

EFFECT OF PRESSURE ON THE FAST MOTIONS IN
ORDERED PHASE PHOSPHOLIPID BILAYERS

CENTRE FOR NEWFOUNDLAND STUDIES

**TOTAL OF 10 PAGES ONLY
MAY BE XEROXED**

(Without Author's Permission)

HARPREET SINGH

EFFECT OF PRESSURE ON THE FAST MOTIONS IN
ORDERED PHASE PHOSPHOLIPID BILAYERS

by

© Harpreet Singh
M.Tech. (IIT Delhi) M.Sc. (Panjab University)

A thesis submitted
in partial fulfillment of the
requirements for the degree of
Master of Science.

Department of Physics and Physical Oceanography
Memorial University of Newfoundland

August, 2005

ST. JOHN'S



NEWFOUNDLAND

Abstract

Application of hydrostatic pressure to phospholipid bilayers increases acyl chain order and raises the main transition temperature. ^2H NMR spectra and quadrupole echo decay times were obtained at ambient pressure and pressures of 85 MPa and 196.1 MPa for ordered phase bilayers of a zwitterionic phospholipid : 16:0-16:0 PC- d_{62} (DPPC- d_{62}) and an anionic phospholipid : 16:0-16:0 PG- d_{62} (DPPG- d_{62}). The extent to which deuterium magnetization following an RF pulse is refocused in the echo after a second pulse is limited by the motions that modulate the orientation-dependent quadrupole interaction. Quadrupole echo decay times were recorded for a temperature range of 60°C to -26°C for both lipids, at ambient pressure and pressures of 85 MPa and 196.1 MPa. The temperature dependences of the echo decay times at ambient pressure are similar for the two lipids. The echo decay times pass through a minimum at the main transition, as the correlation times of some motions change from short to intermediate on the NMR timescale. Upon further cooling in the gel phase, the echo decay time passes through a maximum before falling to a second minimum. This indicates the persistence of some fast motions into the ordered phases. At 196.1 MPa, both lipids undergo a transition to more ordered crystalline phases near 0°C . This is reflected as a plateau in the temperature dependence of quadrupole echo decay times at high pressure. The application of 85 MPa shifts the main transition but does not lower the low temperature minimum in the echo decay time. The behavior of DPPG- d_{62} at 85 MPa is qualitatively similar to that at higher pressure. The q-CPMG pulse sequence is used to separate the contribution of slow and fast motions to the echo decay rate. This work provides insight into how chain packing affects local motion.

Acknowledgements

I wish to express my deep gratitude to my supervisor Professor M.R. Morrow for his guidance, encouragement and financial support over the years; and making me do it right. His expertise, combined with kind patience and positive attitude have helped and encouraged me many times during the project.

I am grateful to the School of Graduate Studies and Department of Physics and Physical Oceanography for financial support as a form of fellowship and graduate assistance. It is my pleasure to acknowledge help from Wayne Holly for keeping our lab. going with an excellent cryogenic facility.

I would like to thank my friends both old and new. They have given freely of laughter and friendship, knowledge and new ideas, and they have made my time at Memorial enriching and joyful.

I thank my family in India, for their unwavering faith in me and for their trust and full support through the tough decisions of recent times. I wish to thank my wife Navneet for her understanding, encouragement and support.

Finally, I would like to thank all my fellow students as well as faculty who have made my experience at Memorial University a memorable and productive one.

St. John's, NL, Canada, July 2005

Harpreet Singh

Contents

1	Introduction	1
1.0.1	Overview of Thesis	3
2	Lipid Background: Structure and Phase Behavior	5
2.1	Chemical structure of DPPC and DPPG	7
2.2	Phase Structures	8
2.3	Phase Behavior of Bilayers	9
2.4	Effect of Pressure on Phase behavior of Lipid Bilayers	11
2.5	Dynamic Properties	12
3	NMR Theory	17
3.1	Hamiltonian	18
3.1.1	The Electric Quadrupole moment	19
3.2	Effect of motions on 2H Quadrupolar Hamiltonian	23
3.3	The Quadrupole Echo	27
3.4	Quadrupole Carr-Purcell-Meiboom-Gill Echo Train	33
3.5	Molecular Motions and Quadrupolar Relaxation	34
4	Experimental Setup	40
4.1	Spectrometer	40

4.2	The High Pressure Probe	42
4.3	Experimental Details	43
4.4	Sample Preparation	44
5	Results and Discussion	46
5.1	Temperature Dependence of DPPC- d_{62} ^2H NMR Spectra at Ambient Pressure and High pressure	47
5.1.1	DPPC- d_{62} at Ambient Pressure	47
5.1.2	DPPC- d_{62} at High Pressure	49
5.2	Temperature Dependence of First Moments of DPPC- d_{62}	52
5.3	Temperature Dependence of DPPG- d_{62} ^2H NMR Spectra at Ambient Pressure and High pressure	54
5.4	Temperature Dependence of First Moments of DPPG- d_{62}	58
5.5	Deuteron Quadrupole Echo Decay	60
5.5.1	Temperature Dependence of DPPC- d_{62} Transverse Relaxation Time at Ambient and High Pressure	61
5.5.2	Temperature Dependence of DPPG- d_{62} Transverse Relaxation Time at Ambient and High Pressure	66
5.6	Quadrupole Carr-Purcell-Meiboom-Gill Decays	69
5.6.1	Quadrupole Carr-Purcell-Meiboom-Gill Decays for DPPC- d_{62} at Ambient and High Pressures	71
5.6.2	Quadrupole Carr-Purcell-Meiboom-Gill Decays for DPPG- d_{62} at Ambient and High Pressures	79
6	Summary and Concluding Remarks	83
A	^2H NMR Spectra	97

List of Figures

2.1	Chemical structure of (a) Dipalmitoyl-sn-glycero-3-phosphocholine (DPPC), (b) Dipalmitoyl-sn-glycero-3- [phospho-rac-(1-glycerol)] (DPPG).	6
2.2	states of aggregation of phospholipids in water (a) bilayer (b) micelles (c) inverted hexagonal cylinders.	7
2.3	Cross-sectional view of (a) Multilamellar vesicles (MLV) and (b) a Lipid Bilayer	9
2.4	Structure of lipid bilayer in the (a) the liquid crystalline (L_α) phase and (b) the gel phase (L_β). The acyl chains of lipids in the (L_α) phase are disordered whereas the chains are highly ordered in the (L_β) phase.	10
2.5	Schematic Pressure-Temperature phase diagram for lipid bilayers, rep- resenting all the different phase transitions with temperature and pres- sure.	12
2.6	Schematic illustration of different possible motions of lipid molecules in bilayers.	14

2.7	Summary of important timescales in NMR experiments, showing the regimes of motion as defined in the text. Above the bar showing τ_c values, selected NMR parameters are shown along with the range of timescales to which they are sensitive. At the bottom, representative motions present in fluid bilayers are shown, along with estimated ranges of their correlation times.	16
3.1	Splitting of Zeeman energy levels by quadrupole interaction.	20
3.2	Schematic illustrating angles that modulate the quadrupole splitting.	24
3.3	Spin-1 powder pattern line shape. The vertical axis is intensity. . . .	26
3.4	Quadrupole echo pulse sequence and the echo formation.	28
3.5	Example of Free Induction Decay, FID.	31
3.6	Quadrupole echo intensity obtained using quadrupole echo pulse sequences: Variation of the echo intensity with τ is used to measure T_2^{QE}	36
4.1	Block diagram of NMR spectrometer	41
4.2	High pressure chamber	43
5.1	^2H NMR spectra of Dipalmitoyl-sn-Glycero-3-Phosphocholine(DPPC- d_{62}) at ambient pressure and at selected temperatures.	48
5.2	^2H NMR spectra of Dipalmitoyl-sn-Glycero-3-Phosphocholine(DPPC- d_{62}) at 85 MPa pressure and at selected temperatures.	50
5.3	^2H NMR spectra of Dipalmitoyl-sn-Glycero-3-Phosphocholine(DPPC- d_{62}) at 196.1 MPa pressure and at selected temperatures.	51
5.4	First moments for DPPC- d_{62} at ambient pressure (circle), 85 MPa (square) and 196.1 MPa (triangle).	53

5.5	^2H NMR spectra of Dipalmitoyl-sn-Glycero-3- [Phospho-rac-(1-glycerol)](DPPG- d_{62}) at ambient pressure and at selected temperatures.	55
5.6	^2H NMR spectra of Dipalmitoyl-sn-Glycero-3- [Phospho-rac-(1-glycerol)](DPPG- d_{62}) at 85 MPa pressure and at selected temperatures.	56
5.7	^2H NMR spectra of Dipalmitoyl-sn-Glycero-3- [Phospho-rac-(1-glycerol)](DPPG- d_{62}) at 196.1 MPa pressure and at selected temperatures.	57
5.8	First moments for DPPG- d_{62} at ambient pressure (blue), 85 MPa (green), and 196.1 MPa (red).	59
5.9	Temperature dependence of Quadrupole echo decay times T_{2e}^{QE} for DPPC- d_{62} at (a) Ambient Pressure (b) 85 MPa Pressure and (c) 196.1 MPa. The sharp phase transitions are marked by dotted lines. The broader low temperature phase transition is marked by a shaded area.	62
5.10	Temperature dependence of T_{2e} : Separate contributions of fast and slow motions.	64
5.11	Temperature dependence of T_{2e} : Separate contributions of fast and slow motions.	65
5.12	Temperature dependence of Quadrupole echo decay times T_{2e}^{QE} for DPPG- d_{62} at (a) Ambient Pressure (b) 85 MPa Pressure and (c) 196.1 MPa. The sharp phase transitions are marked by dotted lines. The broader low temperature phase transition is marked by shaded a area.	67
5.13	Schematic representation of q-CPMG pulse sequence and trains of echoes obtained.	71
5.14	q-CPMG echo decays for DPPC- d_{62} at ambient pressure and 45°C, where A is the amplitude of echo obtained at $2n\tau$ and A(max) is the maximum amplitude for shortest τ	73

5.15	q-CPMG echo decays for DPPC- d_{62} at ambient pressure and 30°C, where A is the amplitude of echo obtained at $2n\tau$ and A(max) is the maximum amplitude for shortest τ	73
5.16	q-CPMG echo decays for DPPC- d_{62} at ambient pressure and 10°C, where A is the amplitude of echo obtained at $2n\tau$ and A(max) is the maximum amplitude for shortest τ	74
5.17	q-CPMG echo decays for DPPC- d_{62} at ambient pressure and -10°C, where A is the amplitude of echo obtained at $2n\tau$ and A(max) is the maximum amplitude for shortest τ	74
5.18	q-CPMG echo decays for DPPC- d_{62} at 196.1 MPa and 50°C, where A is the amplitude of echo obtained at $2n\tau$ and A(max) is the maximum amplitude for shortest τ	77
5.19	q-CPMG echo decays for DPPC- d_{62} at 196.1 MPa and 30°C, where A is the amplitude of echo obtained at $2n\tau$ and A(max) is the maximum amplitude for shortest τ	77
5.20	q-CPMG echo decays for DPPC- d_{62} at 196.1 MPa and 0°C, where A is the amplitude of echo obtained at $2n\tau$ and A(max) is the maximum amplitude for shortest τ	78
5.21	q-CPMG echo decays for DPPG- d_{62} at ambient pressure and 30°C, where A is the amplitude of echo obtained at $2n\tau$ and A(max) is the maximum amplitude for shortest τ	79
5.22	q-CPMG echo decays for DPPG- d_{62} at ambient pressure and 23°C, where A is the amplitude of echo obtained at $2n\tau$ and A(max) is the maximum amplitude for shortest τ	80

5.23	q-CPMG echo decays for DPPG- d_{62} at 196.1 MPa and 58°C, where A is the amplitude of echo obtained at $2n\tau$ and A(max) is the maximum amplitude for shortest τ	80
5.24	q-CPMG echo decays for DPPG- d_{62} at 196.1 MPa and 30°C, where A is the amplitude of echo obtained at $2n\tau$ and A(max) is the maximum amplitude for shortest τ	81
5.25	q-CPMG echo decays for DPPG- d_{62} at 196.1 MPa and -5°C, where A is the amplitude of echo obtained at $2n\tau$ and A(max) is the maximum amplitude for shortest τ	81
A.1	^2H NMR spectra for DPPC- d_{62} at ambient pressure, 50°C to 23°C. . .	98
A.2	^2H NMR spectra for DPPC- d_{62} at ambient pressure, 20°C to -26°C. . .	99
A.3	^2H NMR spectra for DPPC- d_{62} at pressure of 85 MPa, 60°C to 29°C. . .	100
A.4	^2H NMR spectra for DPPC- d_{62} at pressure 85 MPa, 26°C to -26°C. . .	101
A.5	^2H NMR spectra for DPPC- d_{62} at pressure 196.1 MPa, 60°C to 30°C. . .	102
A.6	^2H NMR spectra for DPPC- d_{62} at pressure 196.1 MPa, 30°C to -15°C. . .	103
A.7	^2H NMR spectra for DPPG- d_{62} at ambient pressure, 50°C to 23°C. . .	104
A.8	^2H NMR spectra for DPPG- d_{62} at ambient pressure, 23°C to -26°C. . .	105
A.9	^2H NMR spectra for DPPG- d_{62} at pressure of 85 MPa, 60°C to 29°C. . .	106
A.10	^2H NMR spectra for DPPG- d_{62} at pressure 85 MPa, 26°C to -26°C. . .	107
A.11	^2H NMR spectra for DPPG- d_{62} at pressure 196.1 MPa, 60°C to 24°C. . .	108
A.12	^2H NMR spectra for DPPG- d_{62} at pressure 196.1 MPa, 24°C to -26°C. . .	109

List of Tables

2.1	Luzzati nomenclature.	8
3.1	9 dimensional operator space.	30
3.2	Correlation times, τ_{ci} for the motions in the liquid crystalline phase. .	35
5.1	DPPC- d_{62} phases at ambient pressure.	49
5.2	DPPC- d_{62} phases at 85 MPa.	49
5.3	DPPC- d_{62} phases at 196.1 MPa.	52

Abbreviations

^2H NMR: Deuterium Nuclear Magnetic Resonance

PC: Phosphaticholine

DPPC: 1,2-dipalmitoyl-sn-glycero-3-phosphocholine

DPPC- d_{62} : 1,2-perdeuterodipalmitoyl-sn-glycero-3-phosphocholine

PG: Phosphatidylglycerol

DPPG: 1,2-dipalmitoyl-sn-glycero-3- [phospho-rac-(1-glycerol)]

DPPG- d_{62} : 1,2-perdeuterodipalmitoyl-sn-glycero-3- [phospho-rac-(1-glycerol)]

q-CPMG: Quadrupole Carr-Purcell-Meiboom-Gill pulse sequence

T_2^{QE} : Quadrupole echo decay time

EFG: Electric Field Gradient

PAS: Principal Axis System

Chapter 1

Introduction

Lipids are very important parts of biomembranes. Phospholipids self assemble into lipid bilayers upon hydration. Lipid bilayers embedded with different proteins constitute the cell membrane which differentiates the cell interior from its environment. The lipid molecules are amphiphilic, so lipid bilayers consist of two regions; one is hydrophobic where the other one is hydrophilic.

Lipid bilayers are well studied by a number of different experimental techniques like NMR, IR spectroscopy, ESR and optical spectroscopy etc. ^2H NMR is a very important tool to study structure and many other dynamic properties of bilayers, like correlation times of different motions. Lipid bilayers exist in many phases, depending on temperature and pressure. The most studied phases are the high temperature liquid crystalline phase and the low temperature, more ordered, gel phase. The transition between these two phases is known as the main phase transition. Experimental studies at high pressure have revealed that pressure has an effect on phase behavior of lipid bilayers [1, 2, 3, 4, 5]. The main transition temperature increases with increasing pressure. In dimyristoylphosphaticholine (DMPC), a zwitterionic diacyl lipid with 14-carbon saturated hydrocarbon chains, the main transition temperature

rises by 20°C per 100 MPa of applied pressure [2]. There are a number of pressure-induced ordered phases other than the two phases discussed above. The structures of these phases has been studied by Wong et al. [6] using Raman spectroscopy, Driscoll et al. [7] using ^2H NMR, Peng and Jonas using ^{31}P NMR [8] and others.

Motions in lipid bilayers span a range of characteristic times from short (10^{-10}s) to long (10^{-4}s) [9]. These motions are characterized as fast or slow motions by comparing their correlation times with the NMR time scale. The quadrupole echo pulse sequence consists of two $\frac{\pi}{2}$ radio frequency pulses differing in phase by $\frac{\pi}{2}$ and separated by time τ . This pulse sequence results in a quadrupole echo at $t=2\tau$. The deuteron quadrupole Hamiltonian is orientation dependent. Motions that change the orientation of the average electric field gradient tensor in the principal axis system with characteristic times in the range of NMR experiment time scale, reduce the amplitude of the quadrupole echo. The characteristic time for decay of the quadrupole echo with increasing 2τ is T_2^{QE} , known as the quadrupole echo decay time.

The temperature dependence for echo decay times has been studied at ambient pressure [9, 10, 11, 12]. An abrupt decrease in the echo decay time at main transition was reported. Further cooling in the gel phase leads to an increase in the echo decay time. Previous work done by Morrow and Nidal [10] on DPPC/egg-PG bilayers showed that in the gel phase, T_2^{QE} first increases, reaches a local maximum and then starts decreasing. The double minimum in the temperature dependence of T_2^{QE} at low temperature and ambient pressure for DMPC- $d_{6,13}$ was reported by Meier et al. [9]. The quadrupole echo decay time T_2^{QE} passes through a first minimum at the main transition from the liquid crystalline phase to the gel phase due to slowing down of some fast motions. The second minimum in T_2^{QE} is seen at low temperatures due to freezing of trans-gauche isomerization in lipid molecules.

Temperature and pressure changes affect the nature of the bilayer and may induce

phase changes to more ordered bilayer states. The echo decay times at high pressure are not much studied. Such research would be of particular interest because changes in echo decay time tell about the nature of motions present in high pressure phases.

There are some motions with long correlation times that do not contribute to the motional narrowing but contribute to the quadrupole echo decay time [12]. Bloom and Sternin [12] used Quadrupole Carr-Purcell-Meiboom-Gill Echo (q-CPMG), to separate contributions of these motions to echo decay times. The effect of q-CPMG echo decay rates have been studied by Blicharski [13] and Stohrer et al. [14]. The q-CPMG experiment were performed on both lipids DPPC- d_{62} and DPPG- d_{62} at ambient pressure and high pressure of 196.1 MPa. .

1.0.1 Overview of Thesis

The objective of the present work is to address two questions

- How does pressure affect the freezing out of fast motions in the ordered phase?
- Does headgroup charge affect the freezing out of motion in the ordered phase?

To study the effect of surface charge, the ^2H NMR experiments were performed on two deuterated phospholipids; dipalmitoyl-sn-glycero-3-phosphocholine (DPPC) and dipalmitoyl-sn-glycero-3- [phospho-rac-(1-glycerol)] (DPPG) having different headgroup charge. The experiments were conducted at ambient pressure and elevated pressures of 85 MPa and 196.1 MPa for a wide range of temperatures from 60°C to -26°C. In these experiments quadrupole splittings and quadrupole echo decay times were measured. Quadrupole Carr-Purcell-Meiboom-Gill (q-CPMG) decay were studied under similar conditions. This thesis reports the results of these studies done in an effort to better understand the effect of high pressure on the fast motions in lipid bilayers and how that effect is changed by changing the headgroup charge.

In chapter 2, a brief introduction to the structure and phase behavior of lipid bilayer is presented. In Chapter 3, the NMR theory relevant to the experiments and their interpretation is summarized. Chapter 4 outlines the details of experimental techniques. The results and analysis are presented in Chapter 5, with accompanying discussion; the chapter concludes with suggested extensions of the study, and the relevance of the findings to the biological question is assessed. Chapter 6 is a brief concluding statement. Appendix A includes ^2H NMR spectra not presented in Chapter 5.

Chapter 2

Lipid Background: Structure and Phase Behavior

Phospholipid bilayers have been the subject of intense study for several decades. They are important structural elements of biological membranes. Cell membranes constitute one of the fundamental structural and functional elements of living organisms. The plasma membrane of a cell or the envelope of a virion denotes the outer boundary of the system and distinguishes between the inside and outside of the system [15]. Lipid bilayers can contain proteins and other components (e.g. cholesterol). Comprehensive reviews of membrane properties can be found in the literature [16, 17, 18].

When dispersed in water, phospholipids form bilayer vesicles spontaneously because of their amphiphilic structure. One end of a phospholipid has a polar group (head group). The remainder of the molecule (acyl chain) is hydrophobic with extensive hydrocarbon character. Due to hydrophobic effects, lipids assemble with their head groups in contact with water and hydrophobic acyl chains facing inwards. For most two-chain phospholipids, bilayers are the favored structure, rather than micelles or inverted hexagonal phases [19]. One important feature of lipid bilayer behavior is

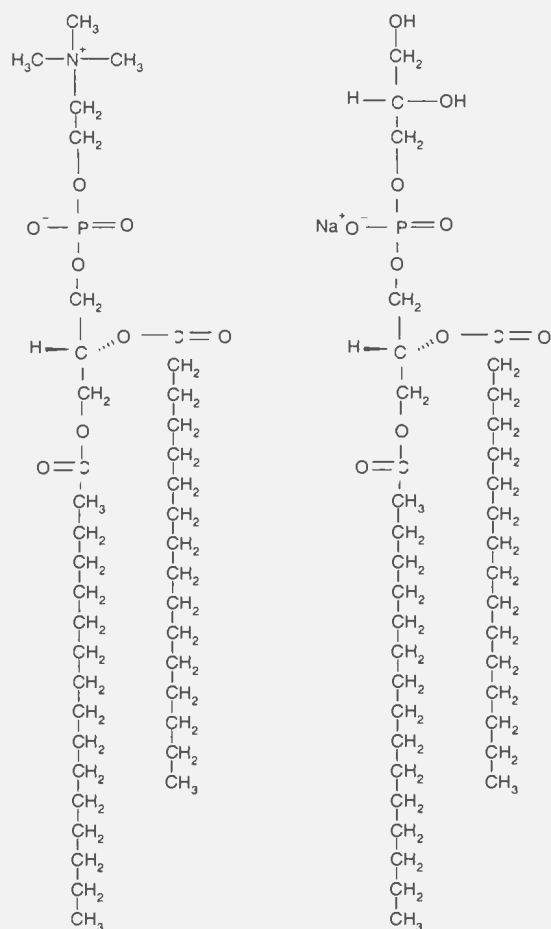


Figure 2.1: Chemical structure of (a) Dipalmitoyl-*sn*-glycero-3-phosphocholine (DPPC), (b) Dipalmitoyl-*sn*-glycero-3-[phospho-*rac*-(1-glycerol)] (DPPG).

their phase behavior. Bilayers undergo the main phase transition from a low temperature gel phase, in which chains are in order, to a high temperature liquid crystalline phase in which chains are more fluid. Bilayer properties depend on acyl chain length [20, 21] and degree of lipid chain unsaturation [22, 23, 24].

Nuclear magnetic resonance has been widely used to study lipid systems. Studying the phase behavior, NMR can be used to find phase transition temperature, but it can also give information about the dynamics of a system on the molecular level.

2.1 Chemical structure of DPPC and DPPG

The focus of the present work is on 1,2-Dipalmitoyl-sn-glycero-3-phosphocholine (DPPC) and 1,2-Dipalmitoyl-sn-glycero-3-[phospho-rac-(1-glycerol)](DPPG). The chemical structures of DPPC and DPPG are as shown in Figure (2.1). DPPC is a zwitterionic phospholipid and DPPG is an anionic phospholipid. Their chains are of same length.

The structures of lipid bilayers have been studied by many experimental techniques, including infrared spectroscopy [25, 26, 27, 28, 29], fluorescent probes [30, 31], neutron diffraction [32, 33, 34], x-ray diffraction [35, 36], proton nuclear magnetic resonance [37, 38, 39] and deuterium nuclear magnetic resonance [40, 41, 42, 43]. Phospholipid molecules has three different structural regions. The polar end of the molecule is known as the *headgroup*. The headgroup region consists of a phosphate group bound to an alcohol and it is the hydrophilic part of the phospholipid molecule. The headgroup is attached to the acyl chains via a glycerol backbone [44].

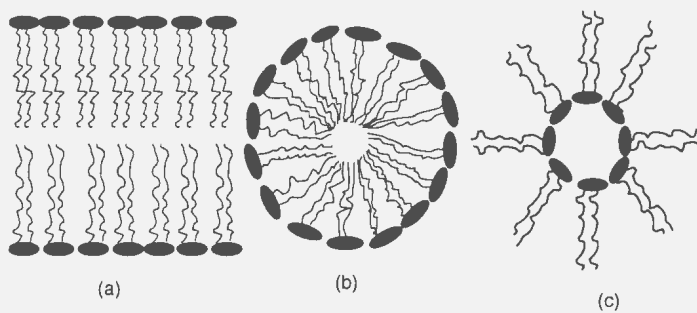


Figure 2.2: states of aggregation of phospholipids in water (a) bilayer (b) micelles (c) inverted hexagonal cylinders.

2.2 Phase Structures

Phospholipid assemblies exist in different phases depending upon hydration or temperatures. Some of these aggregation states of phospholipids in water are shown in fig (2.2).

The most commonly used and widely accepted nomenclature for the lyotropic mesophases is proposed by Luzzati [45]. The lattice type is denoted by a capital letter on the basis of its general topology and geometry. A subscript is used to denote chain conformation.

A list of the meaning of various symbols is given in table 2.1. Depending on the geometrical factors and other conditions, most two chain phospholipids form a structure with two layers of lipid, in which hydrophilic polar headgroups are at the lipid-water interface and hydrophobic tails interact to form an environment that excludes water. This bilayer conformation, shown in fig.(2.2a), is the structural element of biological membranes. Bilayers have a tendency to establish a structure in which

Table 2.1: Luzzati nomenclature.

Lattice type	Chain conformation
L -lamellar	α -fluid (disordered)
P -rippled	β -normal (partially ordered gel)
H -two-dimensional hexagonal	β' -tilted (partially ordered gel)
H_I -hexagonal	c -crystalline
H_{II} - inverted hexagonal	δ -helical
R -rhombohedral	
Q -cubic	
C -crystalline	

there is least contact between water and lipid chains. So, a lipid bilayer closes in on itself, forming a spherical vesicle, a *liposome*.

Liposomes which have single layer are known as unilamellar vesicles (ULV). The focus of the present work is on multilamellar vesicles (MLV), shown in fig. 2.3.

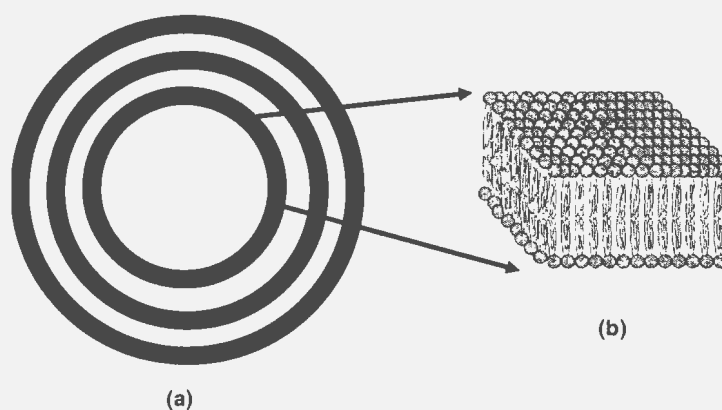


Figure 2.3: Cross-sectional view of (a) Multilamellar vesicles (MLV) and (b) a Lipid Bilayer

2.3 Phase Behavior of Bilayers

Phospholipid bilayers undergo a well defined thermotropic phase transition in which lipid chains change from an ordered or gel phase to a fluid or liquid crystalline state. The high temperature phase is the fluid or liquid crystalline phase (L_{α}). In this phase there are various types of motions like *trans-gauche* isomerization around carbon-carbon bonds, molecular rotations, surface undulations, collective motions etc. The *trans-gauche* isomerization leads to kinks and bends in acyl chains, which expand the bilayer laterally, or perpendicularly to hydrocarbon chain axis. Most lipids in

biomembranes under physiological conditions are in a fluid state.

In the gel phase (L_β) the acyl chains are highly ordered and the lipid headgroups are packed more tightly together compared to the (L_α) phase. In this phase lipid acyl chains are mostly in *all trans* configuration, meaning that all the carbon atoms on one chain lie in one plane. This phase is formed at low temperatures or high pressures. Due to the discrepancy between the headgroup and the chain cross-sectional areas, lipids with larger headgroups (such as DPPC) have acyl chains tilted with respect to the bilayer normal. This phase is denoted by (L_β').

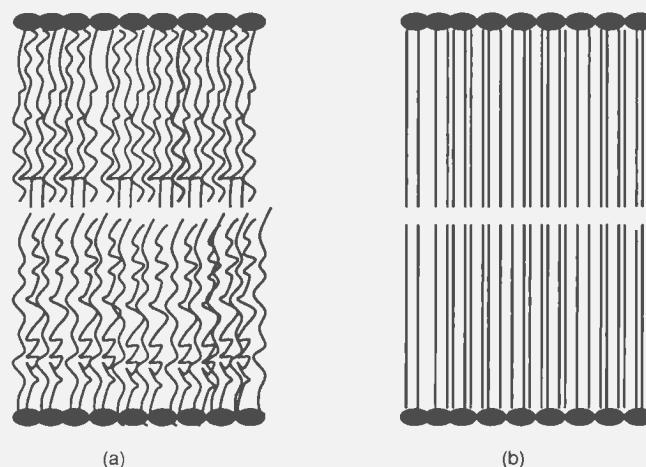


Figure 2.4: Structure of lipid bilayer in the (a) the liquid crystalline (L_α) phase and (b) the gel phase (L_β). The acyl chains of lipids in the (L_α) phase are disordered whereas the chains are highly ordered in the (L_β) phase.

In the (P_β'), there is a reduction in the gauche conformers in the chain. As a result the average cross-sectional area of two acyl chains is slightly less than the cross-sectional area of the choline headgroup [6]. This leads to a periodic ripple in this phase. The inter chain packing in this phase is hexagonal lattice.

The transition between gel phases ($L_{\beta'}$) and ($P_{\beta'}$) is called the *pretransition*. The transitions between the gel phase ($P_{\beta'}$) and the liquid crystalline phase (L_{α}) is called *main transition*. These transition can be induced by changes in temperature as well as by changing the pressure. It is difficult to distinguish the ($L_{\beta'}$) and ($P_{\beta'}$) phase using 2H NMR. At low temperature there is phase transition from the gel phase to another more ordered subgel phase, denoted as L_C . This is known as the subgel transition.

These differences in the phases are characterized by different order and motional properties in the chain region, not by changes in topology of the sample which is MLV in this case.

2.4 Effect of Pressure on Phase behavior of Lipid Bilayers

Effects of pressure on biological systems have been investigated by several research groups [34], [46]. Wong et al [46] used Raman spectroscopy to study lipids at high pressure. Their investigation revealed some pressure-induced gel phases other than the ordinary gel phase (L_{β}) and (P_{β}) discussed in the last section. These phases are named GI to GV corresponding to increasing pressure, where GI and GII are the (L_{β}) and (P_{α}) phases, respectively. In both GII and GIII the chains are extended and tilted with respect to the bilayer normal. The GIII phase is more ordered than GII and the GV phase is the most ordered. Structures of all these phases have been described by Wong et al. [6]. Small angle neutron angle studies [34] have shown another pressure-induced phase, known as interdigitated gel phase, $G_{interdigitated}$. In this phase lipid molecules from opposite sides of the monolayer interpenetrate to form

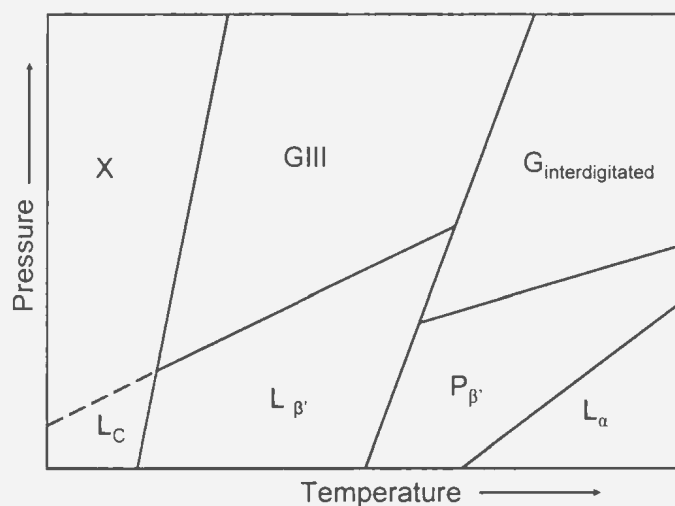


Figure 2.5: Schematic Pressure-Temperature phase diagram for lipid bilayers, representing all the different phase transitions with temperature and pressure.

an interdigitated gel phase. Methyl ends of the chains penetrate between the chains from the other side. Because the methyl chain ends are constrained, there is less motion in this phase. Bilayer properties are affected by the presence of other species [47, 48], including cholesterol [49, 50].

Driscoll et al. [7] used solid state NMR to study the transition between different phases with changes in pressure and temperature. Using the results from Wong [34] and Prasad [51], they established the boundaries of different phases in the phase diagram. A schematic of the pressure/temperature phase diagram for DPPC is shown in fig (2.5).

2.5 Dynamic Properties

In lipid membranes a wide range of motional modes are present. There are fast motions having characteristic time constants of 10^{-14} s for molecular vibrations as

well as slow motions having characteristic time constants of hours or days for lipid flip-flop. As the phospholipid bilayers are anisotropic in nature, so reorientation motions are not isotropic. The reorientations about different molecular axes have very different time scales.

The different possible reorientation motions are given below [52]. The schematic of these motion is shown in fig. 2.6. The extent and correlation times of these motions depends on the bilayer state:

- intramolecular reorientation motions, i.e.,
 - isomerization between different conformations, such as *trans-gauche* isomerization in fatty acid chains,
 - torsional oscillations around single bonds,
 - free or marginally hindered rotations of certain groups or segments, such as methyl groups or the whole head group
- collective processes, such as surface undulations of the bilayers
- Brownian translational diffusion or jump diffusion of the lipid molecule in the lipid bilayer
- anisotropic rotation around the long molecular axis
- anisotropic rotation around the axis perpendicular to the long axis.

The correlation time of *trans-gauche* isomerization was determined using relaxation time measurement and computer simulations by Kothe et al. [9] for DPMC. The correlation times for *trans-gauche* isomerization ranges from 10^{-12} s to 10^{-10} s in the liquid crystalline phase. The fraction of *gauche* conformers increases towards the

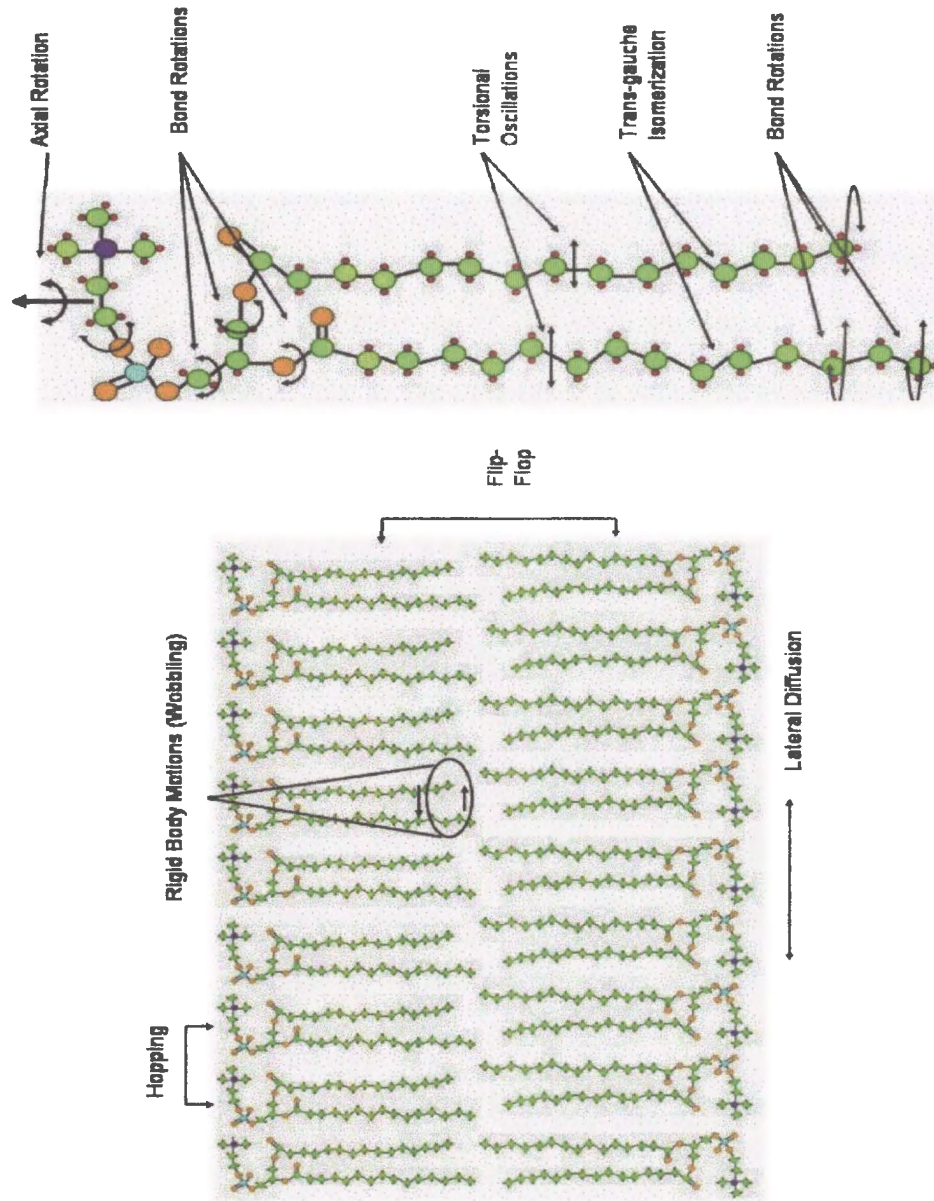


Figure 2.6: Schematic illustration of different possible motions of lipid molecules in bilayers.

chain ends with a decrease in correlation time, τ , for the trans-gauche isomerization. In the liquid crystalline phase, lipid rotation is also fast on ^2H NMR time scale. The correlation time for chain rotation is 10^{-8} in the L_α phase. The lipid molecules also undergo bond vibrations and torsional oscillations, with very short correlation times between 10^{-14} to 10^{-9} s [53, 9, 54]. The other motions in the L_α phase are long axis rotation of the whole molecule, with correlation times between 10^{-9} to 2.10^{-8} s [53, 54] and wobbling motions of the whole molecule, with correlation times between 10^{-9} to 10^{-7} s [53, 54]. In addition to these reorientational motions, slow lateral diffusion of lipid molecules in the plane of bilayer is also observed, having correlation times of $\approx 10^{-5}$ s [14, 55, 12].

In the $L_{\beta'}$ phase the chains are tilted at an angle of approximately 30° with respect to the bilayer normal [56, 57]. The chains are packed in a distorted hexagonal lattice (Wong et al. [6]). The reorientational motions around the molecular long axis slow down with correlation times of 10^{-5} s just above 0°C [53]. The correlation times of trans-gauche isomerization still remain below 10^{-7} s [53, 54, 58, 9, 59, 60]. The bond vibrations and torsional oscillations have similar correlation times as in L_α phase, between 10^{-13} s to 10^{-10} s. The head groups are still highly mobile in the $P_{\beta'}$ as well as in $L_{\beta'}$ phase, with correlation times for the head group reorientations between 10^{-9} s to 10^{-6} s.

After sufficient incubation around 0°C , DPPC- d_{62} and DPPG- d_{62} convert to an L_C phase in which most molecular motions are frozen out. The FTIR and Raman spectra in this phase show highly ordered chains packed in a parallel or perpendicular orthorhombic lattice [25, 6]. The ^2H NMR spectra shows full quadrupole splitting and ^{13}C -NMR shows full asymmetric tensors [9, 61, 62]. The head group motions are also completely suppressed when the lipid converts to the L_C phase [63, 64, 65].

The different motions in the lipid bilayers are classified into slow and fast motions

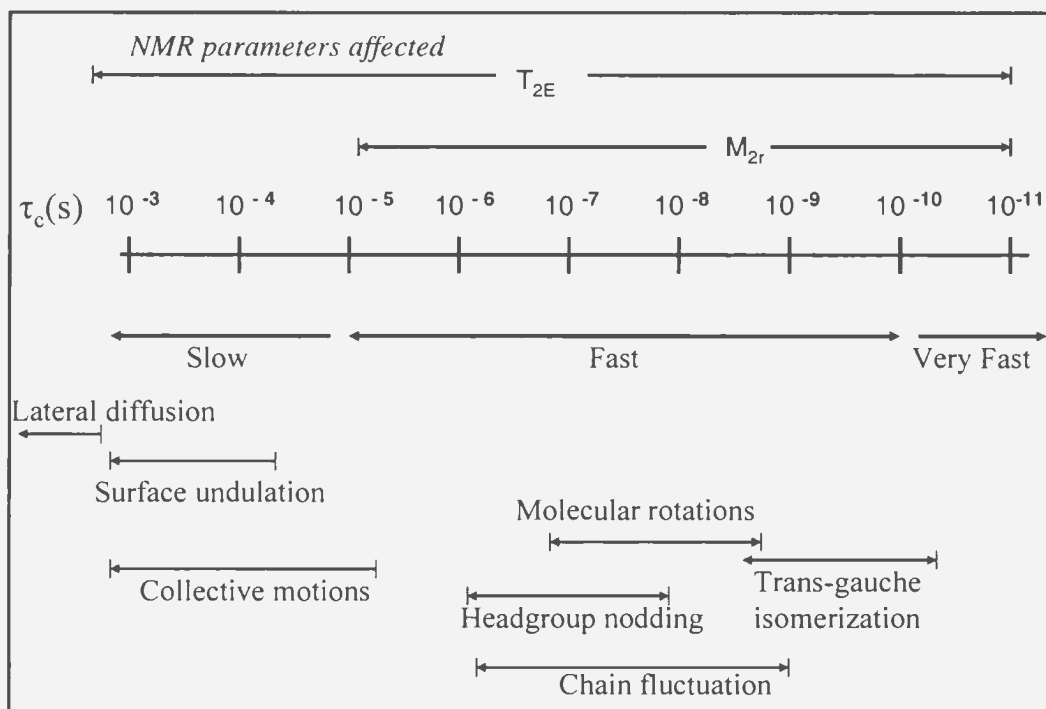


Figure 2.7: Summary of important timescales in NMR experiments, showing the regimes of motion as defined in the text. Above the bar showing τ_c values, selected NMR parameters are shown along with the range of timescales to which they are sensitive. At the bottom, representative motions present in fluid bilayers are shown, along with estimated ranges of their correlation times.

by comparing their correlation times with the time scale of the present NMR experiment. The range of time scales of interest for present work are shown in fig.(2.7). The NMR parameters affected by motions in the these ranges are also shown, as well as representative motions present in fluid bilayers.

Chapter 3

NMR Theory

Lipid bilayers are partially ordered systems. In such systems molecular motions are anisotropic. Orientation-dependent interactions that perturb Zeeman levels, such as chemical shift, dipole-dipole interaction, quadrupolar interactions, are partially averaged by molecular motions. Changes in molecular motions due to external effects like temperature or pressure variations, can be detected by probing the relevant interactions using NMR. This chapter deals with the basic theory behind ^2H -NMR spectroscopy. The splitting of Zeeman energy levels due to quadrupolar interactions in the absence of molecular motions is presented first. The quadrupole splitting expression is then extended by including the effects of motions which modulate the spectrum.

The principle of NMR can be described briefly as follows. Atomic nuclei with intrinsic spin have a magnetic moment. In the presence of a magnetic field the nuclear magnetization precesses about that field with a frequency that depends upon the magnetic field and the magnetic moment of the nucleus. Application of a current oscillating at this characteristic frequency to a coil oriented perpendicular to the applied field can tip the nuclear magnetization away from the field. If the duration of

this radio frequency is selected to leave the nuclear magnetization perpendicular to the applied field, the nuclear magnetization can be detected via the oscillating voltage induced in the coil. This effect is called Nuclear Magnetic Resonance (NMR). Perturbation of the precession frequency gives us information about the environment of the nuclear spin. For a spin-1 nucleus, such as deuterium, the precession is perturbed by the orientation-dependent quadrupole interaction.

3.1 Hamiltonian

The evolution of the spin system depends on the motions and interactions present in the system and its surroundings, in short-on its Hamiltonian.

The Hamiltonian of a deuterium nucleus in a high external magnetic field (H_0) is composed of the Zeeman interaction (H_Z), the quadrupole interaction (H_Q), the dipolar interaction (H_D) and the chemical shift interaction (H_C) [66]:

$$H = H_Z + H_Q + H_D + H_C \quad (3.1)$$

Deuterium has a nucleus with spin angular momentum $I=1$ and its magnetic moment is a factor of 6.5 smaller than that of the spin $I=\frac{1}{2}$ nucleus of hydrogen for which it is often substituted [67]. The maximum quadrupole splitting of ^2H in a C- ^2H bond is about 252 kHz, which is much less than the Larmor frequency 23 MHz in magnetic field of 3.5T. The ^2H - ^2H dipolar splittings for a methylene group are at most a few kHz. The ^2H - ^1H dipolar splittings are of the order of 10 kHz. Chemical shift dispersion is about 1 kHz. Thus in a ^2H -NMR experiment, dipolar interactions with other nuclei and chemical shift dispersion may be neglected, and deuterium may be treated as an isolated spin-1 nucleus. The quadrupolar interactions are then treated

as a first order perturbation. The Hamiltonian of equation (3.1) then reduces to

$$H = H_Z + H_Q \quad (3.2)$$

3.1.1 The Electric Quadrupole moment

Consider a collection of N deuterons in a magnetic field H_0 along z -axis. In the absence of any quadrupole interaction, the Zeeman interactions splits the ground state nuclear energy levels of the system as shown in fig (3.1).

The Hamiltonian for the Zeeman interactions is

$$H_Z = -\vec{\mu} \cdot \vec{H}_0 = -\gamma\hbar\omega_0 I_Z \quad (3.3)$$

where $\vec{\mu}$ is the nuclear magnetic moment, \vec{H}_0 is the external magnetic field, γ is the nuclear gyromagnetic ratio ($\gamma = 2\pi \times 6.536 \times 10^6 s^{-1} T^{-1}$ for deuterium), \hbar is Planck's constant divided by 2π , $\omega_0 = \gamma H_0$ is the nuclear Larmor frequency, and I_Z is the z -component of the nuclear spin momentum. The allowed values of I_Z are $m = -1, 0, 1$ and the energy of the interaction is

$$E_m = -m\hbar\omega_0. \quad (3.4)$$

In the $C-^2H$ bond, the electron density has a highly anisotropic distribution which creates an EFG. For a nucleus with an electric quadrupole moment, eQ , this interaction between the EFG and eQ results in a shift of these nuclear Zeeman levels [68]. This is shown in fig (3.1).

The energy of a nuclear charge distribution $\rho(\vec{r})$ in an electrical potential $V(\vec{r})$ is [68]

$$E = \int \rho(\vec{r})V(\vec{r})d^3 \vec{r}, \quad (3.5)$$

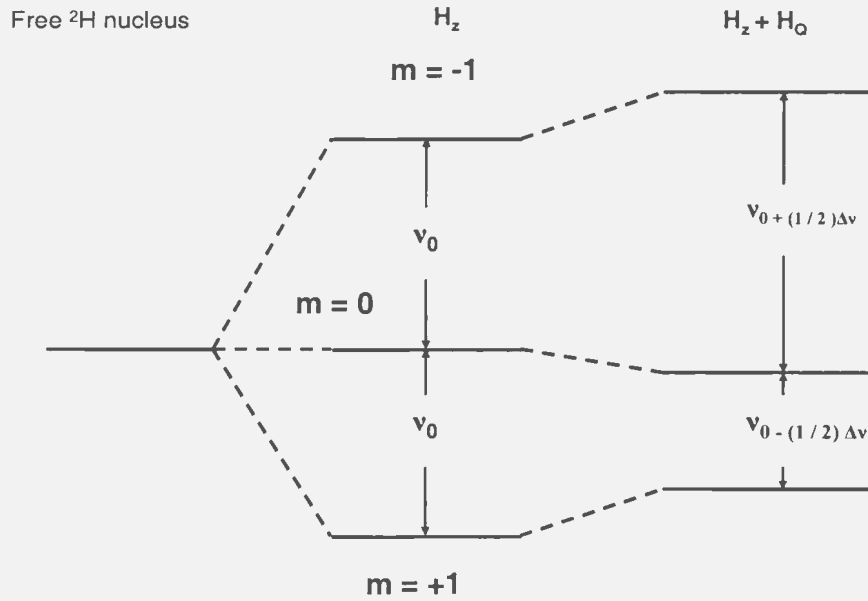


Figure 3.1: Splitting of Zeeman energy levels by quadrupole interaction.

where the integral is over the nuclear volume. We can find the expression for the energy using an expansion of $V(\vec{r})$ is the Taylor's series about the origin [68, 69]

$$V(\vec{r}) = V(0) + \sum_{\alpha} x_{\alpha} \frac{\partial V}{\partial x_{\alpha}} \Big|_{\vec{r}=0} + \frac{1}{2!} \sum_{\alpha, \beta} x_{\alpha} x_{\beta} \frac{\partial^2 V}{\partial x_{\alpha} \partial x_{\beta}} \Big|_{\vec{r}=0} + \dots \quad (3.6)$$

Using Eq. (3.6) in Eq. (3.5), Eq. (3.5) may be written as

$$E = V(0) + \int \rho(\vec{r}) d^3 \vec{r} + \sum_{\alpha} V_{\alpha} \int x_{\alpha} \rho(\vec{r}) d^3 \vec{r} + \frac{1}{2} \sum_{\alpha, \beta} V_{\alpha \beta} \int x_{\alpha} x_{\beta} \rho(\vec{r}) d^3 \vec{r} + \dots \quad (3.7)$$

where x_{α} ($\alpha=1,2,3$) stands for x, y, or z respectively. The quantity

$$V_{\alpha, \beta} = \frac{\partial^2 V}{\partial x_{\alpha} \partial x_{\beta}} \Big|_{\vec{r}=0} \quad (3.8)$$

is the symmetric traceless second order tensor, called EFG tensor. The first term, $E^{(0)}$, is the energy of a point charge in the electric potential $V(0)$ and the second term, $E^{(1)}$, is zero because all integrals which involve odd powers of x_α vanish for nuclear states with definite parity. The third term, $E^{(2)}$, is the electric quadrupole interaction [68] and it can be written as

$$E^{(2)} = \frac{1}{2} \sum_{\alpha,\beta} V_{\alpha,\beta} Q_{\alpha,\beta}^N \quad (3.9)$$

where the nuclear quadrupole moment is defined [68, 69] by

$$Q_{\alpha,\beta}^N = \int (3x_\alpha x_\beta - \delta_{\alpha\beta} r^2) \rho dr. \quad (3.10)$$

In the above equation the integral is over the nuclear volume. This tensor V is symmetric with respect to an interchange of α and β , $V_{\alpha\beta} = V_{\beta\alpha}$. The trace of V vanishes due to the Laplace equation

$$\nabla^2 V = \sum_{\alpha} V_{\alpha\alpha} = 0. \quad (3.11)$$

A symmetric, traceless, second rank tensor has only five independent components. This symmetric second rank tensor is diagonalized by using the coordinate transformation through Euler angles (α, β, γ) , which brings us from the laboratory coordinate system into the principal axis system (PAS) of the electric field gradient tensor. With the assumption

$$|V_{yy}| \leq |V_{xx}| \leq |V_{zz}| \quad (3.12)$$

where the principal value of electric field gradient is defined as

$$eq = V_{zz} \quad (3.13)$$

and asymmetry parameter is

$$\eta = \left| \frac{V_{xx} - V_{yy}}{V_{zz}} \right|. \quad (3.14)$$

This imposes the inequality

$$0 \leq \eta \leq 1. \quad (3.15)$$

The quadrupole Hamiltonian, H_Q , is given by the scalar product of electric field gradient tensor with quadrupole moment tensor, and can be expressed as [69]

$$H_Q = \frac{eQ}{6I(2I-1)} \sum_{\alpha,\beta} V_{\alpha\beta} \left[\frac{3}{2} (I_\alpha I_\beta + I_\beta I_\alpha) - \delta_{\alpha\beta} I^2 \right]. \quad (3.16)$$

This can be written in the principal axis system as [69, 68]

$$H_Q = \frac{eQ}{6I(2I-1)} [V_{xx}(3I_x^2 - I^2) + V_{yy}(3I_y^2 - I^2) + V_{zz}(3I_z^2 - I^2)]. \quad (3.17)$$

Using the asymmetry parameter and principal value we have

$$H_Q = \frac{e^2qQ}{4I(2I-1)} [(3I_z^2 - I^2) + \eta(I_x^2 - I_y^2)]. \quad (3.18)$$

The laboratory coordinate system is defined by the direction of \vec{H}_0 , and in general, does not coincide with the PAS of the electric field gradient tensor. We need to transform electric field gradient from PAS to laboratory coordinate system, in order to find how H_Q effects the Zeeman energy levels. This is done by using Wigner rotation matrices in the spherical coordinate system [11, 70], to get the Hamiltonian in laboratory coordinate system

$$H_Q = \frac{e^2qQ}{4I(2I-1)} [3I_z^2 - I(I+1)] [(3 \cos^2 \beta - 1) + \eta \sin^2 \beta \cos 2\alpha]. \quad (3.19)$$

Thus, the quadrupole interaction shifts the nuclear energy levels, to first order by the amount

$$E_m = \frac{e^2qQ}{8}(3m^2 - 1)[(3 \cos^2 \beta - 1) + \eta \sin^2 \beta \cos 2\alpha]. \quad (3.20)$$

The levels with $m = \pm 1$ are shifted up as shown in the fig (3.1), by an amount Δ

$$\Delta = \frac{e^2qQ}{8}[(3 \cos^2 \beta - 1) + \eta \sin^2 \beta \cos 2\alpha]. \quad (3.21)$$

The $m=0$ level is lowered by the amount 2Δ . According to selection rules $\Delta m = \pm 1$, there are two possible transitions among shifted Zeeman energy levels. As a result we observe a doublet which is symmetrically displaced about ω_0 with quadrupole splitting of

$$\omega_Q = 6\Delta = \frac{3e^2qQ}{4\hbar}[(3 \cos^2 \beta - 1) + \eta \sin^2 \beta \cos 2\alpha]. \quad (3.22)$$

The quadrupole splitting, ω_Q depends upon, (α, β) , the orientation of the electric field gradient tensor in the principal axis system relative to magnetic field. In the case of C-²H bonds, the EFG tensor is nearly axially symmetric ($\eta \leq 0.05$), so term containing the η in Eq. (3.22) is neglected and Eq. (3.22) becomes

$$\omega_Q = 6\Delta = \frac{3e^2qQ}{4\hbar}(3 \cos^2 \beta - 1) \quad (3.23)$$

where $\frac{e^2qQ}{\hbar} = 167 \text{ kHz}$ is the quadrupole coupling constant for the deuterium in a C-²H bond.

3.2 Effect of motions on ²H Quadrupolar Hamiltonian

In lipid bilayers a wide range of motional modes are present. For energy levels and quadrupole splitting derived in the last section we assumed a static C-²H bond, which

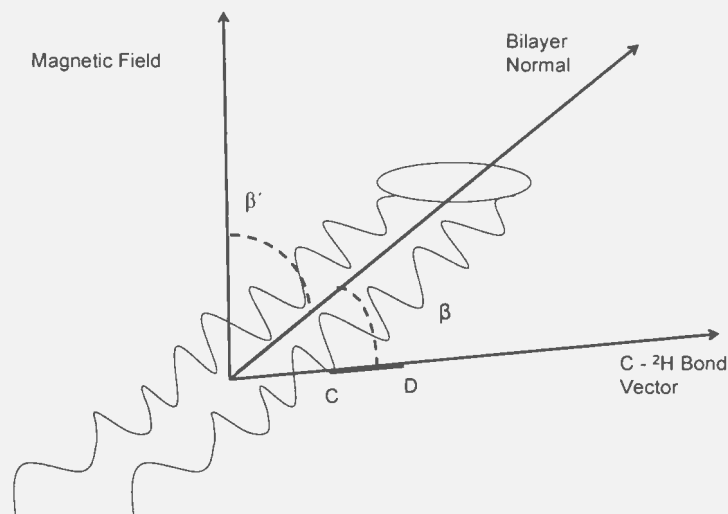


Figure 3.2: Schematic illustrating angles that modulate the quadrupole splitting.

is not applicable in the general case. In the presence of molecular motions the quadrupole interaction is modulated by molecular motions. The resulting expression for splittings is obtained by making a two-step transformation from a molecule-fixed principal axis frame to the laboratory frame. The first step is a transformation from the principal axis frame to a bilayer-fixed frame through Euler angles α, β and γ . The second step is a transformation from the bilayer fixed frame to the laboratory frame through Euler angles α', β' and γ' . In phospholipid bilayers, the bilayer normal is an axis of symmetry for motions and therefore the bilayer fixed frame is introduced so that one can take into account the effect of this molecular motion.

In the case of axially symmetric motions α', γ' and γ are arbitrary. They can be set to zero for simplification [11, 68]. The quadrupole splitting in the presence of molecular motions is then [11]

$$\omega_Q = \frac{3e^2qQ}{8\hbar} [(3 \cos^2 \beta' - 1) \langle (3 \cos^2 \beta - 1) + \eta \sin^2 \beta \cos 2\alpha \rangle] \quad (3.24)$$

where $\langle \dots \rangle$ denotes the time average over the duration of the ^2H NMR experiment. It is important to consider the time average as molecular reorientation may change α and β , while β' (the angle between the bilayer fixed frame and the laboratory frame, as shown in fig (3.2) can be taken as fixed for a particular molecule.

The above analysis applies to a specific orientation of the electric field gradient tensor. For a sample of multilamellar vesicles, bilayer normal orientations will be spherically distributed. Such a sample is known as ‘powder sample’. In this case, β' is not unique but takes all values. This results in superposition of quadrupole splitting doublets giving rise to powder spectral line shape similar to as shown in fig (3.2).

For an axially symmetric field gradient which has $\eta=0$, the quadrupole splitting is [11]

$$\omega_Q = \frac{3e^2qQ}{8\hbar} [(3 \cos^2 \beta' - 1) \langle (3 \cos^2 \beta - 1) \rangle]. \quad (3.25)$$

The quadrupole splitting is often expressed in terms of the orientational order parameter, S_{CD} , where S_{CD} is defined as

$$S_{CD} = \frac{1}{2} \langle (3 \cos^2 \beta - 1) \rangle. \quad (3.26)$$

The quadrupole splitting in terms of S_{CD} is then

$$\omega_Q = \frac{3e^2qQ}{4\hbar} (3 \cos^2 \beta' - 1) S_{CD}. \quad (3.27)$$

There is a significant difference between the spectrum from a liquid-crystalline phase bilayer and that of a gel phase bilayer. In the liquid crystal phase the motions are fast and axially symmetric and hence the spectra are relatively narrow [71]. As the sample passes through the main transition and enters the gel phase the motions are slower and no longer axially symmetric. The average S_{CD} indicates the amount of motion experienced by C- ^2H bond on the NMR time scale. The chain order in the

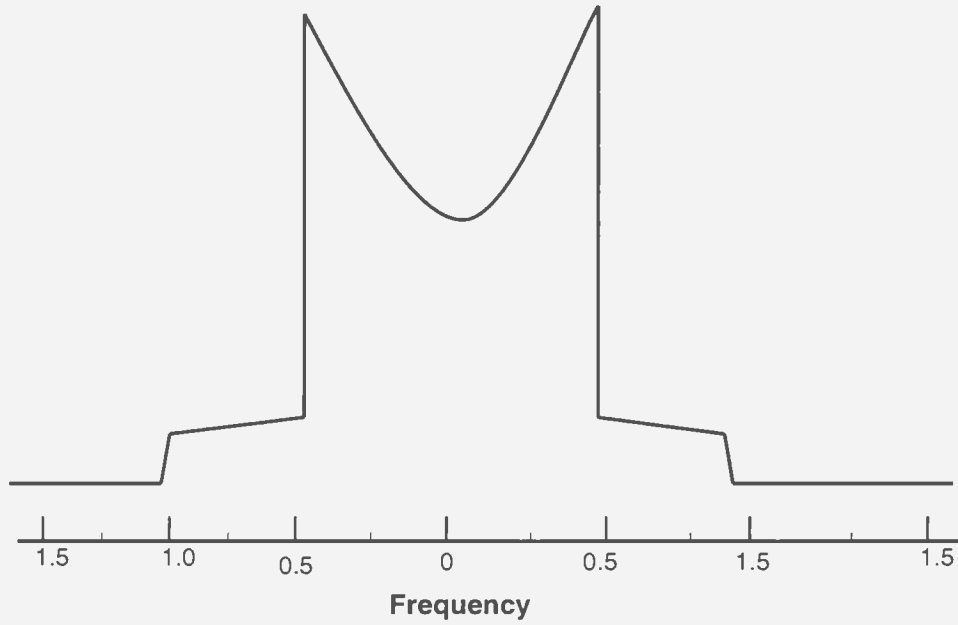


Figure 3.3: Spin-1 powder pattern line shape. The vertical axis is intensity.

gel phase increases as the amplitude of chain motions decreases. The commonly used method for spectrum analysis is ‘method of moments’. This method was used for analysis of experimental results in this work. In the case of ^2H NMR spectra such as the one shown in fig (3.3), the n^{th} spectral moment of the half spectrum is given by [11]

$$M_n = \frac{\int_0^\infty f(\omega)\omega^n d\omega}{\int_0^\infty f(\omega)d\omega} \quad (3.28)$$

where $f(\omega)$ is the spectral intensity as a function of frequency. The first spectral moment (M_1) gives the mean quadrupole splitting and is thus related to mean orientational order through [11]

$$M_1 = \frac{4\pi}{3\sqrt{3}} \langle (\omega_Q)^2 \rangle = \frac{\pi}{\sqrt{3}} \frac{e^2 q Q}{h} \langle S_{CD} \rangle. \quad (3.29)$$

The second spectral moment (M_2) gives the mean square quadrupole splitting by [11]

$$M_2 = \frac{4\pi^2}{5} \langle (\omega_Q)^2 \rangle. \quad (3.30)$$

Since the M_1 is directly proportional to $\langle S_{CD} \rangle$, it is useful in studying the temperature dependence of the orientational order parameter.

3.3 The Quadrupole Echo

The main pulse sequence used in this work was the quadrupole echo sequence [72]. It consists of two $\frac{\pi}{2}$ radio frequency pulses differing in phase by $\frac{\pi}{2}$ and separated by time τ as shown in fig (3.4). The quadrupole echo technique is used to avert the problem of dead time associated with the receiver of the spectrometer [72, 68, 73]. For a typical RF coil with $Q \approx 10^2$, it takes several μs for the signal due to a strong RF pulse to ring down to noise level. Reducing the Q of the coil to shorten the dead time is not acceptable as it reduces the the sensitivity of circuit. This problem is solved by applying a second pulse at time $t = \tau$ after the first pulse. The first pulse tips the net magnetization 90° away from the equilibrium position. The resulting precession of magnetization is called the FID. The FID decays at a characteristic time due to dephasing of nuclear spins that give rise to the net magnetic field. The second $\frac{\pi}{2}$ pulse of the quadrupole echo sequence is used to invert the accumulated phase and thus refocus the nuclear spins at time 2τ after the first pulse as shown in fig (3.4). If the pulse separation is chosen such that the echo will occur after the receiver dead time, an undistorted ^2H NMR spectrum is obtained. The amplitude of the echo observed at time 2τ depends on the molecular motions present during the time. The complete refocusing of deuteron magnetization is possible if the quadrupole interaction for each spin is unchanged during the 2τ duration of the experiment. Therefore the echo

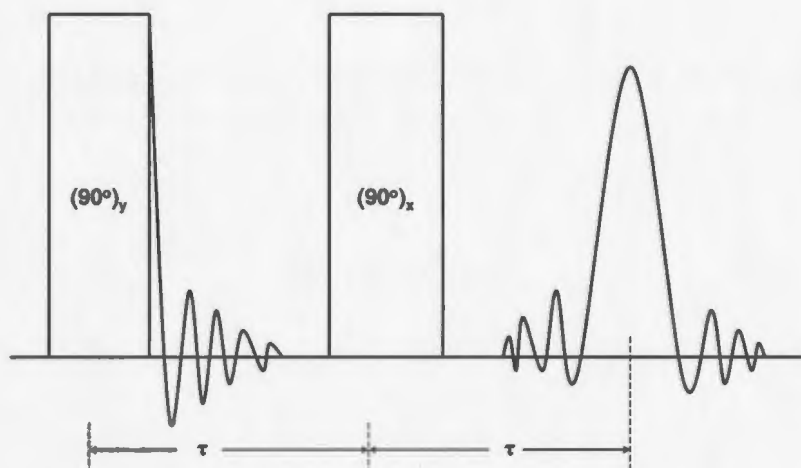


Figure 3.4: Quadrupole echo pulse sequence and the echo formation.

amplitude decreases with increasing pulse separation. The characteristic time for decay of the echo is denoted by T_{2e}^{QE} . This is used as a parameter to study the effect of temperature and pressure on the lipid bilayers [74].

The quantum mechanical treatment of the quadrupole echo is conveniently done in the terms of evolution of the density matrix [72, 68, 73] following the two pulses. The time dependent density matrix for a spin-1 system is expressed in the terms of nine $((2I+1)^2) 3 \times 3$ matrices in an operator space. The operator space \mathcal{O}_i has 9 dimensions. Its representation is given in table 3.1. We can express the relevant Hamiltonians in the terms of the basis operators \mathcal{O}_i [75]. The Zeeman Hamiltonian for a magnetic field applied along the z-axis can be given by

$$\hat{H}_z = -\sqrt{2}\omega_0\mathcal{O}_3. \quad (3.31)$$

The axially symmetric quadrupolar Hamiltonian is then given by

$$\hat{H}_Q = -\sqrt{\frac{2}{3}}\omega_Q\mathcal{O}_4. \quad (3.32)$$

For a magnetic field applied along the x-axis in the rotating frame, the Hamiltonian is

$$\hat{H}_x = -\sqrt{2}\omega_0\mathcal{O}_1. \quad (3.33)$$

For a magnetic field applied along the y-axis in the rotating frame, the Hamiltonian is

$$\hat{H}_y = -\sqrt{2}\omega_0\mathcal{O}_2. \quad (3.34)$$

The state of the system can be described by a set of coefficients $c_i(t)$ which define a time dependent vector

$$\vec{C} = (c_0(t), c_1(t), c_2(t), \dots) \quad (3.35)$$

in the space spanned by the basis operators \mathcal{O}_i .

The equilibrium state represented in terms of the spin system is this,

$$\vec{C} = (1, 0, 0, I_0, 0, 0, 0, 0). \quad (3.36)$$

If a radio frequency (RF) pulse of duration τ_y and strength ω_1 is applied along the y-axis in the rotating frame, the Hamiltonian \hat{H}_y is given by equation 3.34. The evolution of the state vector under the influence of \hat{H}_y is [75] determined from the equation of motion

$$\frac{dc_i(t)}{dt} = i \sum_q c_j(t) \text{Tr} \mathcal{O}_i [\mathcal{O}_j, \hat{H}_y]. \quad (3.37)$$

The time evolution of vector $\vec{C}(t)$ using the above equation of motion, is given as

$$\vec{C}(\tau_y) = (1, I_0 \sin \theta, 0, I_0 \cos \theta, 0, 0, 0, 0) \quad (3.38)$$

Table 3.1: 9 dimensional operator space.

$$\begin{aligned}
\mathcal{O}_1 &= \frac{1}{\sqrt{2}}I_x = \frac{1}{2} \begin{pmatrix} 0 & 1 & 0 \\ 1 & 0 & 1 \\ 0 & 1 & 0 \end{pmatrix} & \mathcal{O}_2 &= \frac{1}{\sqrt{2}}I_y = \frac{1}{2} \begin{pmatrix} 0 & -i & 0 \\ i & 0 & -i \\ 0 & i & 0 \end{pmatrix} \\
\mathcal{O}_3 &= \frac{1}{\sqrt{2}}I_z = \frac{1}{2} \begin{pmatrix} 1 & 0 & 0 \\ 0 & 0 & 0 \\ 0 & 0 & -1 \end{pmatrix} & \mathcal{O}_4 &= \frac{1}{\sqrt{6}}(3I_z^2 - 2) = \frac{1}{2} \begin{pmatrix} 1 & 0 & 0 \\ 0 & -2 & 0 \\ 0 & 0 & 1 \end{pmatrix} \\
\mathcal{O}_5 &= \frac{1}{\sqrt{2}}(I_x I_z - I_z I_x) = \frac{1}{2} \begin{pmatrix} 0 & 1 & 0 \\ 1 & 0 & -1 \\ 0 & -1 & 0 \end{pmatrix} & \mathcal{O}_6 &= \frac{1}{\sqrt{2}}(I_y I_z - I_z I_y) = \frac{1}{2} \begin{pmatrix} 0 & -i & 0 \\ i & 0 & i \\ 0 & -i & 0 \end{pmatrix} \\
\mathcal{O}_7 &= \frac{1}{\sqrt{2}}(I_x^2 - I_y^2) = \frac{1}{2} \begin{pmatrix} 0 & 0 & 1 \\ 0 & 0 & 0 \\ 1 & 0 & 0 \end{pmatrix} & \mathcal{O}_8 &= \frac{1}{\sqrt{2}}(I_x I_y - I_y I_x) = \frac{1}{2} \begin{pmatrix} 0 & 0 & -i \\ 0 & 0 & 0 \\ i & 0 & 0 \end{pmatrix} \\
\mathcal{O}_9 &= 1 = \frac{1}{2} \begin{pmatrix} 1 & 0 & 0 \\ 0 & 1 & 0 \\ 0 & 0 & 1 \end{pmatrix}
\end{aligned}$$

where $\theta = \omega_1 \tau_y$ represents the angle of rotation by RF pulse. If we apply a ' $\frac{\pi}{2}$ pulse', the magnitude and direction is such that $\theta = \frac{\pi}{2}$. At the end of a $\frac{\pi}{2}$ pulse the z-component of magnetization is thus rotated onto the x-axis

$$\vec{C}(\tau_y) = (1, I_0, 0, 0, 0, 0, 0, 0, 0). \quad (3.39)$$

Here, the transverse relaxation during the time of the pulse is neglected because we assume $\tau_\omega \ll T_2$, where T_2 is the transverse relaxation time characterizing the dephasing of the spins about the z-axis in the xy-plane of the rotating frame. After completion of the first pulse the evolution of the system for time τ is governed by quadrupolar interaction Hamiltonian (Eq (3.32)). This couples \mathcal{O}_1 with \mathcal{O}_6 , so that the state of the system at time τ after the first pulse is

$$\vec{C}(\tau_y + \tau) = (1, I_0 \cos \omega_Q \tau, 0, 0, 0, 0, I_0 \sin \omega_Q \tau, 0, 0). \quad (3.40)$$

The coil in the NMR experiment is perpendicular to the magnetic field H_0 and can detect only the transverse magnetization M_x and M_y . Thus after the $\frac{\pi}{2}$ pulse the

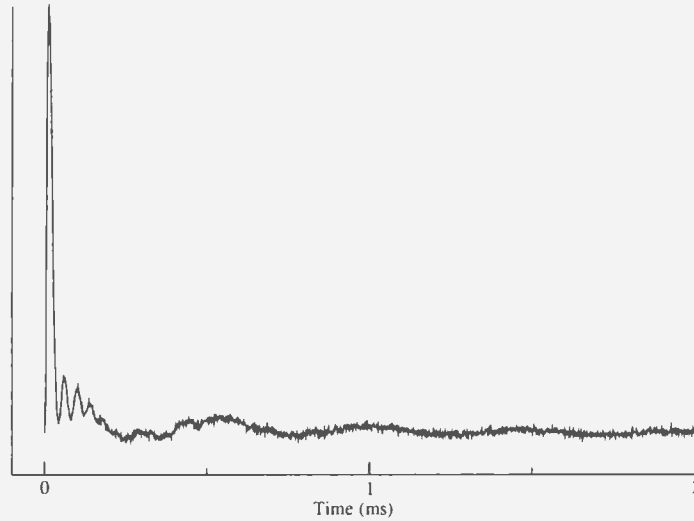


Figure 3.5: Example of Free Induction Decay, FID.

signal in the rotating frame is $\langle \hat{M}_x \rangle$, which is proportional to $\langle \hat{I}_x \rangle$

$$\langle \hat{I}_x \rangle = \sqrt{2}c_1 = \sqrt{2}I_0 \cos(\omega_Q \tau). \quad (3.41)$$

If we include the effects of the transverse relaxation, we get

$$\vec{C}(\tau_y + \tau) = (1, I_0 \cos(\omega_Q \tau) e^{-\frac{t}{T_2}}, 0, 0, 0, 0, I_0 \sin(\omega_Q \tau) e^{-\frac{t}{T_2}}, 0, 0) \quad (3.42)$$

where T_2 is the transverse relaxation time. This signal is called FID as shown in fig (3.5). The components with different ω_Q dephase and lead to decrease in the amplitude of FID.

The second radio frequency (RF) pulse, of duration τ_x and strength ω_2 , is applied along the x-axis following the first pulse after time t . It is described by the Hamiltonian of Eq (3.33),

$$\hat{H}_x = -\sqrt{2}\omega_0 \mathcal{O}_1.$$

After this second pulse, the system is allowed to evolve under the quadrupole Hamiltonian, Eq (3.32). Only C_1 and C_6 are not zero. Again H_Q couples \mathcal{O}_1 and \mathcal{O}_6 , but with different initial conditions. After time t following the second pulse,

$$c_1(t) = I_0(\cos(\omega_Q\tau) \cos(\omega_Q t) - \cos(2\phi) \sin(\omega_Q\tau) \sin(\omega_Q t))e^{-\frac{t}{T_2}} \quad (3.43)$$

$$c_6(t) = I_0(\cos(\omega_Q\tau) \sin(\omega_Q t) + \cos(2\phi) \sin(\omega_Q\tau) \cos(\omega_Q t))e^{-\frac{t}{T_2}}. \quad (3.44)$$

If the rotation resulting from the second pulse is $\pi/2$, this leads to

$$c_1(t) = I_0(\cos(\omega_Q(t - \tau)))e^{-\frac{t+\tau}{T_2}} \quad (3.45)$$

$$c_6(t) = I_0(\sin(\omega_Q(t - \tau)))e^{-\frac{t+\tau}{T_2}}. \quad (3.46)$$

The observed signal is proportional to the ensemble average of $c_1(t)$ over the spectrum of ω_Q 's. At time $t=\tau$, $c_1(t)$ becomes independent of ω_Q . The quadrupolar echo pulse sequence thus refocuses the FID completely at time 2τ (if relaxation is neglected). By choosing a τ longer than the receiver dead time, the distortion free spectrum is obtained by taking the Fourier transform of this time domain signal.

By using a quadrupole echo sequence

$$\left(\frac{\pi}{2}\right)_y - \tau - \left(\frac{\pi}{2}\right)_x - t -$$

and measuring the amplitude of quadrupole echo as a function of the separation time, τ , one can calculate transverse relaxation rate from

$$A(2\tau) = A(0)e^{-\frac{2\tau}{T_2^{QE}}} \quad (3.47)$$

where we use T_2^{QE} to distinguish this decay from the decay of other modes.

3.4 Quadrupole Carr-Purcell-Meiboom-Gill Echo Train

The state of the system at $t=\tau$ after the second pulse, that is after the pulse sequence $(\frac{\pi}{2})_y - \tau - (\frac{\pi}{2})_x - t-$, is the same, if we neglect spin-lattice relaxation, as the state of the system just after the $(\frac{\pi}{2})_y$ except for a decrease in c_1 by a factor of $e^{-\frac{2\tau}{T_2^{QE}}}$, such that

$$\vec{C}(2\tau) = (1, I_0 e^{-\frac{2\tau}{T_2^{QE}}}, 0, 0, 0, 0, 0, 0, 0). \quad (3.48)$$

If we repeat the $\tau - (\frac{\pi}{2})_x - \tau$ part of the sequence again, the state of the system at $t=4\tau$ is

$$\vec{C}(4\tau) = (1, I_0 e^{-\frac{4\tau}{T_2^{QE}}}, 0, 0, 0, 0, 0, 0, 0). \quad (3.49)$$

By using the pulse sequence

$$(\frac{\pi}{2})_y - (\tau - (\frac{\pi}{2})_x - t-)_n$$

and measuring the amplitudes of the signal at times $t = 2n\tau$, one can obtain in a single experiment, a series of amplitude which give us T_2^{q-CPMG} through,

$$A(2n\tau) = A(0) e^{-\frac{2n\tau}{T_2^{q-CPMG}}}. \quad (3.50)$$

This is called the Carr-Purcell-Meiboom-Gill (CPMG) echo train [76]. This was modified by Bloom [76] to be suitable for a spin-1 system in order to study adiabatic motions. This pulse sequence is also referred as MW-4 sequence by Blicharski and others [13].

The q-CPMG can be used to separate the contributions of slow and fast motions to echo decay rate. The contributions to echo decay rate can be approximated as a superposition of effects from two classes, fast and slow, of motions. The result is

$$R = \frac{1}{T_{2e}^{q-CPMG}} = \sum_i M_2^i \tau_i + \sum_j M_2^j \frac{\tau^2}{3\tau_j}, \quad (3.51)$$

where τ is the pulse separation, $\tau_i \ll \tau$ and $\tau_j \gg \tau$ are the correlation times of fast and slow motions respectively. In the above equation, the contributions of the slow motions (long correlation times) to echo decay rate are dependent on pulse separation τ , and are reduced by a factor of $\frac{\tau^2}{3\tau_j^2}$. This suggests, q-CPMG can be used to suppress the contribution of slow motions to echo decay by selecting an appropriate pulse separation τ . In this case the q-CPMG pulse sequence acts as a low pass filter.

3.5 Molecular Motions and Quadrupolar Relaxation

The quadrupole echo sequence consists of two $\pi/2$ radio frequency pulses separated by an interval τ . The quadrupole echo is formed at time 2τ . The deuteron quadrupole Hamiltonian is orientation dependent. Motions that change orientation of the average electric field gradient tensor in the principal axis system with characteristic times in the range of NMR experiment time scale, reduce the amplitude of the quadrupole echo as shown in fig (3.6). The characteristic time for decay of the quadrupole echo with increasing 2τ is T_2^{QE} .

As discussed in chapter two, there are many types of motions which may affect the quadrupole echo decay. These include bilayer surface undulation [77], diffusion along the curved surface [12], collective bilayer modes [14], intermolecular motions (*chain fluctuation and molecular rotations*) and intramolecular motions (*trans-gauche isomerization*) [9]. Orders of magnitude of correlation times for these motions in the liquid crystalline phase and gel phase have been estimated [77, 73]. Approximate

correlation times for some of these motions in the liquid crystalline phase are given in table 3.2.

Table 3.2: Correlation times, τ_{ci} for the motions in the liquid crystalline phase.

Motions	τ_{ci}
Bilayer undulations [73, 77]	100 μ s
Lateral diffusion [73, 12]	100ms
Collective bilayer modes [14]	10 μ s
Chain rotation and fluctuation [9]	10 ⁻⁸ s
trans-gauche isomerization [9]	10 ⁻¹⁰ s

A given motion, j can be characterized by a correlation time τ_{cj} . The extent to which this motion modulates the quadrupole Hamiltonian can be characterized by the second moment, ΔM_2 , of the modulation. For motions which give rise to motional narrowing

$$\Delta M_2 = M_2 - M_{2r} \quad (3.52)$$

where M_2 is the full second moment of the interaction and M_{2r} is the residue second moment of motionally narrowed spectrum [78].

If the Larmor Frequency is modulated by a set of independent, adiabatic motions labelled by index $i=1,2,3,\dots$, each motion is characterized by correlation time τ_i and range of frequencies having second moments M_2^i respectively, such that $M_2^i \tau_i^2 \ll 1$. The relaxation rate is then the sum of the rates due to the different modes such that,

$$R = \sum_i R_i. \quad (3.53)$$

The classification of motions as fast or slow motion depends upon the relationship between correlation time, τ_c , and the reduction in the apparent second moment ΔM_2 .

For fast motions, the correlation times are related to ΔM_2 by $\Delta M_2 \cdot \tau_c^2 \ll 1$, while those for slow motion are related by $\Delta M_2 \cdot \tau_c^2 \gg 1$. The quadrupole relaxation is characterized by the effective transverse relaxation time, T_{2e}^{QE} , the inverse of the transverse relaxation rate averaged over all deuterons in a given sample.

$$\frac{1}{T_{2e}^{QE}} = R \quad (3.54)$$

In 2H NMR the dominant interaction responsible for T_{2e}^{QE} is the quadrupole interaction.

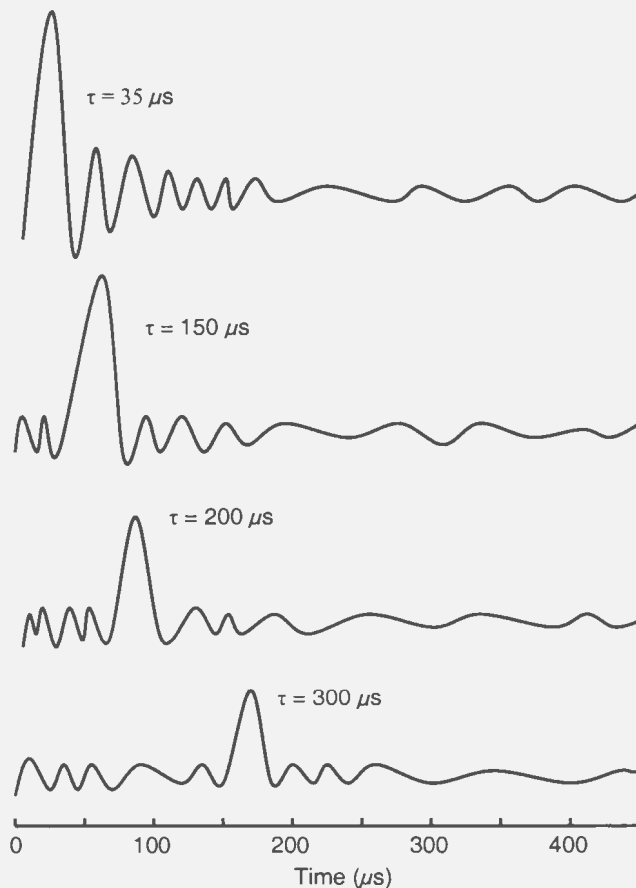


Figure 3.6: Quadrupole echo intensity obtained using quadrupole echo pulse sequences: Variation of the echo intensity with τ is used to measure T_2^{QE} .

Fast Motion:

In the short correlation time limit, the general theory of motional averaging leads to a result for isotropic motions which is essentially independent of the details of the motion for large class of systems [78, 79]. For fast motions, which contributes to motional narrowing, the general theory of motional averaging gives [78, 12]

$$R_i = \Delta M_2^i \tau_{ci}. \quad (3.55)$$

The decay rate is proportional to correlation time for fast motions.

Slow Motion:

The result obtained in this limit depends on the nature of the motion and also on how the measurements are made. In a two-pulse echo experiment in which the separation, τ , of the pulses is sufficiently large to satisfy $\Delta M_2 \cdot \tau_c^2 \gg 1$, and in which the random rotational jumps of the molecule are large, the contributions to relaxation rate, R , results is given as

$$\frac{1}{R} = T_{2e} = p\tau_c \quad (3.56)$$

where $p \geq 1$ [78]. The decay rate is inversely proportional to correlation time for slow motions.

Intermediate motion:

Based on the above, we expect for the slow motions $R \propto \frac{1}{\tau_c}$ and for fast motions $R \propto \tau_c$. In the case of the intermediate motion situation $\Delta M_2 \cdot \tau_c^2 \approx 1$, and the value of T_{2e} must go through minimum for intermediate values of τ_c . Pauls et al. [78] propose, for the intermediate τ_c regime,

$$R = \frac{1}{T_{2e}} = \frac{\Delta M_2 \cdot \tau_c}{1 + p\Delta M_2 \cdot \tau_c^2} \quad (3.57)$$

which reduces to expression (3.55) for short τ_c and to (3.57) for long τ_c . In the liquid crystalline phase, away from the phase transition, slow motions contribute significantly to relaxation. These motions may include bilayer surface undulations, lateral diffusion and collective lipid motions [14, 12]. The contributions to echo decay rate, R , are inversely proportional to correlation times of these slow motions as discussed above. There are fast motions too like chain fluctuation, molecular rotations and *trans-gauche* isomerization, their contributions to echo decay rate are proportional to their correlation times. As a result, the contributions from slow and fast motions sum to a constant and T_{2e} remains relatively independent of temperature in the liquid crystal phase.

As the temperature decreases below the main transition the correlation times of all motions gets longer (all the motions slow down). The bilayer surface undulations, lateral diffusion and collective lipid motions slow down and their correlation times increase. They freeze out on the NMR time scale of the present experiment and do not affect the echo decay rate. Just below the main transition, the correlation times of the some faster motions, possibly molecular rotations, become comparable to the pulse separation so T_{2e} reaches a minimum. The correlations times of chain fluctuations and molecular rotations increase, and they enter the slow motion regime. Further decreases in temperature (increases in τ_c) results in a increase in T_{2e} . The echo decay time, T_{2e} , increases with a decrease in temperature until it reaches a maximum in the gel phase. On cooling below this temperature, the remaining fast motion is *trans-gauche* isomerization and it is expected to contribute significantly to T_{2e} . This leads to a decrease in T_{2e} after it passes through a maximum. At still lower temperature *trans-gauche* isomerization slows down with further decrease in temperature and leads to a second minimum in the temperature vs. T_{2e} curve.

In the subsequent chapters, the effect of pressure on DPPC- d_{62} and DPPG- d_{62} lipid

bilayers will be probed by measuring and comparing the 2H transverse relaxation time for the samples at ambient pressure and under high pressure.

Chapter 4

Experimental Setup

All spectra for the variable pressure experiments were obtained using a 3.5T superconducting magnet (Nalorac Cryogenics, Martinez, CA), in conjunction with a locally constructed solid state spectrometer [80] and a locally constructed high pressure cell [81].

4.1 Spectrometer

The wide line spectrometer is made up of components including a 1 KW radio transmitter, quadrature detection section with 12-bit digitizing oscilloscope, a computer for data collection and a pulse sequence programmer. A block diagram of the 3.5T spectrometer is shown in fig 4.1. The general operation is described briefly below.

The frequency synthesizer provides signals with frequencies 33.2 MHz (*local oscillator signal*) and 10 MHz (*intermediate frequency*). The 10.0 MHz signal is fed to a phase splitter and edited into pulses with phases of 0° , 90° , 180° and 270° in the pulse generator, under control by the pulse programmer (which controls the output and the duration (t_p)). The 10 MHz pulses are sent to mixers contained in a

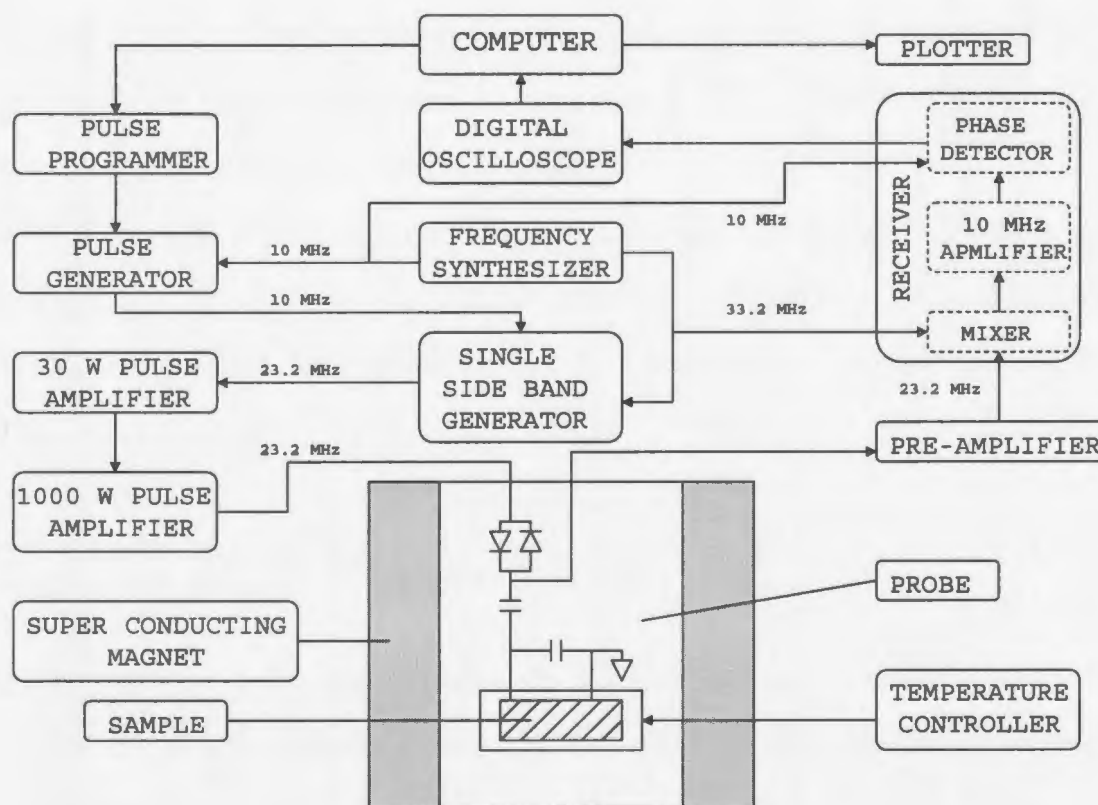


Figure 4.1: Block diagram of NMR spectrometer

single-side-band generator. The 33.2 MHz signal is sent to both the receiver and the single-side-band generator, where it is mixed with the 10.0 MHz signal to generate pulses at the deuteron resonance frequency of 23.2 MHz. These pulses are then sent, via a pulse amplifier, to a home built transmitter amplifier. The 1 KW amplifier transmits short pulses at the resonance frequency with an amplitude of about 275 volts into the RF coil (Probe). The spin system (sample) produces a weak signal in response to a pair of high power pulses through the coil. This signal is amplified in the preamplifier and then fed into the receiver system which contains a mixer, 10.0 MHz amplifier, and a quadrature detector. The mixer mixes the 23.2 MHz carrier wave, which is modulated by the FID, with the 33.2 MHz local oscillator signal from

the frequency synthesizer and generates a 10.0 MHz carrier wave modulated by the FID signal. This is sent to the quadrature detector which separates the real and imaginary parts of the FID signal by comparing the FID signal with the reference signal coming from the frequency synthesizer.

The FID signals are then digitized, by the digital oscilloscope, with a desired sampling rate. To begin the Fourier transform from the top of echo, it is necessary to shift the points in the accumulated signal by a fraction of the dwell time [11]. The method of oversampling was also used [82, 83] to improve the signal to noise ratio.

4.2 The High Pressure Probe

The high-pressure probe used for this work was designed by Dr. B. Bonev [81]. It is capable of measurements between -30°C to 80°C (For present work we used the temperature range -25°C to 60°C) at pressures up to 270 MPa. A drawing of the high pressure probe is shown in the fig 4.2.

A hydraulic jack was used to pressurize the system using AW ISO 32 grade pressure transmitting fluid . A pressure stabilizer with a temperature controller was used to maintain the constant pressure in the system. When the temperature of the sample chamber was increased (decreased), the temperature of the pressure stabilizer was decreased (increased). This stabilized the sample chamber pressure, which was monitored by Bourdon type pressure gauge. The temperature of the sample was controlled using a PID temperature controller. To reach temperatures below room temperature, the sample chamber was cooled using nitrogen as exchange gas. The nitrogen gas was blown through copper piping, which was submerged in liquid nitrogen. This gas passed through tubing coiled within the walls of the oven around the sample.

The sequence included a 0.1 s pre-sequence interval and a 0.4 s recovery to allow the sample to completely equilibrate before the next pulse. Spectra were acquired by averaging 4000 transient to obtain adequate signal to noise ratio. The FID decays were phased shifted and contracted [83] giving an effective dwell time of 4 μ s for the liquid crystalline phase and 2 μ s for the gel phase. Frequency spectra were obtained by Fourier transforming the time domain data. For echo decay (T_2^{QE}) measurements, pulse separations were varied from 35 μ s to 500 μ s.

The experimental parameters for the q-CPMG experiments differ for the liquid crystalline and gel phases. In the liquid crystalline phase, we obtained 8 to 40 echoes using pulse separation times, τ , between 0.075 ms to 0.500 ms. In the gel phase, we obtained 16 to 40 echoes using pulse separation times between 0.030 ms to 0.105 ms. During q-CPMG experiments, the dwell time in liquid crystalline phase was 5 μ s and in gel phase 2 μ s. 2000 scans were collected in both cases.

Data were collected on a 386 PC. A Turbo C program was used for the data analysis. A microprocessor based, PID temperature controller having resolution of $\pm 0.1^\circ\text{C}$, was used to control the temperature around the sample. A thermocouple was used as sensor for temperature measurement. Experiments were carried out for series of temperatures starting at 60°C to -25°C , descending in steps of 3°C (2°C near the main phase transition), and 5°C steps below 0°C to -25°C . Samples were allowed to reach thermal equilibrium by allowing it to cool down for one and half hours before starting each experiment.

4.4 Sample Preparation

All deuterated lipids were purchased from Avanti Polar Lipids (Birmingham, AL) in powder form. Phospholipids were used without further purification. For preparing

multilamellar vesicles (MLV), first any solvent was removed from the powder sample by vacuum-drying overnight. 25-30 mg of lipid was then dissolved in ethanol in a round bottom flask. The ethanol was evaporated by heating the contents at 40°C and then further vacuum-dried overnight. This deposited a layer of dried lipid on the inner surface of the flask, which facilitated reproducible hydration of the sample. The sample was hydrated using approximately 200 μ l of 0.1 M phosphate buffer having pH 6.9-7.0. The contents in the round bottom flask were rotated while maintained above the transition temperature of the lipid for 25 minutes.

To maximize the amount of sample in the sample tube, samples were centrifuged for a minute so that excess buffer could be removed without removing too much lipid. Following preparation, samples were heat sealed in polyethylene containers which were made by cutting an appropriately sized portion of polyethylene pipette, heat sealing one end, and putting sample into the half closed container. The other end was then heat sealed to make a pillow. These containers were used because standard NMR glass tubes can not transmit pressure to the sample.

Chapter 5

Results and Discussion

Lipid bilayers are complex molecular systems, with a variety of motions characterized by different correlation times τ_c . There are fast motions like chain fluctuation, molecular rotations, *trans-gauche* isomerization [9] and slow motions like undulation, diffusion along the curved surface, and collective bilayer modes. Echo decay times depend on how much motions modulate the deuterium quadrupole Hamiltonian, which is orientation dependent. Solid state ^2H NMR is a very important tool to study different ordered phases of phospholipid systems. The present work was done to study the effect of pressure on these motions, in particular fast motions that persist in ordered phase phospholipids. The experiments were conducted at different temperatures from 60°C to -26°C , at ambient pressure and elevated pressures of 85 MPa, 196.1 MPa. ^2H NMR spectra and echo decay times were obtained and are interpreted in terms of fast and slow motions. High pressure studies have provided evidence of many pressure induced gel phases including GIII, GIV, GV, $G_{interdigitated}$. These are in addition to well known ambient pressure gel phases $P_{\beta'}$, $L_{\beta'}$ and liquid crystal phase, L_{α} . The incubation of samples at low temperature for long times can also induce the subgel phase, L_C . During experiments and discussion, no attempt is made to explain the

structure and properties of these phases. Wong et al. [6] have done extensive work on pressure induced gel phases and have discussed the structure of the five pressure induced gel phases which are encountered during these experiments. ^2H NMR was used to locate the boundaries between the different ordered phases of phospholipids by Driscoll et al. [7].

5.1 Temperature Dependence of DPPC- d_{62} ^2H NMR Spectra at Ambient Pressure and High pressure

5.1.1 DPPC- d_{62} at Ambient Pressure

Fig (5.1) shows the temperature dependence of deuterium NMR spectra for DPPC- d_{62} at ambient pressure. The spectra show a clear main transition from a high temperature liquid crystalline phase to more ordered a low temperature gel phase at 36°C . Above this temperature the lipid chains are experiencing fast axially symmetric motions, so spectra are the superpositions of Pake doublets. The spectra below the main phase transition temperature are characteristic of gel phase. They indicate slow axially asymmetric motions of lipid chains. $L_{\beta'}$ phase and $P_{\beta'}$ phase are not distinguished here as it is very difficult to distinguish them using ^2H NMR only.

There are some common features of all gel phase ^2H spectra as there is intensity at ± 63 kHz. The intensity of this component varies with changes in temperature or pressure. In fig (5.1), between the temperature 3°C and -1°C there is growth in intensity of ± 63 kHz component, which means there is a gradual transition from the ordinary gel phase to a more ordered gel phase. This new phase is know as the

subgel phase and is denoted by L_C by Driscoll et al. [7]. L_C is also reported by other research groups, in model phospholipid bilayers at ambient pressure. The formation of this phase requires incubation of the sample at low temperature, around 0°C in this case. To form a subgel phase, the temperature must be low enough for the subgel phase to be thermodynamically stable but not so low as to freeze out motions that allow rearrangement of lipid in to the ordered phase. The observed phases DPPC- d_{62}

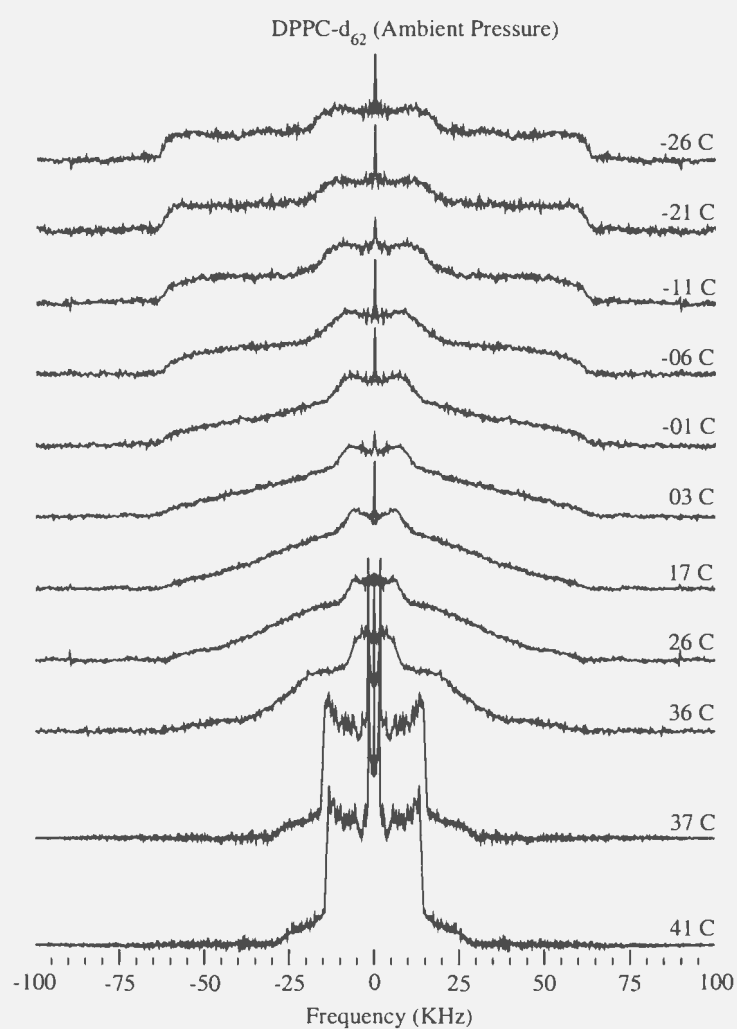


Figure 5.1: ^2H NMR spectra of Dipalmitoyl-*sn*-Glycero-3-Phosphocholine(DPPC- d_{62}) at ambient pressure and at selected temperatures.

Table 5.1: DPPC- d_{62} phases at ambient pressure.

Temperature	50°C to 37°C	36°C to 03°C	-01°C to -26°C
Phases	Liquid crystal Phase L_{α}	Gel phase $L_{\beta'}$	Subgel phase L_C

at ambient pressure are summarized in the table 5.1.

5.1.2 DPPC- d_{62} at High Pressure

Deuterium NMR spectra for perdeuterated DPPC- d_{62} were also obtained at elevated pressures of 85 MPa and 196.1 MPa. Temperature was varied while keeping the pressure constant at 85 MPa and 196.1 MPa. Fig (5.2) shows deuterium ^2H NMR spectra for DPPC- d_{62} at selected temperatures and a constant pressure of 85 MPa. The main phase transition from the high temperature liquid crystalline phase to the lower temperature gel phase takes place at 57°C. The elevation in main phase transition temperature is consistent with previous work done in this lab [50]. Between temperatures -1°C to -11°C there is a gradual change in the spectrum as intensity at ± 63 kHz gradually increases. This reflects the phase transition from ordinary gel phase $L_{\beta'}$ to the subgel phase L_C . The ^2H NMR spectra of DPPC- d_{62} at ambient pressure and 85 MPa are qualitatively similar, aside from the shift in temperature. The temperature ranges for observed phases, for DPPC- d_{62} at 85 MPa are summarized in the table 5.2.

Another set of isobaric spectra for DPPC- d_{62} were obtained at a pressure of 196.1 MPa. These are shown in fig (5.3). The main transition temperature at this pressure

Table 5.2: DPPC- d_{62} phases at 85 MPa.

Temperature	60°C to 57°C	56°C to 11°C	7°C to -26°C
Phases	Liquid crystal Phase L_{α}	Gel phase $L_{\beta'}$	Subgel phase L_C

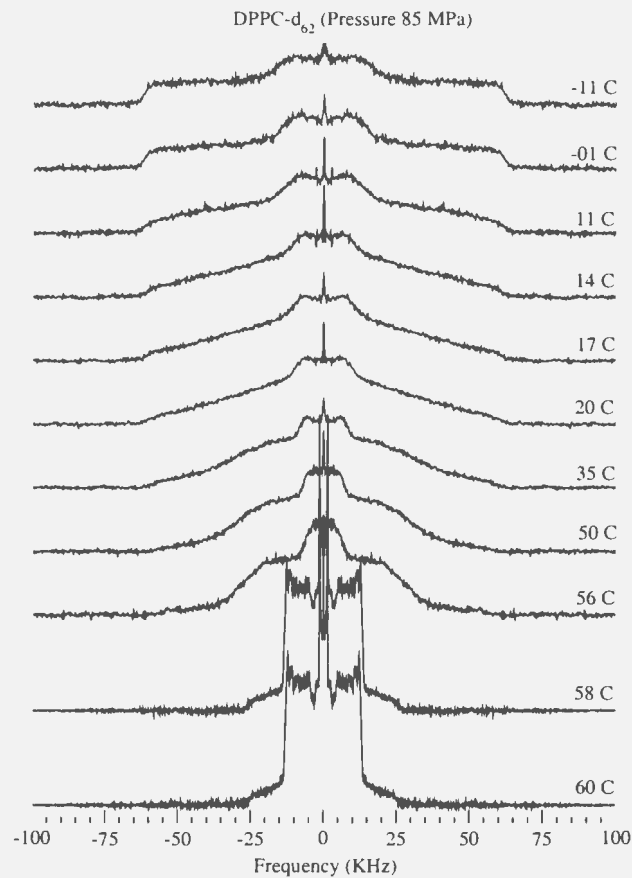


Figure 5.2: ^2H NMR spectra of Dipalmitoyl-*sn*-Glycero-3-Phosphocholine(DPPC- d_{62}) at 85 MPa pressure and at selected temperatures.

is quite high and was not observed during the present set of experiments, for which the maximum temperature was 60°C . As shown in fig (5.3), the spectrum at 60°C is quite different from the ordinary gel phase spectrum at ambient pressure. This spectrum is characteristic of the interdigitated gel phase which denoted as $G_{interdigitated}$. This suggests the liquid phase to gel phase transition at ambient pressure is replaced by a liquid crystal phase to interdigitated gel phase, $G_{interdigitated}$ near 200 MPa [7, 50]. The interdigitated gel phase has been reported by other workers using deuterium NMR and using different techniques like neutron diffraction [34], and Fourier-transform

infrared spectroscopy [25]. In this phase the chains from opposite sides of the bilayer

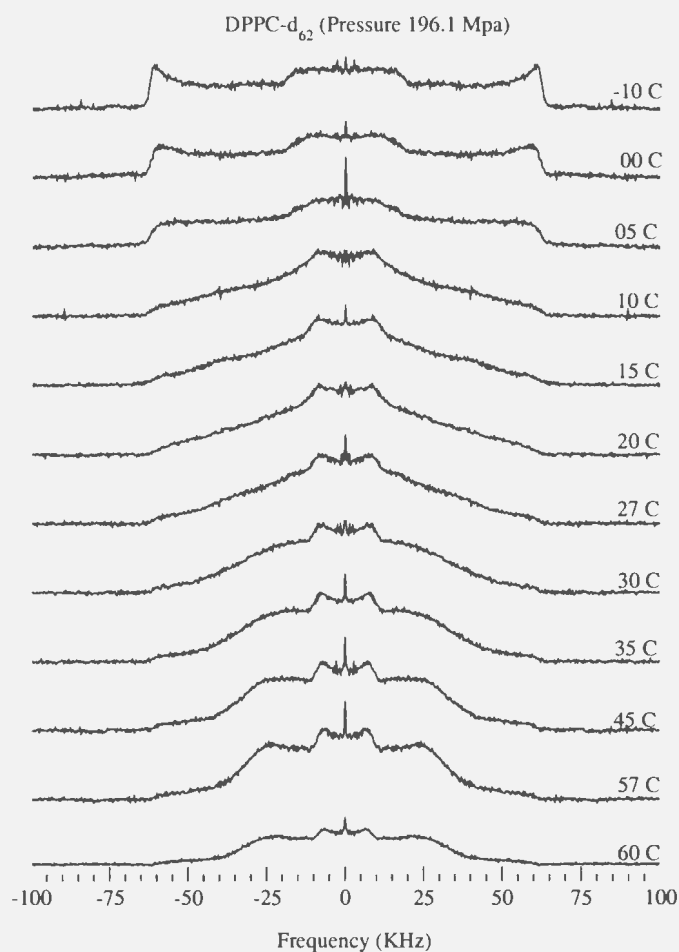


Figure 5.3: ^2H NMR spectra of Dipalmitoyl-*sn*-Glycero-3-Phosphocholine(DPPC- d_{62}) at 196.1 MPa pressure and at selected temperatures.

(monolayers) interpenetrate. This restricts the motion of methyl ends of the chains. Between 30°C to 27°C, the spectra change from being characteristic of $G_{interdigitated}$ and likely reflect another gel phase GIII. This phase has been reported by Peng et al. [41]. The structure of the GIII phase has been described by Wong et al. [6]. In GIII, chains are fully extended and tilted with respect to bilayer normal and the inter chain orientations are highly ordered. The spectra in fig. (5.3) indicate that the GIII

phase exists between temperatures 27°C to 10°C at 196.1 MPa for DPPC- d_{62} . Below this temperature, the spectrum becomes more axially symmetric with splittings corresponding to the full quadrupole interaction. The central component due to methyl group deuterons, between ± 20 kHz is narrowed by rotation about the symmetry axis of methyl group. The observation of the full quadrupole interaction indicates that CD bonds are static on NMR time scale. This highly ordered phase is denoted as phase X [7]. The temperature ranges of observed phases, for DPPC- d_{62} at 196.1 MPa are summarized in table 5.3.

Table 5.3: DPPC- d_{62} phases at 196.1 MPa.

Temperature	60°C to 30°C	27° to 10°C	5°C to -15°C
Phases	Interdigitated gel $G_{interdigitated}$	Gel phase GIII	X

5.2 Temperature Dependence of First Moments of DPPC- d_{62}

The moments of ^2H NMR spectra provide a complete description of the distribution of quadrupole splittings [11]. For spectra with line shape $f(\omega)$, the n^{th} moment of the spectrum is given by [11], [71], [75]

$$M_n = \frac{\int_{-\infty}^{\infty} f(\omega)\omega^n d\omega}{\int_{-\infty}^{\infty} f(\omega)d\omega} \quad (5.1)$$

where $\omega = 0$ corresponds to the Larmor frequency ω_0 . As the first order quadrupolar powder spectrum is symmetric around ω_0 , all the odd moments of ^2H NMR spectrum vanish. For this reason spectral moments are normally defined for positive frequencies only to give,

$$M_n = \frac{\int_0^\infty f(\omega)\omega^n d\omega}{\int_0^\infty f(\omega)d\omega}. \quad (5.2)$$

Using the above equation, the first spectral moment (M_1) gives the mean quadrupole splitting and is thus related to mean orientational order [11]. The second spectral moment (M_2) gives the mean square quadrupole splitting [11].

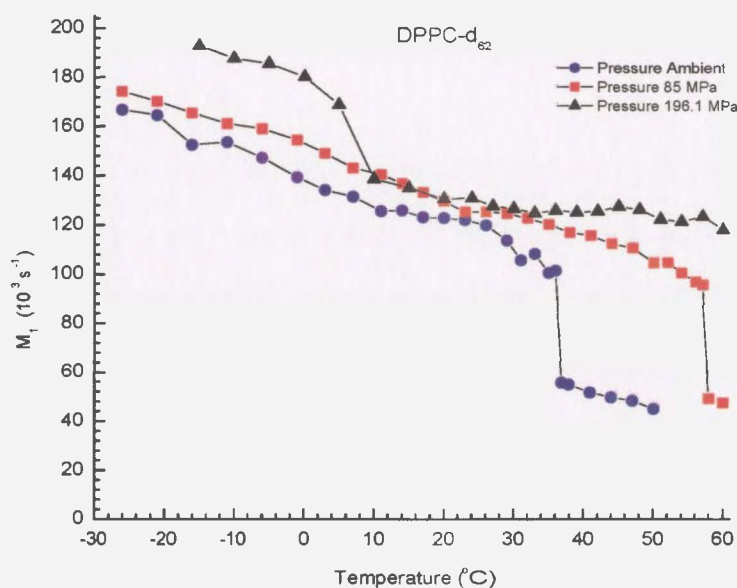


Figure 5.4: First moments for DPPC- d_{62} at ambient pressure (circle), 85 MPa (square) and 196.1 MPa (triangle).

First spectral moments for DPPC- d_{62} at ambient and elevated pressures are shown in fig (5.4). These were obtained from the spectra shown in figs (5.1), (5.2), and (5.3). There is sharp jump in the first moment as the phase changes from liquid crystalline to the more ordered gel phase.

The first moments analysis illustrates the phase changes described in the last sections. The main phase transition at ambient pressure takes place at 37°C. At a

pressure of 85 MPa, the main transition was shifted to 57°C. The main transition at 196.1 MPa is not seen in fig (5.4), as it is beyond the range of the present set of experiments. In the gel phase, as the temperature is lowered, first moments increase because the lipids molecules are getting more ordered. At 196.1 MPa there is a prominent change in first moment at 5°C. As shown in the previous section, there is a phase change at this temperature from GIII to phase X. This supports the observation of such a phase change of 85 MPa described in the previous section. Not all the ordered-ordered phase transitions discussed in the last section are apparent from temperature dependence of M_1 .

An indication of the uncertainty can be obtained by comparing separate runs on a given sample and by observing the scatter of M_1 results about a smooth curve at temperatures far from a transition. Based on these considerations, the uncertainty in M_1 appears to be less than $\pm 5\%$ for typical spectra obtained in this work.

5.3 Temperature Dependence of DPPG- d_{62} ^2H NMR Spectra at Ambient Pressure and High pressure

^2H NMR experiments were also performed on DPPG- d_{62} at ambient pressure and elevated pressures of 85 MPa and 196.1 MPa for a wide range of temperature (60°C to -26°C). Spectra at selected temperatures for DPPG- d_{62} at ambient pressure are shown in fig (5.5). At ambient pressure DPPG- d_{62} undergoes the main phase transition from liquid crystalline phase to ordered gel phase at 35°C.

Below this temperature, the shape of the spectrum changes gradually in the gel phase. Around 7°C, there is a gradual increase in the intensity at ± 63 kHz, which is

pressure of 85 MPa, the main transition was shifted to 57°C. The main transition at 196.1 MPa is not seen in fig (5.4), as it is beyond the range of the present set of experiments. In the gel phase, as the temperature is lowered, first moments increase because the lipids molecules are getting more ordered. At 196.1 MPa there is a prominent change in first moment at 5°C. As shown in the previous section, there is a phase change at this temperature from GIII to phase X. This supports the observation of such a phase change of 85 MPa described in the previous section. Not all the ordered-ordered phase transitions discussed in the last section are apparent from temperature dependence of M_1 .

An indication of the uncertainty can be obtained by comparing separate runs on a given sample and by observing the scatter of M_1 results about a smooth curve at temperatures far from a transition. Based on these considerations, the uncertainty in M_1 appears to be less than $\pm 5\%$ for typical spectra obtained in this work.

5.3 Temperature Dependence of DPPG- d_{62} ^2H NMR Spectra at Ambient Pressure and High pressure

^2H NMR experiments were also performed on DPPG- d_{62} at ambient pressure and elevated pressures of 85 MPa and 196.1 MPa for a wide range of temperature (60°C to -26°C). Spectra at selected temperatures for DPPG- d_{62} at ambient pressure are shown in fig (5.5). At ambient pressure DPPG- d_{62} undergoes the main phase transition from liquid crystalline phase to ordered gel phase at 35°C.

Below this temperature, the shape of the spectrum changes gradually in the gel phase. Around 7°C, there is a gradual increase in the intensity at ± 63 kHz, which is

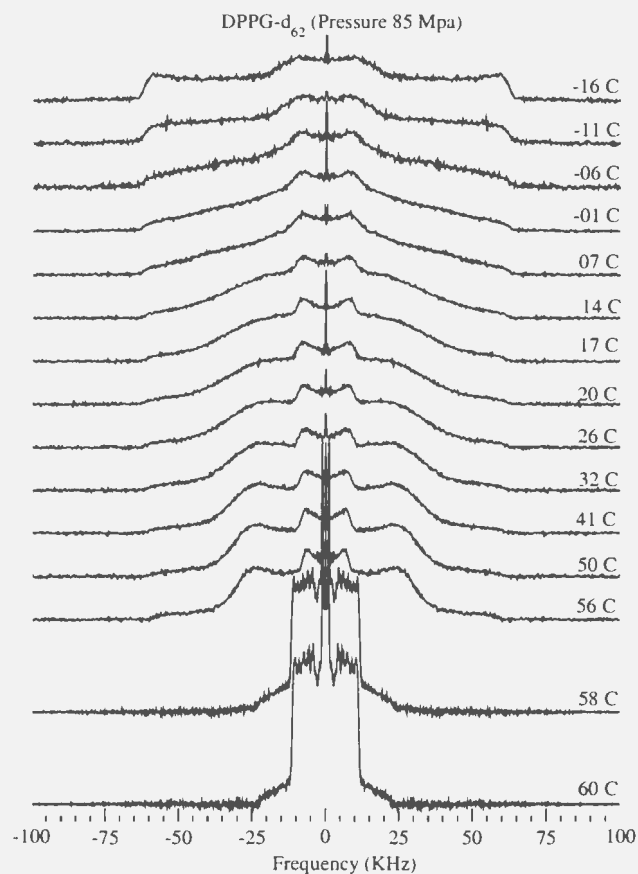


Figure 5.6: ^2H NMR spectra of Dipalmitoyl-sn-Glycero-3- [Phospho-rac-(1-glycerol)](DPPG- d_{62}) at 85 MPa pressure and at selected temperatures.

the characteristic spectrum of L_{β}' , but is similar to the DPPC- d_{62} spectrum identified as being characteristic of interdigitated gel phase at higher pressure. Therefore, it appears DPPG- d_{62} at 85 MPa undergoes a phase transition from the liquid crystalline phase directly into the more ordered interdigitated gel phase, $G_{interdigitated}$. Between 26°C and 17°C, there is gradual change in the spectra from one that is characteristic of $G_{interdigitated}$ to one that is characteristic of another gel phase GIII. On further cooling, there is a gradual change in the spectra until there is prominent increase in intensity at ± 63 kHz between 7°C and -6°C. This indicates an order-order phase

transition from GIII to an immobilized lipid phase X.

The sequence of phase transitions for DPPG- d_{62} at 85 MPa is liquid crystal phase, interdigitated gel phase, GIII, and phase X.

The phase behavior of DPPG- d_{62} at 196.1 MPa as shown in fig. (5.7), is quite similar to that of DPPC- d_{62} at same pressure. The main transition temperature is higher than 60°C, so at 60°C DPPG- d_{62} is in the interdigitated gel phase, $G_{interdigitated}$. From 60°C to 30°C there is gradual change in the spectrum. Between 30°C and 27°C the spectra become characteristic of the GIII phase.

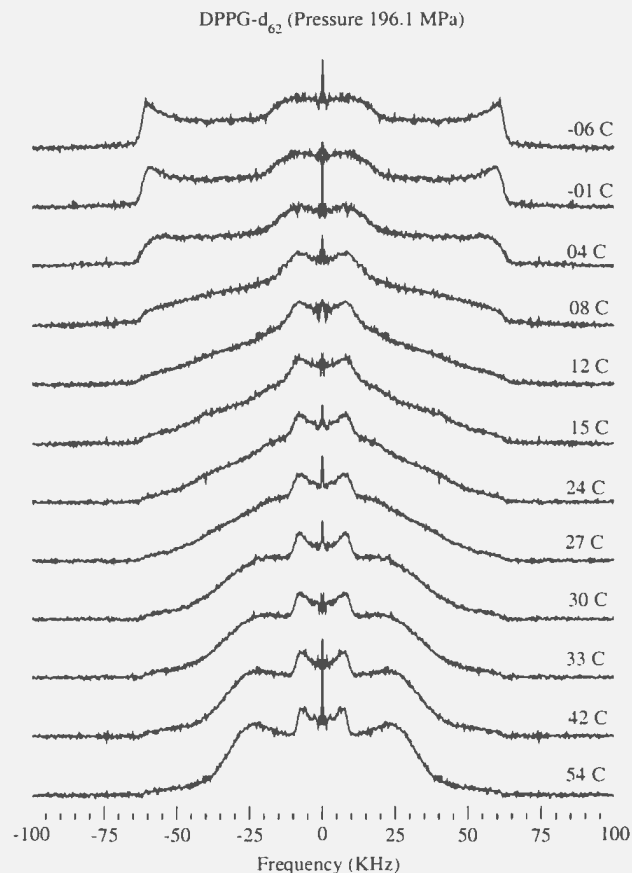


Figure 5.7: ^2H NMR spectra of Dipalmitoyl-sn-Glycero-3- [Phospho-rac-(1-glycerol)](DPPG- d_{62}) at 196.1 MPa pressure and at selected temperatures.

The GIII phase appears to exist between 27°C to 10°C. Below this temperature there is a change in the spectrum as it becomes more axially symmetric with splittings corresponding to the full quadrupole interaction. The central component due to methyl group deuterons is again narrowed by the rotation about the symmetry axis of methyl group. This phase is denoted as phase X [7]. The sequence of observed phases for DPPG- d_{62} at 196.1 MPa appears to be interdigitated gel phase, GIII phase and then phase X. At ambient pressure the accessible phases are liquid crystalline phase L_α , the gel phase $L_{\beta'}$, and the subgel phase, L_C .

The observed phases at 85 Mpa are liquid crystalline phase L_α , interdigitated gel phase, $G_{interdigitated}$, the gel phase GIII and phase X. The sequence of the phase changes for DPPG- d_{62} is consistent with the partial phase diagram shown by Driscoll et al. [7].

5.4 Temperature Dependence of First Moments of DPPG- d_{62}

The spectral moments shown in figure (5.8) are obtained from spectra of DPPG- d_{62} at ambient pressure, 85 MPa, and 196.1 MPa shown in figs (5.5), (5.6), (5.7) respectively. The main phase transition from liquid crystalline phase to gel phase gives rise to a sharp jump in the corresponding M_1 values. At ambient pressure, the main phase transition occurs at 35°C. Below this temperature there is a further gradual increase in M_1 as the lipid bilayers become more ordered on cooling. The subgel transition around -1°C is not very apparent from the changes in the first moments, M_1 . There is also a sharp jump in M_1 at 56°C for DPPG- d_{62} at 85 MPa. This jump in M_1 at 85 MPa is large as compared to the jump in M_1 at the ambient pressure main phase transition.

As discussed in the previous section, the phase just below the main phase transition is not the ordinary gel phase L_{β}' , but rather the interdigitated gel phase $G_{interdigitated}$. The chain order in the interdigitated gel phase just below the main transition is higher than the normal gel phase just below the main transition. First moments are proportional to average orientational order parameter of carbon deuterium bonds. Comparing the ambient pressure first moments to high pressure ones just above their respective main transition temperature, the high pressure moments are lower. This implies that, the lipids at high pressure enter the gel phase from lower average chain

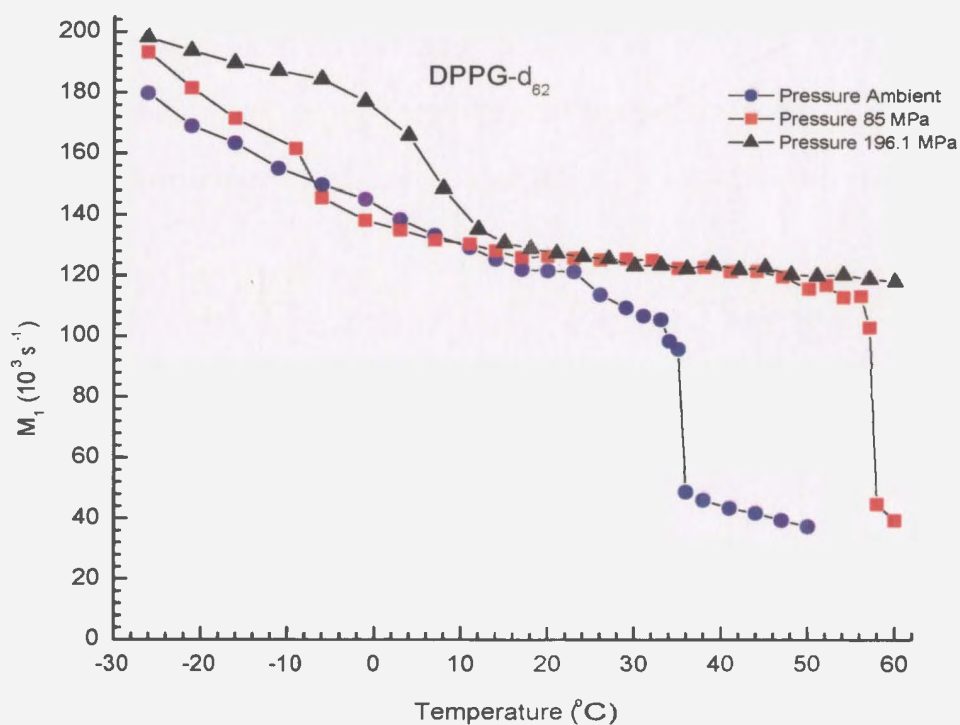


Figure 5.8: First moments for DPPG- d_{62} at ambient pressure (blue), 85 MPa (green), and 196.1 MPa (red).

orientation order than lipids at ambient pressure.

There is another sharp increase in M_1 at -6°C for DPPG- d_{62} at 85 MPa pressure. This corresponds to the transition from GIII phase to more ordered immobilized lipid phase X. The phase transition from normal gel phase $L_{\beta'}$ to subgel phase L_C is gradual, but the phase transition from GIII phase to phase X is sudden. The phase X at high pressures displays the same spectra as the subgel phase at ambient pressure.

The moments for DPPG- d_{62} at 196.1 MPa are higher, as the lipid is in interdigitated gel phase at 60°C . The transition from $G_{interdigitated}$ to gel phase GIII around 30°C , is not apparent from changes in M_1 . There is slow increase in the M_1 until 10°C where there is significant increase in M_1 . There appears to be a phase transition from GIII phase to more ordered immobilized phase X at 10°C , as discussed above. The main phase transitions are quite sharp, but the temperature ranges over which phase transition at high pressures and low temperature occur are blurred.

5.5 Deuteron Quadrupole Echo Decay

The deuteron quadrupole Hamiltonian is orientation dependent and motions that change the orientation of the EFG tensor principal axis system, with correlation times comparable to the characteristic time of NMR experiment, affect the extent to which the magnetization is refocused using the deuteron quadrupole echo pulse sequence described in the section 3.3. Information on how the fast and slow motions are affected by pressure can be obtained from deuteron quadrupole relaxation time T_{2e}^{QE} . The quadrupole relaxation time is obtained by varying the quadrupole echo pulse separation τ and taking the initial slope from the semi-logarithmic plot of echo amplitude versus time of echo formation.

5.5.1 Temperature Dependence of DPPC- d_{62} Transverse Relaxation Time at Ambient and High Pressure

Transverse relaxation times T_{2e}^{QE} for DPPC- d_{62} were obtained for a wide range of temperatures from 60°C to -26°C at ambient pressure and pressures of 85 MPa and 196.1 MPa. The temperature dependence of T_{2e}^{QE} at ambient pressure is shown in figure (5.9a). Over the temperature range investigated at ambient pressure, DPPC- d_{62} goes from liquid crystalline phase to gel phase and then to subgel phase around 0°C. In the liquid crystalline phase the echo decay time, T_{2e}^{QE} , stays approximately independent of temperature. On cooling, DPPC- d_{62} passes through its main transition to the gel phase, and there is sudden decrease in T_{2e}^{QE} . As temperature is reduced further in gel phase, T_{2e}^{QE} passes through a maximum.

The temperature dependence of T_{2e}^{QE} for DPPC- d_{62} at 85 MPa is shown in fig.(5.9b). It is qualitatively similar to temperature dependence of T_{2e}^{QE} at ambient pressure. The main phase transition is shifted to higher temperature by high pressure and so is the corresponding first minimum in T_{2e}^{QE} . Another noticeable difference is that the maximum in T_{2e}^{QE} at 85 MPa is lower than the maximum in T_{2e}^{QE} at ambient pressure. The temperature profile of T_{2e}^{QE} at ambient pressure and at 85 MPa pressure is explained as follows.

As described in section 3.5, using Equations (3.55) and (3.57), we know that the contributions of fast motions to echo decay rate, R , is proportional to their correlation times. For slow motions contributions to echo decay rate are inversely proportional to their correlation times. In the liquid crystal phase, both fast motions (such as molecular rotation, chain fluctuation and trans-gauche isomerization) and slow motions (such as collective bilayer motion, lateral diffusion and surface undulations) are present. The effects of fast and slow motions on echo decay rate are opposite to

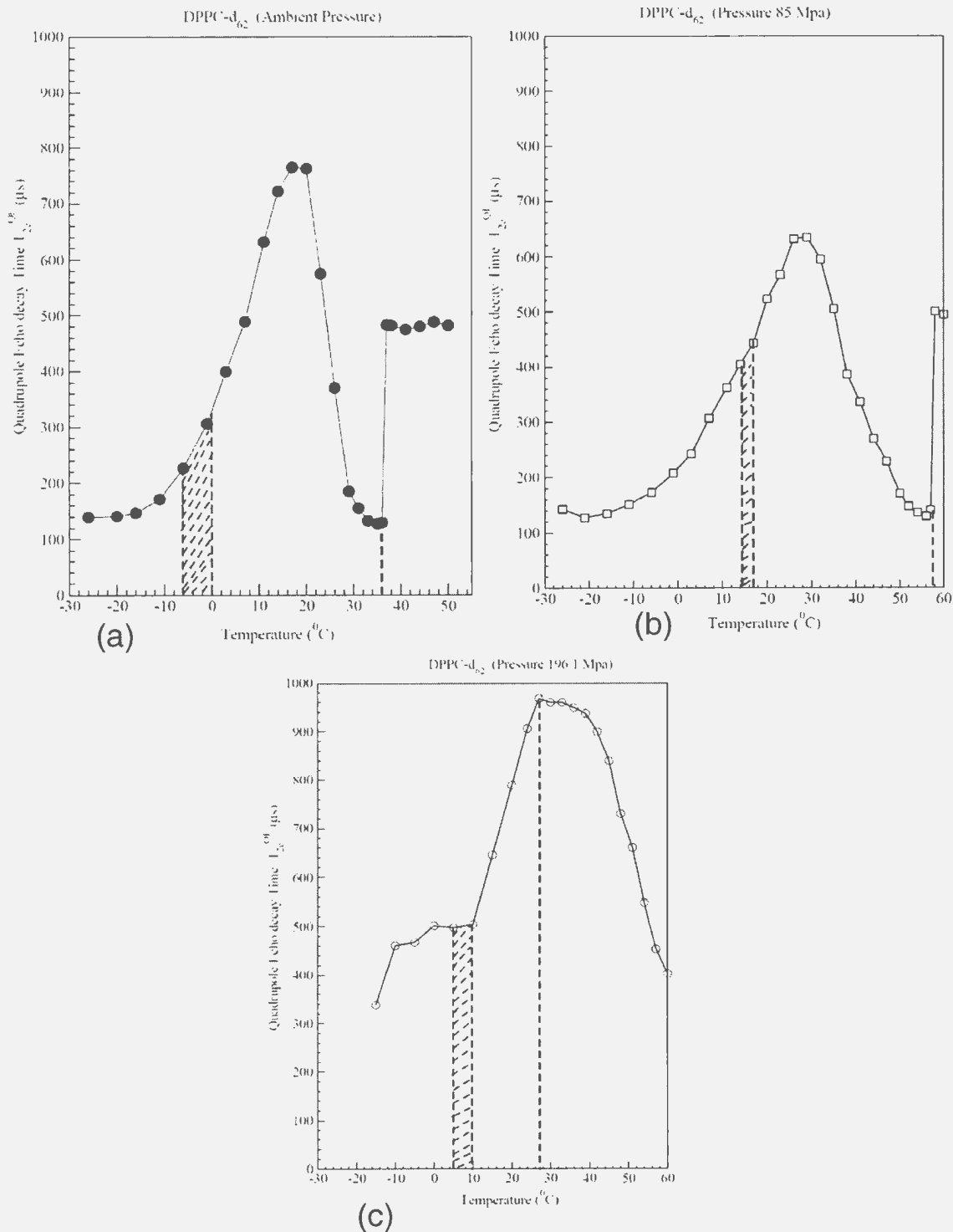


Figure 5.9: Temperature dependence of Quadrupole echo decay times T_{2e}^{QE} for DPPC- d_{62} at (a) Ambient Pressure (b) 85 MPa Pressure and (c) 196.1 MPa. The sharp phase transitions are marked by dotted lines. The broader low temperature phase transition is marked by a shaded area.

each other, so echo decay rate in the liquid crystalline phase remains approximately independent of temperature. On cooling through the main transition, the liquid crystalline phase L_α is changed to ordered gel phase $L_{\beta'}$.

In the ordered gel phase, the correlation times of both fast and slow motions increase, and all motions slow down. The motions which were slow in the liquid crystalline phase get even slower in the gel phase and effectively freeze out on the NMR time scale of present experiment. As a result, their contributions to the echo decay rate decrease. The correlation times of faster motions like molecular rotations and chain fluctuations get longer, just below the main transition, so that these motions now fall into the slow motion regime. Their contributions to echo decay rate in the gel phase are thus inversely proportional to their correlation times. The inverse of echo decay rate is echo decay time, T_{2e}^{QE} . A reduction in echo decay rate gives rise to an increase in T_{2e}^{QE} value with further cooling, as the correlation times of these motions get longer. The echo decay time T_{2e}^{QE} increases in gel phase until it reaches a maximum.

On further cooling, the echo decay time T_{2e}^{QE} starts decreasing, and this implies that some fast motion is still present. This fast motion which begins to dominate echo decay rate, may be trans-gauche isomerization. The contribution to echo decay rate from this motion is directly proportional to its correlation time, as it is in the fast motion regime. With decreasing temperature, the correlation times of trans-gauche isomerization get longer, so the echo decay rate increases and the echo decay time decreases. The echo decay times thus approach a second minimum at low temperature. Below this temperature, the trans-gauche isomerization will slow down enough to move into the slow motion regime and its contribution to echo decay rate becomes inversely proportional to its correlation times. This leads to a rise in echo decay times below the second minimum, as shown in fig. 5.9b. In fig. (5.9a,b), the range of

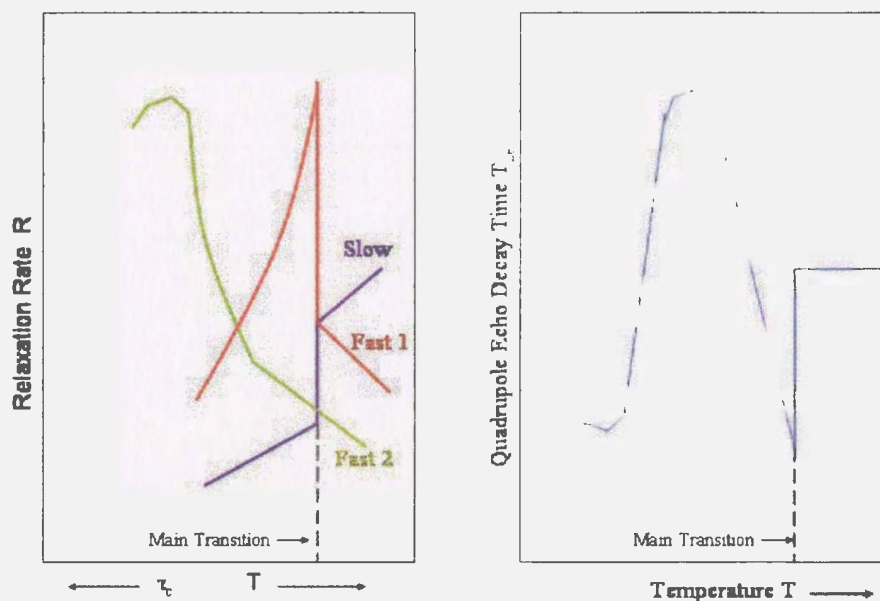


Figure 5.10: Temperature dependence of $T_{2\epsilon}$: Separate contributions of fast and slow motions.

the subgel transition is shaded, as the subgel transition is not a sharp transition. A schematic of the contributions of fast and slow motions to echo decay rate is shown in fig (5.10).

The temperature dependence of echo decay times for DPPC- d_{62} at a pressure of 196.1 MPa is shown in fig (5.9c). The sequence of phase transitions for DPPC- d_{62} at this pressure is interdigitated gel phase, GIII gel phase and the immobilized phase X. At 60°C and a pressure of 196.1MPa, DPPC- d_{62} is in the interdigitated gel phase. The present motions are molecular rotations and others which are in the slow motion regime and fast motion such as trans-gauche isomerization. In interdigitated gel phase, the rate at which motions like molecular rotations slow on cooling is fast as compared to the case in the ordinary gel phase at ambient pressure. This gives rise

to a higher maximum echo decay time, $T_{2\epsilon}^{QE}$, at 196.1 MPa as compared to ambient pressure.

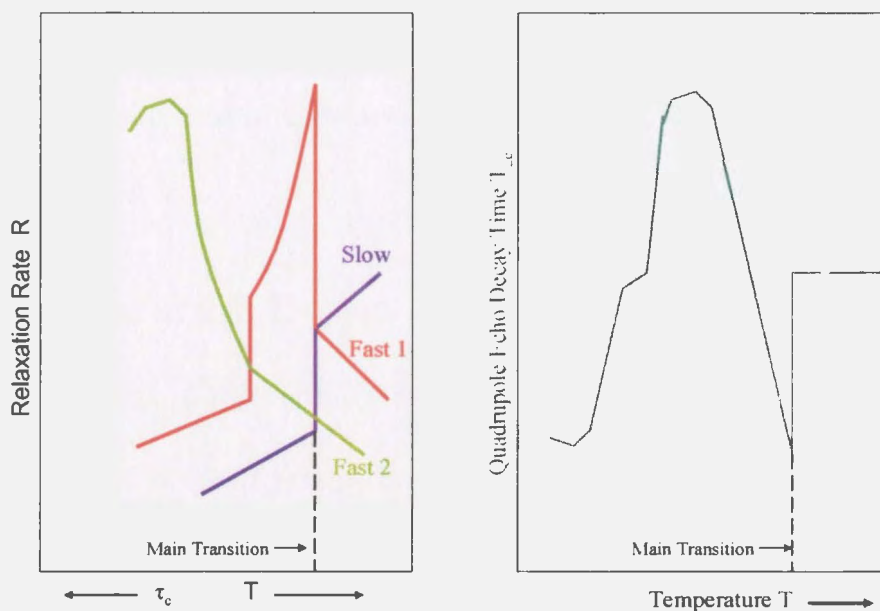


Figure 5.11: Temperature dependence of $T_{2\epsilon}$: Separate contributions of fast and slow motions.

The phase transition between 30°C and 27°C from the interdigitated gel phase to the GIII gel phase, is marked by a dotted line in fig. (5.9c). Below this temperature, trans-gauche isomerization appears to be the dominant process and contributes to echo decay rates in the fast motions regime. On cooling, the correlation times for trans-gauche motions increase, which leads to a decrease in echo decay times. The transition from the GIII phase to the phase X is not sudden and is marked as a shaded area in fig (5.9c).

A plateau in the echo decay time is observed as the phase X is established. The spectra in phase X are nearly symmetric spectra with full quadrupole splitting. The

phase X is an immobilized phase, having only a few motions. At the beginning of phase X, the motions like molecular rotations slow sharply. The rapid decrease in rate R for these motions counters the fast rise in R from fast trans-gauche isomerization and the overall increase in R is slowed. This give rise to a plateau in the temperature dependence of T_{2e}^{QE} for DPPC- d_{62} at high pressure at the beginning of phase X. The schematic of contributions of slow and fast motions to echo decay rate is shown in fig (5.11).

5.5.2 Temperature Dependence of DPPG- d_{62} Transverse Relaxation Time at Ambient and High Pressure

To study the effect of head group charge on the freezing out of motions in ordered phase phospholipids, echo decay times were also obtained for the anionic phospholipid DPPG- d_{62} . The temperature dependence of echo decay times for DPPG- d_{62} at ambient pressure and high pressures of 85 MPa, 196.1 MPa is shown in fig (5.12a,b,c) respectively. The temperature dependence of echo decay times for DPPG- d_{62} at ambient pressure is qualitatively similar to DPPC- d_{62} at same pressure. The echo decay times in the liquid crystalline phase L_{α} for DPPG- d_{62} are shorter as compared to DPPC- d_{62} in the same phase. The main phase transition is marked by a line, while transition to the subgel phase is shown as a shaded area.

At a pressure of 85 MPa the sequence of phases for DPPG- d_{62} is characteristic of high pressure. These are the interdigitated gel phase, the GIII phase and the immobilized phase X. This is quite different from the sequence of phases for DPPC- d_{62} at a pressure of 85 MPa which is similar to that of low pressure. This implies a shift of ordered phase boundaries to lower pressure for DPPG- d_{62} . The echo decay times for DPPG- d_{62} at 85 MPa also show behavior characteristic of high pressure. At

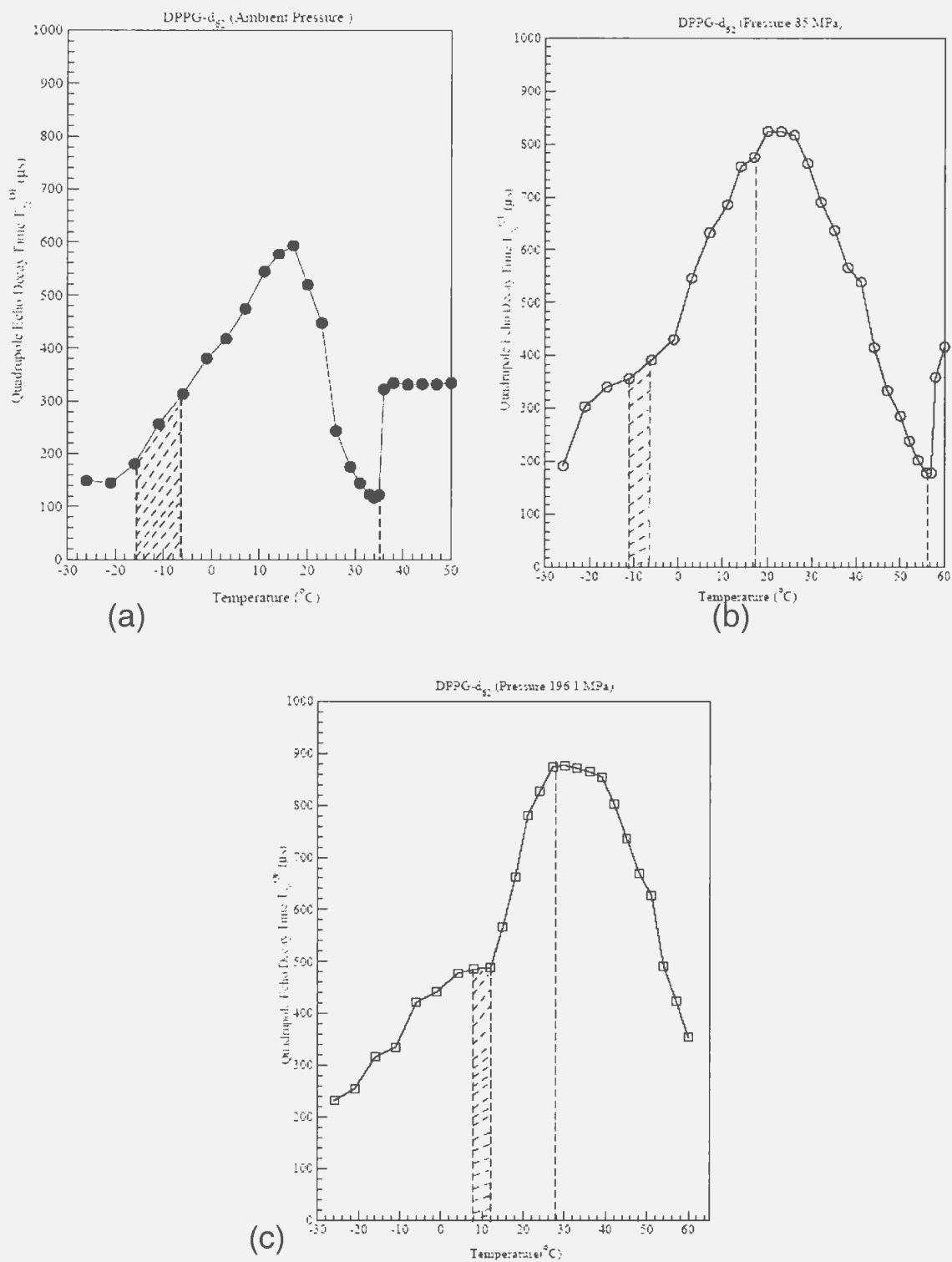


Figure 5.12: Temperature dependence of Quadrupole echo decay times T_{2e}^{QE} for DPPG- d_{62} at (a) Ambient Pressure (b) 85 MPa Pressure and (c) 196.1 MPa. The sharp phase transitions are marked by dotted lines. The broader low temperature phase transition is marked by shaded a area.

the main phase transition from liquid crystalline phase L_α to interdigitated gel phase at 57°C, there is a decrease in echo decay times. The change in echo decay times at the main phase transition is not as sharp as in DPPC- d_{62} . On cooling through the interdigitated gel phase, motions like molecular rotations slow down and their contributions to echo decay rate become inversely proportional to their correlation times. This lead to an increase in echo decay times on cooling. The rate at which these motions slow on cooling is faster in the interdigitated gel phase than in the ordinary gel phase. As a result, the echo decay times for DPPG- d_{62} at a pressure of 85 MPa reach a higher maximum. Around -5°C, as the phase X is established, there is a plateau in the echo decay times. The sudden freezing of motions like molecular rotations etc. in phase X cause this plateau, as explained in the previous section (5.11). On further cooling, the echo decay times decrease and go towards a second minimum.

The echo decay times for DPPG- d_{62} at a pressure of 196.1 MPa are shown in fig 5.12c. The temperature dependence of echo decay times for DPPG- d_{62} is qualitatively similar to that of DPPC- d_{62} at same pressure. At 60°C, DPPG- d_{62} is in the interdigitated gel phase, and in this phase the intermediate motions like molecular rotations freeze out more rapidly as the temperature is lowered. This gives a higher maximum in the echo decay times. On cooling towards the immobilized phase X, trans-gauche isomerization becomes a dominant process and results in a fall in the echo decay times for temperatures below that of the T_{2e}^{QE} maximum. Residual motions like molecular rotations freeze-out as the phase X is established. This leads to a plateau in the temperature dependence of the echo decay times. On further cooling in phase X, the echo decay times decrease and go towards a second minimum.

The overall behavior of DPPG- d_{62} and DPPC- d_{62} at ambient pressure and a pressure of 196.1 MPa are qualitatively similar to each other. At 85 MPa the ordered-

ordered boundaries shifted to lower pressure for DPPG- d_{62} . The contribution in terms of slow and fast motions are given in fig. 5.10 for ambient pressure and in fig. 5.11 for pressures of 85 MPa and 196.1 MPa. These are explained in the previous section.

5.6 Quadrupole Carr-Purcell-Meiboom-Gill Decays

There are some motions whose correlation times are too long for them to contribute to motional narrowing of spectra, but which still contribute to the quadrupole echo decay [12]. Bloom and Sternin [12] used the quadrupole Carr-Purcell-Meiboom-Gill (q-CPMG) pulse sequence to separate contributions to echo decay rate of such slow adiabatic motions from fast motions which are more effective in motional narrowing of deuterium spectra. These adiabatic bilayer motions may include diffusion of molecules around curved vesicle surfaces [12] and collective bilayer, surface undulations [14]. The separation of contributions, from slow and fast motions, to the echo decay rate, in particular, would be useful for understanding of the freezing of fast motions in ordered phase.

In the q-CPMG pulse sequence, the second pulse of the quadrupole echo pulse sequence is replaced by a sequence of N such pulses as shown below,

$$\left(\frac{\pi}{2}\right)_y - \tau - \left(\frac{\pi}{2}\right)_x - t - .$$

As a result, instead of getting one quadrupole echo we get a train of echoes with decreasing amplitudes at times $2n\tau$, as shown in fig. 5.13, where n is an integer. The rate of decrease of the amplitude of the train of echoes can be measured to determine the transverse relaxation time denoted by T_2^{q-CPMG} . The relaxation rate for a specific deuteron is sum of the rates due to different modes, in case of q-CPMG experiment is given as

$$R = \sum_i R_i = \frac{1}{T_2^{q-CPMG}} = \sum_i M_2^i \tau_i \left[1 - \frac{\tau_i}{\tau} \tanh\left(\frac{\tau}{\tau_i}\right) \right], \quad (5.3)$$

where τ_i is the correlation time of one motion and τ is the pulse separation of the q-CPMG pulse sequence. This formula derived by Blicharski et al. [13] describes the response of the nuclear system to the q-CPMG pulse train in the weak-collision case.

The motions for which $\tau_j \ll (\Delta M_2^j)^{-\frac{1}{2}}$, can contribute to motional narrowing. Such motions generally also satisfy $\tau_j \ll \tau$, so that their contributions to echo decay rate are given as

$$R = \frac{1}{T_2^{q-CPMG}} \approx \sum_j M_2^j \tau_j. \quad (5.4)$$

This above equation is independent of pulse separation. In this limit, $T_2^{q-CPMG} \approx T_2^{QE}$.

The motions for which $\tau_k \gg (\Delta M_2^k)^{-\frac{1}{2}}$, do not contribute to motional narrowing. For these motions it is possible to select a q-CPMG pulse sequence which satisfies $\tau_k \gg \tau$, so that their contributions to echo decay rate depend on pulse separation and are given by

$$R = \frac{1}{T_2^{q-CPMG}} \approx \sum_k M_2^k \frac{\tau^2}{3\tau_k}. \quad (5.5)$$

The slow motion contributions to echo decay rate are reduced by a factor of $\frac{\tau^2}{3\tau_k^2}$ as compared to their contributions to quadrupole echo decay rate, while the contributions from the fast motions are not affected. By virtue of this technique, the contributions to echo decay due to slow motions can be suppressed by selecting small τ and q-CMPG can be used as a low pass filter for the spectrum of correlation times.

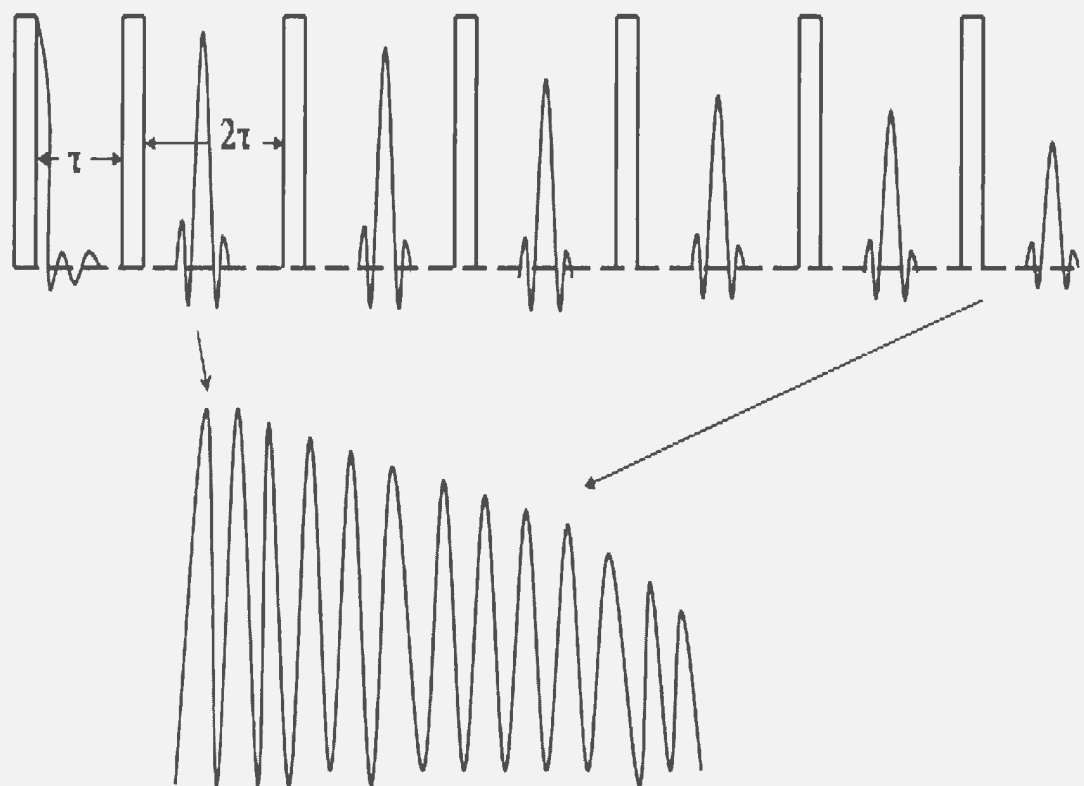


Figure 5.13: Schematic representation of q-CPMG pulse sequence and trains of echoes obtained.

5.6.1 Quadrupole Carr-Purcell-Meiboom-Gill Decays for DPPC- d_{62} at Ambient and High Pressures

Q-CPMG experiments were conducted on DPPC- d_{62} for a series of temperatures at ambient pressure and a pressure of 196.1 MPa. Q-CPMG echo decays for DPPC- d_{62} at ambient pressure and a temperature of 45°C are shown in fig 5.14. DPPC- d_{62} is in liquid crystalline phase at this temperature and pressure. For a molecule undergoing a particular set of motions, the observed q-CPMG decay rate is a sum of contributions from each motion. There are different populations of deuterons in the bilayer system having different environments, so the total signal is the sum from all these populations. The decays in fig.(5.14) are clearly dependent on the pulse separation τ

which indicates that slow adiabatic motions like collective motions, lateral diffusion, surface undulations contribute significantly to decay of the quadrupole echo in the liquid crystalline phase. The decay rates for long pulse separations are non-exponential, but reach a common decay rate for large values of $2n\tau$.

This indicates that each molecule is subject to some common fast motion in addition to various slow (adiabatic) motions. For these slow motions there may be a distribution of correlation times. The q-CPMG decay rate is a sum of contributions from all of the motions affecting the molecule. The contributions to echo decay rate from slow motions (having correlation times long compared to pulse separation, τ) are inversely proportional to the correlation time.

For q-CPMG echo decays at short τ values, the contributions from slow motions are small. The observed decays are largely exponential with a rate determined primarily by the common fast motion. For large τ values, the signals from those molecules whose slow motions have the shortest correlation times decay quickly. For molecules having slow motions with longer correlation times, the fast motions contribute to the echo decay rate more significantly. It is the signal from these molecules which remains at large values of $2n\tau$. The τ dependence of the echo decay rates, contains information about the distribution of slow motions.

Figure 5.15 shows the q-CPMG echo decay rates for DPPC- d_{62} at ambient pressure and 30°C. The temperature is 5°C below the main phase transition, so the DPPC- d_{62} is in the gel phase, L_{β}' . The quadrupole echo decay times at this temperature are just coming out of the first minimum, as shown in fig. 5.9a. The q-CPMG echo decay rates are not very much dependent on pulse separation, τ . This suggests that the motions which contribute to the motional narrowing (non-adiabatic motions) of spectra also contribute significantly to echo decay at this temperature in the gel phase. At the main phase transition, the correlation times of all the motions get

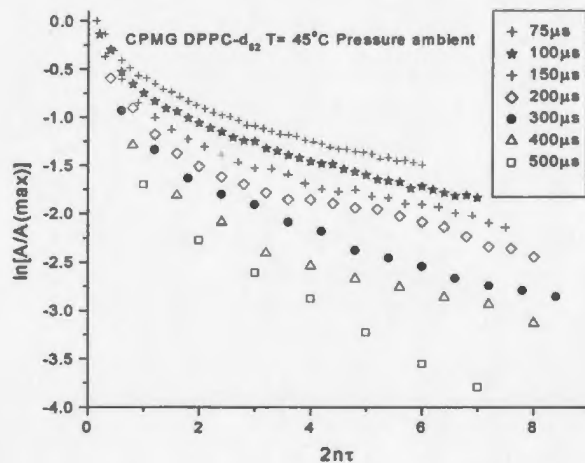


Figure 5.14: q-CPMG echo decays for DPPC- d_{62} at ambient pressure and 45°C, where A is the amplitude of echo obtained at $2n\tau$ and $A(\max)$ is the maximum amplitude for shortest τ .

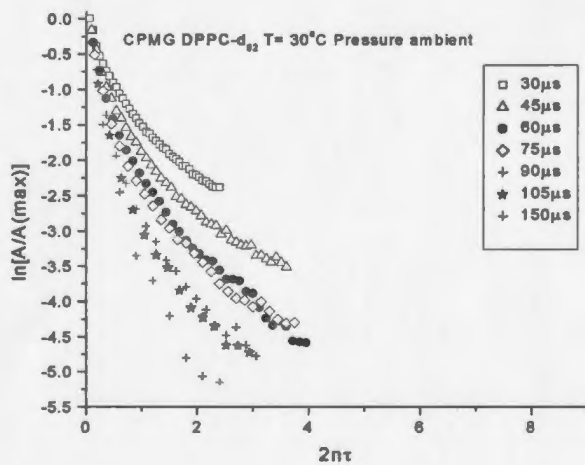


Figure 5.15: q-CPMG echo decays for DPPC- d_{62} at ambient pressure and 30°C, where A is the amplitude of echo obtained at $2n\tau$ and $A(\max)$ is the maximum amplitude for shortest τ .

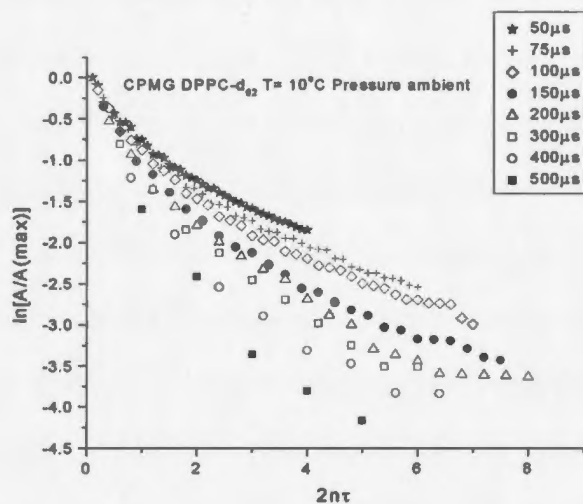


Figure 5.16: q-CPMG echo decays for DPPC- d_{62} at ambient pressure and 10°C, where A is the amplitude of echo obtained at $2n\tau$ and $A(\max)$ is the maximum amplitude for shortest τ .

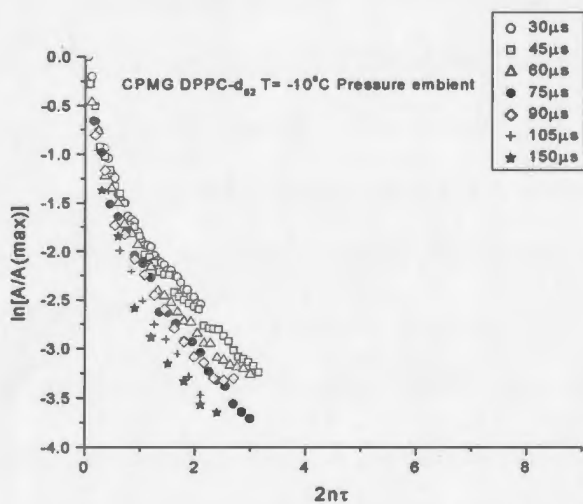


Figure 5.17: q-CPMG echo decays for DPPC- d_{62} at ambient pressure and -10°C, where A is the amplitude of echo obtained at $2n\tau$ and $A(\max)$ is the maximum amplitude for shortest τ .

longer. The slow adiabatic motions that contributed to the echo decay in the liquid crystalline phase are now frozen on the NMR time scale of the present experiment and do not contribute to decay rate to the same extent as they do in the liquid crystalline phase. The molecular rotations and other local motions which were fast in the liquid crystalline phase, are now in the slow motion regime, but their correlation times may still be short compared to the slow adiabatic motions of liquid crystalline phase. These motions may still be in the regime where their contributions to q-CPMG decay go as $M_2^k \frac{\tau^2}{3\tau_k}$. If, however, their correlation times are shorter than the correlation times of the adiabatic motions in the liquid crystalline phase, the result will be a faster decay of q-CPMG echo decay train as seen.

This is consistent with the expectation, from the temperature dependence of T_2^{QE} in the gel phase, that, at this temperature, the main contributions to echo decay are from motions like molecular rotations (section 5.6), and that the slower motions (collective motions, surface undulations, lateral diffusion etc) are frozen out in the gel phase on the time scale of the present NMR experiment.

Another set of q-CPMG echo decays were obtained at 10°C and are shown in fig 5.16, where the quadrupole echo decay times are near the maximum. As the correlation times for the local (rotation, wobble etc) motions gets longer on cooling further in the gel, T_2^{q-CPMG} will get longer. The q-CPMG echo decays appear to become more dependent on pulse separation unlike the echo decay rates at 30°C. This suggests that the correlation times for the significant slow motions are becoming longer. These motions may be the molecular rotations whose correlation times now fall in the adiabatic motion regime. The decay rates for large τ values again reach a common decay rate, indicating important contributions from fast motions too. As discussed in section 5.6, at this temperature the contributions from the fast trans-gauche isomerization begin to dominate the quadrupole echo decays, while the

motions like molecular rotations become less effective as they slow further.

The ^2H NMR spectrum for DPPC- d_{62} shown in fig. 5.1, at ambient pressure and -11°C is a nearly axially symmetric spectrum with full quadrupole splitting. This suggests the absence of motions which contribute to the motional narrowing of the ^2H NMR spectrum. The q-CPMG echo decay rates in the subgel phase L_C , at -10°C are shown in fig. 5.17. The q-CPMG echo decays are almost independent of pulse separation, suggesting that the decay is dominated by a fast motion with a correlation time approaching the characteristic time for the experiment. This may be trans-gauche isomerization which is still in the fast motion regime at this temperature.

The q-CPMG experiments for DPPC- d_{62} at ambient pressure can be summarized as follows. In the liquid crystalline phase both slow and fast motions contribute to the echo decay rate. At 30°C , just below the first minimum, all motions slow down and molecular rotations and other local motions contribute significantly to echo decay. At 10°C , as the quadrupole echo decay times pass maximum, both fast and slow motions contribute to echo decay. In the subgel phase, the dominant process is a fast motion, which may be trans-gauche isomerization.

The q-CPMG echo decay rates for DPPC- d_{62} in the interdigitated gel phase were obtained at 50°C and a pressure of 196.1 MPa, as shown in fig. 5.18. The temperature is 7°C below the main phase transition. The τ dependence of echo decay rates indicate the presence of slow motions. The decay are more exponential which may indicate a narrower distribution of slow motions. These results are not sufficient to distinguish motions in the two ordered phases more fully but the difference is interesting in light of the difference in chain packing.

A q-CPMG echo decay for DPPC- d_{62} was also obtained at same pressure and 30°C (fig. 5.19), where the quadrupole echo decay time reaches a maximum. The q-CPMG decays are qualitatively similar to those at 50°C and 196.1 MPa but the

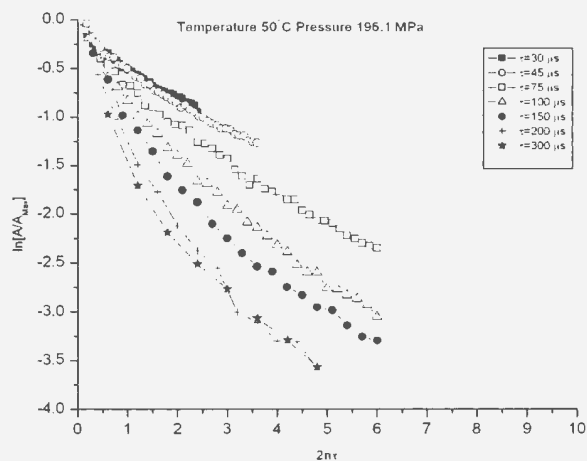


Figure 5.18: q-CPMG echo decays for DPPC- d_{62} at 196.1 MPa and 50°C, where A is the amplitude of echo obtained at $2n\tau$ and $A(\max)$ is the maximum amplitude for shortest τ .

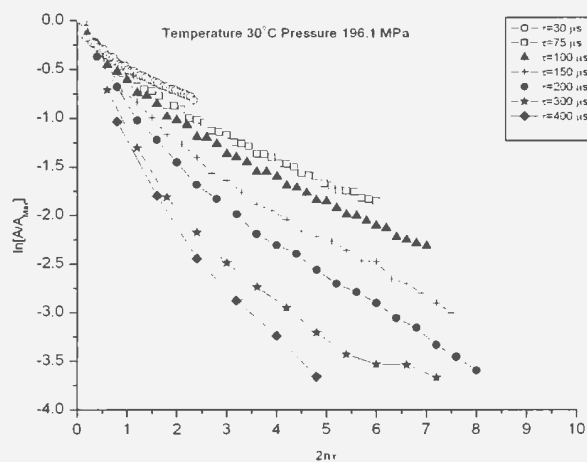


Figure 5.19: q-CPMG echo decays for DPPC- d_{62} at 196.1 MPa and 30°C, where A is the amplitude of echo obtained at $2n\tau$ and $A(\max)$ is the maximum amplitude for shortest τ .

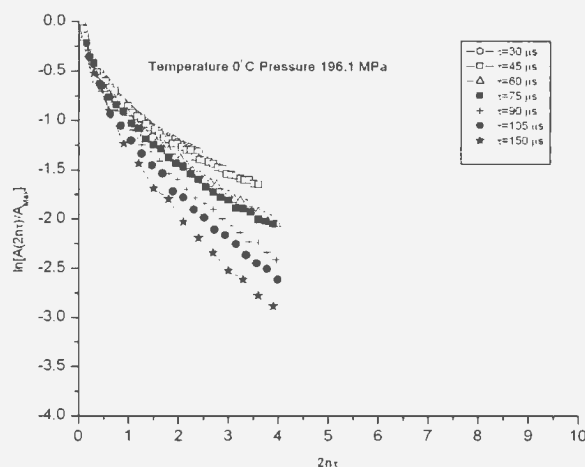


Figure 5.20: q-CPMG echo decays for DPPC- d_{62} at 196.1 MPa and 0°C, where A is the amplitude of echo obtained at $2n\tau$ and $A(\max)$ is the maximum amplitude for shortest τ .

rate for a given pulse separation is lower (longer decay times).

The q-CPMG decay for DPPC- d_{62} was also obtained in the immobilized phase X. The acyl chains are almost rigid in the phase X, and little motion is present. This is also indicated by the q-CPMG echo decay rates at 0°C and 196.1 MPa shown in fig. 5.20. The decay rates are not very dependent on the pulse separation, suggesting the decay is dominated by motions which contribute to motional narrowing ($\tau_j \ll (\Delta M_2^j)^{-\frac{1}{2}}$). This fast motion may be the trans-gauche isomerization. The q-CPMG decay rates separate the contributions from the slow and fast motions to the echo decay rate, and provide the information on the effect of pressure on these motion.

5.6.2 Quadrupole Carr-Purcell-Meiboom-Gill Decays for DPPG- d_{62} at Ambient and High Pressures

The q-CPMG echo decays were also obtained for DPPG- d_{62} at ambient and a pressure of 196.1 MPa for selected temperatures. Fig 5.21 shows the echo decay rates for DPPG- d_{62} in the gel phase at 30°C, 5°C below the main phase transition. The decays are qualitatively similar to DPPC- d_{62} at the same pressure and temperature. The decay is likely dominated by motions that were fast in the liquid crystalline phase but slow in the gel phase. The fast decay of the q-CPMG train suggests that the correlation time for these motions, while in the slow regime, is still shorter than that for the adiabatic motions responsible for the τ dependence of q-CPMG decay in the liquid crystalline phase. The non-exponential shape of the decay suggests that populations with different slow motions still exist in the gel phase.

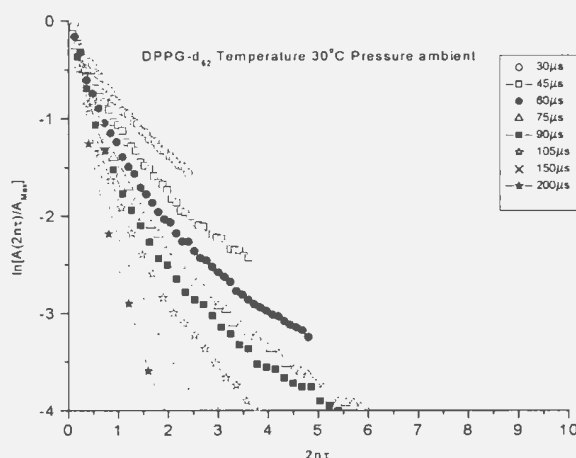


Figure 5.21: q-CPMG echo decays for DPPG- d_{62} at ambient pressure and 30°C, where A is the amplitude of echo obtained at $2n\tau$ and $A(\max)$ is the maximum amplitude for shortest τ .

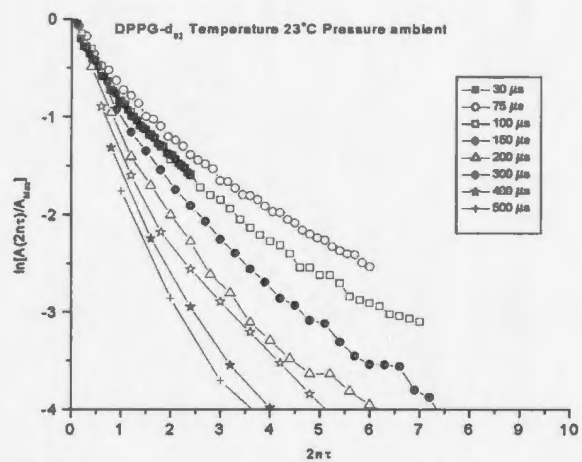


Figure 5.22: q-CPMG echo decays for DPPG- d_{62} at ambient pressure and 23°C, where A is the amplitude of echo obtained at $2n\tau$ and $A(\max)$ is the maximum amplitude for shortest τ .

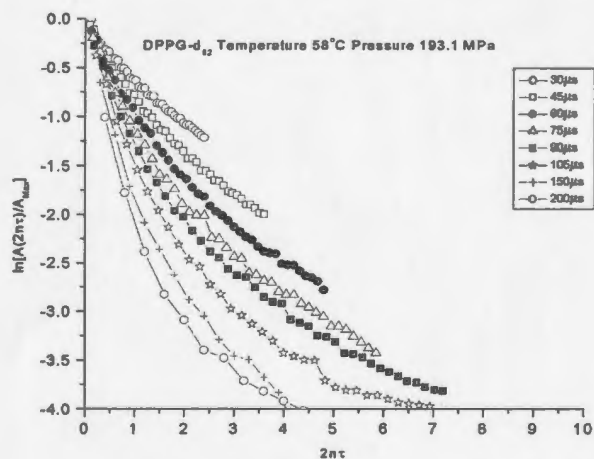


Figure 5.23: q-CPMG echo decays for DPPG- d_{62} at 196.1 MPa and 58°C, where A is the amplitude of echo obtained at $2n\tau$ and $A(\max)$ is the maximum amplitude for shortest τ .

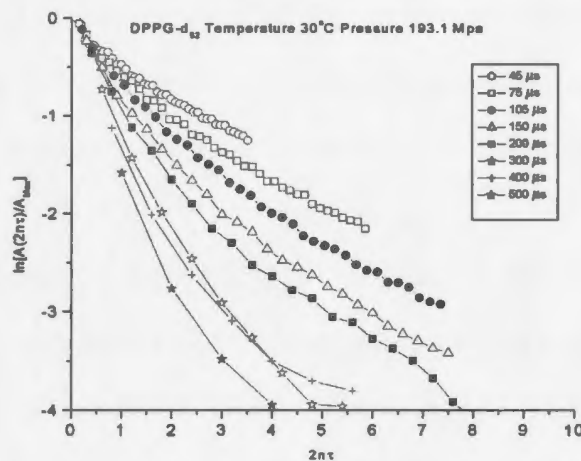


Figure 5.24: q-CPMG echo decays for DPPG- d_{62} at 196.1 MPa and 30°C, where A is the amplitude of echo obtained at $2n\tau$ and $A(\max)$ is the maximum amplitude for shortest τ .

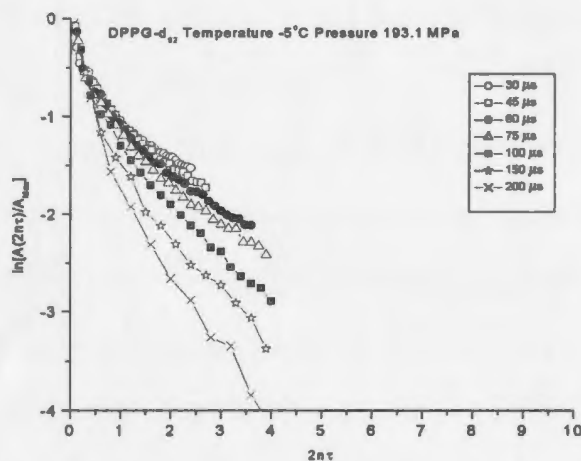


Figure 5.25: q-CPMG echo decays for DPPG- d_{62} at 196.1 MPa and -5°C, where A is the amplitude of echo obtained at $2n\tau$ and $A(\max)$ is the maximum amplitude for shortest τ .

Another q-CPMG decay was obtained at ambient pressure and 23°C, as the quadrupole echo decay times approaches the maximum, as shown in fig 5.22. The q-CPMG decays slow with decreasing temperature below the main transition. This indicates an increase in the correlation times for slow motions that dominate the echo decay in this range.

The qualitative behavior of q-CPMG decay rates for DPPG- d_{62} at a pressure of 196.1MPa is quite similar to DPPC- d_{62} at same pressure. The decay rates in the interdigitated gel phase at 58°C are shown in fig 5.23. The decays are more exponential which may indicate a narrower distribution of slow motions. Fig 5.24 shows the echo decay rates at 30°C, as quadrupole echo decay times reach a maximum. The rate for a given pulse separation is lower compared to the decay rate at 58°C and 196.1 MPa. This lead to an increase in the echo decay times.

On cooling, as the DPPG- d_{62} approaches the phase X, all the motions slows down as indicated by the ^2H NMR spectra which display full quadrupole splitting in the phase X (fig. 5.7). The q-CPMG decay rates were obtained in phase X for DPPG d_{62} at 5°C and pressure of 196.1 MPa, shown in fig. 5.25. The decay rates are less dependent of the pulse separation. This suggest that slow motions (molecular rotations etc.) do not contribute to the decay rates significantly and the decays are dominated by the fast motions which contribute to the motional narrowing of spectra. These fast motions may be trans-gauche isomerization, which are the dominant process in phase X. The qualitatively behavior of q-CPMG decays for DPPG d_{62} are quite similar to DPPC d_{62} under similar conditions.

Chapter 6

Summary and Concluding Remarks

Quadrupole echo decay times were obtained for DPPC- d_{62} and DPPG- d_{62} at ambient and high pressures for a range of temperature, to study the effect of pressure on freezing out of fast motions. To study the affect of head group charge on freezing out of motions in the ordered phase, the experiments were performed on two different types of lipids, anionic lipid DPPG- d_{62} and zwitterionic lipid DPPC- d_{62} . The q-CPMG experiments were performed at selected temperature and at ambient and pressure of 196.1 MPa, to separate the contribution of slow and fast motions to echo decay rate.

The temperature dependences of echo decay times for DPPC- d_{62} and DPPG- d_{62} are qualitatively similar at ambient pressure. The echo decay time passes through a minimum at the main transition, increase to maximum as the correlation times for molecular motions increase in the gel phase and then drop towards a second minimum as the trans-gauche isomerization slows and begins to dominate echo decay. Trans-gauche isomerization starts dominating the echo decay rate, just above the emergence of CD bond spectra characteristic of subgel phase.

At a pressure of 196.1 MPa, the phase behaviors of both lipids are different from

their ambient pressure behavior. The sequence of phases at this pressure is interdigitated gel phase, GIII phase and phase X. The intermediate motions like molecular rotations etc. freeze out more rapidly as the temperature is lowered in the interdigitated gel phase. This is reflected by a higher maximum in the temperature dependence of the echo decay times. Trans-gauche isomerization also appears to slow down at a faster rate on cooling towards the immobilized phase.

A plateau in echo decay times was observed as the immobilized phase X is established. The axially symmetric spectrum in phase X with full quadrupole splitting indicates the freezing out of most motions. The sharp increase in the molecular rotational correlation times and the presence of fast trans-gauche isomerization leads to a plateau in echo decay times.

The phase X at high pressures and the subgel phase at low pressure are not distinct phases. The subgel transition at ambient pressure is quite gradual where the transition to phase X at high pressures is sharp. This is also reflected by the sudden change in M_1 values when the transition to phase X takes place.

At an intermediate pressure of 85 MPa, the phase behaviors of DPPC- d_{62} and DPPG- d_{62} are totally different. The phase behavior DPPC- d_{62} is characteristic of lower pressure while DPPG- d_{62} behavior is characteristic of high pressure sequence of phases. The main phase transition to the interdigitated gel phase is also indicated by a larger jump in M_1 values compared to the jump for the transition to the ordinary gel phase at ambient pressure. This suggests that the intermediate pressure ordered-ordered phase boundaries are shifted to lower pressure for DPPG- d_{62} . The lower maximum in echo decay times for DPPC- d_{62} at 85 MPa compared to maximum at ambient pressure indicates that the correlation times of trans-gauche isomerization in the ordered gel phase are increasing slowly at 85 MPa.

The decay rates from q-CPMG experiments were analyzed in terms of contribu-

tions from slow and fast motions. The results indicate the presence of both fast and slow motions in the liquid crystalline phase. As the echo decay times pass through the first minimum, the slowest motions freeze out and some faster motions slow into the slow motion regime. Some of these motions slow down more quickly on cooling towards the maximum, where again the presence both fast and slow motions is indicated by q-CPMG decays. For temperatures below the maximum, the dominant process is fast trans-gauche isomerization, which leads to the decrease in echo decay times on cooling towards the subgel phase. The q-CPMG decay rates in subgel phase and in phase X confirms the absence of most motions. The q-CPMG experiments confirm the results obtained from quadrupole echo experiments.

For the future work, the phase diagram of DPPC is well established at high temperature, but at low temperature the phase boundaries are not very clear. The boundary between phase X and subgel phase at low temperature should be better established. The phase diagram for DPPG is not well known, as indicated by our experiments showing that the ordered-ordered phase boundaries at intermediate pressure shift to lower pressure for DPPG. A full phase diagram for DPPG should be developed. The q-CPMG experiments can be done at more selected temperatures, so obtain better information about motions.

Bibliography

- [1] G. Weber and H. G. Drickamer. The effect of high pressure upon proteins and other biomolecules. *Quarterly Review of Biophysics*, 16:89–112, 1983.
- [2] B. B. Bonev and M. R. Morrow. Effect of pressure on the dimyristoylphosphatidylcholine bilayer main transition. *Physical Review E*, 55(5):5825–5833, 1997.
- [3] T. Inoue, I. Motoda, N. Hiramatsu, M. Suzuki, and K. Sato. Pressure effect on phase behavior of binary mixtures of *cis*-unsaturated fatty acids. *Chemistry and Physics of Lipids*, 82:63–72, 1996.
- [4] J. Jonas, C. L. Xie, A. Jonas, P. J. Grandinetti, D. Campbell, and D. Driscoll. High-resolution ^{13}C NMR study of pressure effects on the main phase transition in l- α -dipalmitoyl phosphatidylcholine vesicles. *Proceedings of the National Academy of Sciences*, 85:4115–4117, 1988.
- [5] B. B. Bonev and M. R. Morrow. Effects of hydrostatic pressure on bilayer phase behavior and dynamics of dilauroylphosphatidylcholine. *Biophysical Journal*, 70:2727–2735, 1996.

- [6] P. T. T. Wong, D. J. Siminovitch, and H. H. Mantsch. Structure and properties of model membranes : new knowledge from high pressure vibrational spectroscopy. *Bichimica et Biphysics Acta*, 947:139–171, 1988.
- [7] D. A. Driscoll, J. Jonas, and A. Jonas. High pressure ^2H nuclear magnetic resonance study of the gel phases of dipalmitoylphosphatidylcholine. *Chemistry and Physics of Lipids*, 58:97–104, 1991.
- [8] X. Peng and J. Jonas. High-pressure ^{31}P NMR study of dipalmitoylphosphatidylcholine bilayers. *Biochemistry*, 31:6383–6390, 1992.
- [9] P. Meier, E. Ohmes, and G. Kothe. Multipulse dynamic nuclear magnetic resonance of phospholipid membranes. *Journal of Chemical Physics*, 85:3598–3614, 1986.
- [10] M. R. Morrow, N. Abu-Libdeh, J. Stewart, and K. M. W. Keough. Interaction of pulmonary surfactant protein SP-A with DPPC/egg-PG bilayers. *Biophysical Journal*, 85:2397–2405, 2004.
- [11] J. H. Davis. The description of membrane lipid conformation , order and dynamics by ^2H NMR. *Bichimica et Biphysics Acta*, 737:117–171, 1983.
- [12] M. Bloom and E. Sternin. Transverse nuclear spin relaxation in phospholipids bilayer membranes. *Biochemistry Journal*, 26:2101–2105, 1987.
- [13] J.S. Blicharski. Nuclear spin relaxation in the presence of mansfield-ware-4 multiple sequence. *Canadian Journal Physics*, 64:733–735, 1986.
- [14] J. Stohrer, G. Grobner, D. Reimer, K. Weisz, C. Mayer, and G. Kothe. Collective lipid motions in bilayers membranes studied by transverse deuteron spin relaxation. *Journal of Chemical Physics*, 95:672–678, 1991.

- [15] P. Yeagle. *The Structure of Biological Membranes*. CRC Press Inc., Boca Raton, 1992.
- [16] G. Cevc and D. Marsh. *Phospholipid Bilayers*. John Wiley and sons Inc., USA, 1987.
- [17] J.H. Davis. In *Cholesterol in Membrane Models*. edited by L. Finegold., CRC Press Inc., Boca Raton, 1993.
- [18] G. Cvec. *Phospholipids Handbook*. Marcel Dekker, Inc., USA, 1993.
- [19] M. R. Morrow, P. J. Davis, C. S. Jackman, and K. M. W. Keough. Thermal history alters cholesterol effect on transition of 1-palmitoyl-2-linoleoyl phosphatidylcholine. *Biophysical Journal*, 71:3207–3214, 1996.
- [20] M. R. Morrow, J. P. Whitehead, and D. Lu. Chain-length dependence of lipid bilayer properties near the liquid crystal to gel phase transition. *Biophysical Journal*, 63:18–27, 1992.
- [21] H. Ichimori, T. hata, T. Yoshioka, and H. Matsuki. Thermotropic and barotropic phase transition on bilayer membranes of phospholipids with varying acyl chain-length. *Chemistry and Physics of Lipids*, 89:97–105, 1997.
- [22] H. Ichimori, T. Hata, H. Matsuki, and S. Kaneshina. Effect of unsaturated acyl chains on the thermotropic and barotropic phase transitions of phospholipid bilayer membranes. *Chemistry and Physics of Lipids*, 100:151–164, 1999.
- [23] K. P. Coolbear, C. B. Berde, and K. M. W. Keough. Gel to liquid-crystalline phase transitions of aqueous dispersions of polyunsaturated mixed-acid phosphatidylcholines. *Biochemistry*, 22:1466–1473, 1983.

- [24] K. M. W. Keough, B. Giffin, and N. Kariel. The influence of unsaturation on the phase transition temperatures of a series of heteroacid phosphatidylcholines containing twenty-carbon chains. *Biochimica et Biophysica Acta*, 902:1–10, 1987.
- [25] D. J. Siminovitch, P. T. T. Wong, and H. H. Mantsch. High pressure infrared spectroscopy of lipid bilayers: new tests for interdigitation. *Biochimica et Biophysica Acta*, 900:163–167, 1987.
- [26] P. T. T. Wong and C.H. Huang. Structural aspects of pressure effects on infrared spectra of mixed-chain phosphatidylcholine assemblies in D₂O. *Biochemistry*, 28:1259–1263, 1989.
- [27] R. Buchet, D. Carrier, P. T. T. Wong, and I. Jona. Pressure effects on sarcoplasmic reticulum: a fourier transform infrared spectroscopic study. *Biochimica et Biophysica Acta*, 1023:107–118, 1990.
- [28] C. T. Choma and P. T. T. Wong. The structure of anhydrous and hydrated dimyristoylphosphatidyl glycerol: a pressure tuning infrared spectroscopic study. *Chemistry and Physics of Lipids*, 61:131–137, 1992.
- [29] D. Carrier and P. T. T. Wong. Effect of dehydration and hydrostatic pressure on phosphatidylinositol bilayers: an infrared spectroscopic study. *Chemistry and Physics of Lipids*, 83:141–152, 1996.
- [30] C. R. Mateo, P. Tauc, and J. C. Brochon. Pressure effects on the physical properties of lipids bilayers detected by *trans*-parinaric acid fluorescence decay. *Biophysical Journal*, 65:2248–2260, 1993.

- [31] T. Ahn and C. H. Yun. Phase properties of liquid-crystalline phosphatidylcholine/phosphatidylethanolamine bilayers revealed by fluorescent probes. *Archives of Biochemistry and Biophysics*, 369(2):288–294, 1999.
- [32] R. Winter, A. Gabke, C. Czeslik, and P. Pfeier. Power-law fluctuations in phase-separated lipid membranes. *Physical Review E*, 60(6):7354–7359, 1999.
- [33] C. Czeslik, J. Erbes, and R. Winter. Lateral organization of binary-lipid membranes - evidence for fractal-like behaviour in the gel-fluid coexistence region. *Europhysics Letters*, 37(8):577–582, 1997.
- [34] L. F. Braganza and D. L. Worchester. Hydrostatic pressure induces hydrocarbon chain interdigitation in single-component phospholipid bilayers. *Biochemistry*, 25:2591–2596, 1986.
- [35] C. Czeslik, O. Reis, R. Winter, and G. Rapp. Effect of high pressure on the structure of dipalmitoylphosphatidylcholine bilayer membranes: a synchrotron-X-ray diffraction and FT-IR spectroscopy study using the diamond anvil technique. *Chemistry and Physics of Lipids*, 91:135–144, 1998.
- [36] S. T. Nagle, H. I. Petrache, and J. F. Nagle. Structure and interactions of fully hydrated dioleoylphosphatidylcholine bilayers. *Biophysical Journal*, 75:917–925, 1998.
- [37] B. S. Lee, S. A. Mabry, A. Jonas, and J. Jonas. High-pressure proton NMR study of lateral self-diffusion of phosphatidylcholines in sonicated unilamellar vesicles. *Chemistry and Physics of Lipids*, 78:103–117, 1995.

- [38] X. Peng, A. Jonas, and J. Jonas. One and two dimensional ^1H -NMR studies of pressure and tetracaine effects on sonicated phospholipid vesicles. *Chemistry and Physics of Lipids*, 75:59–69, 1995.
- [39] J. Zhang, X. Peng, A. Jonas, and J. Jonas. NMR study of the cold, heat, and pressure unfolding of ribonuclease a. *Biochemistry*, 34:8631–8641, 1995.
- [40] M. Laffleur, B. Fine, E. Sternin, P. R. Cullis, and M. Bloom. Smoothed orientational order profile of lipid bilayers by ^2H -Nuclear Magnetic Resonance. *Biophysical Journal*, 56:1037–1041, 1989.
- [41] X. Peng, A. Jonas, and J. Jonas. High pressure ^2H study of the order and dynamics of selectively deuterated dipalmitoyl phosphatidylcholine in multilamellar aqueous dispersions. *Biophysical Journal*, 68:1137–1144, 1995.
- [42] D. C. Fiech, B. B. Bonev, and M. R. Morrow. Effect of pressure on dimyristoylphosphatidylcholine headgroup dynamics. *Physical Review E*, 57(3):3334–3343, 1998.
- [43] D. A. Driscoll, S. Samarasinghe, S. Adamy, J. Jonas, and A. Jonas. Pressure effects on dipalmitoylphosphatidylcholine bilayers measured by ^2H nuclear magnetic resonance. *Biochemistry*, 30:3322–3327, 1991.
- [44] L. W. Jelinski. Solid state deuterium NMR studies of polymer chain dynamics. *Annual Review of Materials Science*, 15:337–359, 1985.
- [45] V. Luzzati. In *Biological Membranes*. Vol. 1, edited by D. Chapman, Academic Press, London, 1968.

- [46] R. Winter and W. C. Pilgrim. A SANS study of high pressure phase transitions in model biomembranes. *Berichte der Bunsen-Gesellschaft - Physical Chemistry Chemical Physics*, 93:708–717, 1989.
- [47] R. D. Jacobs, B. S. Hudson, and H. C. Anderson. A theory of phase transitions and phase diagrams for one- and two- component phospholipid bilayers. *Biochemistry*, 16(20):4349–4358, 1977.
- [48] M. B. Sankaram and T. E. Thompson. Deuterium magnetic resonance study of phase equilibria and membrane thickness in binary phospholipid mixed bilayers. *Biochemistry*, 31:8258–8268, 1992.
- [49] O. Reis, R. Winter, and T. W. Zerda. The effect of high external pressure on DPPC-cholesterol multilamellar vesicles: a pressure-tuning fourier transform infrared spectroscopy study. *Biochimica et Biophysica Acta*, 1279:5–16, 1996.
- [50] B. B. Bonev and M. R. Morrow. ^2H NMR studies of dipalmitoylphosphatidylcholine and dipalmitoylphosphatidylcholine-cholesterol bilayers at high pressure. *Canadian Journal of Physics*, 76:1512–1519, 1998.
- [51] S. K. Prasad, R. Shashidhar, B. P. Gaber, and S. C. Chandershakhar. Pressure studies of two hydrated phospholipids 1,2-dimyristoyl-phosphatidylcholine and 1,2-dipalmitoyl-phosphatidylcholine. *Chemistry and Physics of Lipids*, 143:227–235, 1987.
- [52] A. Blume. Dynamic properties. In *Phospholipids Handbook*, pages 455–509. edited by G. Cvec., Marcel Dekker, Inc., USA, 1993.
- [53] C. Mayer, K. Mueller, K. Weisz, and G. Kothe. Deuteron NMR relaxation studies of phospholipid membranes. *Liquid Cryst.*, 3:797–806, 1988.

- [54] C. Mayer, G. Groebner, K. Mueller, K. Weisz, and G. Kothe. Orientation-dependent deuteron spin-lattice relaxation times in bilayer membranes. *Chemical Physics Letters*, 165:155–161, 1990.
- [55] B. A. Cornell and J. M. Pope. Low frequency and diffusive motion in aligned phospholipid multilayers studied by pulsed NMR. *Chemistry and Physics of Lipids*, 27:151–164, 1980.
- [56] A. Tardieu, V. Luzzati, and F.C. Reman. Structure and polymorphism of the hydrocarbon chains of lipids: a study of lecithin-water phases. *Journal of Molecular Biology*, 4:711–33, 1973.
- [57] M.J. Janiak, D.M. Small, and G.G. Shipley. Temperature and compositional dependence of the structure of hydrated dimyristoylphosphatidylcholine. *Journal of Biological Chemistry*, 254:6068, 1979.
- [58] D. G. Cameron, H. L. Casal, H. H. Mantsch, Y. Boulanger, and I. C. Smith IC. The thermotropic behavior of dipalmitoyl phosphatidylcholine bilayers. a fourier transform infrared study of specifically labeled lipids. *Biophysical Journal*, 35:1–16, 1981.
- [59] P Meier, E Ohmes, G Kothe, A Blume, J. Weldner, and H. Eibl. Molecular order and dynamics of phospholipid membranes. a deuteron magnetic resonance study. *Journal of Physical Chemistry*, 87:4904–4912, 1983.
- [60] D. G. Cameron, E. F. Gudgin, and H. H. Mantsch. Dependence of acyl chain packing of phospholipids on the head group and acyl chain length. *Biochemistry*, 15:4496–500, 1981.

- [61] R. J. Wittebort, A. Blume, T. H. Huang, S. K. D. Gupta, and R. G. Griffin. ^{13}C -NMR investigations of phase transitions and phase equilibria in pure and mixed phospholipid bilayers. *Biochemistry*, 14:3487–502, 1982.
- [62] R. J. Wittebort, C. F. Schmidt, and R. G. Griffin. Solid-state ^{13}C NMR of the lecithin gel to liquid-crystalline phase transition. *Biochemistry*, 14:4223–8, 1981.
- [63] H. H. Fuldner. Characterization of a third phase transition in multilamellar dipalmitoyllecithin liposomes. *Biochemistry*, 20:5702, 1981.
- [64] L. Trahms, W. Klabe, and E. D. Boroske. ^1H -NMR study of the three low temperature phases of DPPC-water systems. *Biophysical Journal*, 42:285–293, 1983.
- [65] L. Trahms and W. Klabe. Headgroup mobility in the low temperature phase (L_c) of DPPC. *Molecular Crystals and Liquid Crystals*, 123:333–345, 1985.
- [66] A. R. Grimmer and B. Blumich. *NMR: solid state NMR*. Vol. 30, edited by P. Diehl, E. Fluck, H. Gunther, R. Kosfeld, and J. Seelig., Springer- verlag, Berlin, 1994.
- [67] R. C. Weast. *Handbook of Chemistry and Physics*. The Chemical Rubber Co. , Ohio, 1970.
- [68] J. H. Davis. Deuterium nuclear magnetic resonance spectroscopy in partially ordered systems. In *Isotopes in the Physical and Biomedical Sciences*. edited by E. Buncl and J. R. Jones, Elsevier Science Publishers B. V., Amsterdam., volume 2, 1991: 99-157.
- [69] C. P. Slichter. *Principles of Magnetic Resonance*. Springer-Verlag, 1990.

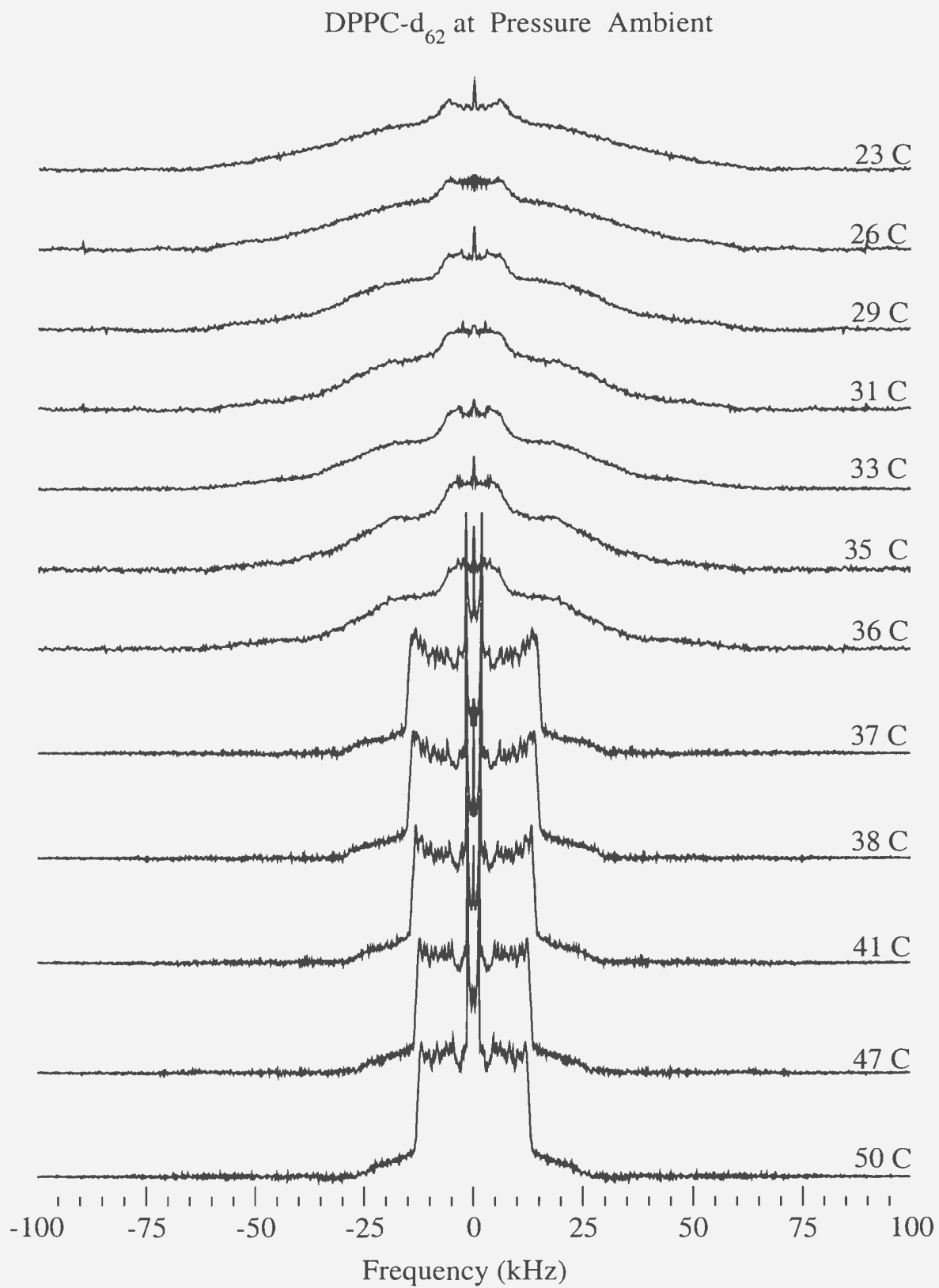
- [70] R. Zare. *Angular Momentum*. John Wiley and Sons, New York, 1988.
- [71] J. Seelig. Deuterium magnetic resonance: Theory and application to lipid membranes. *Quarterly Reviews of Biophysics*, 10(3):353–418, 1977.
- [72] J. H. Davis, K. R. Jeffrey, M. Bloom, M. I. Valic, and T. P. Higgs. Quadrupole echo deuteron magnetic resonance spectroscopy in ordered hydrocarbon chains. *Chemical Physics Letters*, 42:390–394, 1976.
- [73] M. Bloom, C. Morrison, E. Sternin, and J. L. Thewalt. *Pulsed Magnetic Resonance: NMR, ESR, Optics*. edited by D. M. S. Bagguley, Clarendon Press, Oxford 274- 316, 1992.
- [74] J. H. Davis. The influence of membrane proteins on lipid dynamics. *Chemistry and Physics of Lipids*, 40:223–258, 1986.
- [75] J. H. Davis. Deuterium nuclear magnetic resonance spectroscopy in partially ordered systems. *Journal of Computational Chemistry*, 20:1153–1164, 1999.
- [76] E. Sternin. *PhD Thesis*. University of British Columbia,. Vancouver, 1988.
- [77] M. Bloom and E. Evans. *Biologically inspired Physics*,. edited by L. Peliti, Plenum press. , New York, 137-146, 1992.
- [78] K. P. Pauls, A. L. MacKay, O. Soderman, M. Bloom, A. K. Tanjea, and R. S. Hodges. Dynamis properties of backbone of integral membrane polypeptide measured by ^2H NMR. *European Biophysics Journal*, 12:1–11, 1985.
- [79] A. Abragam. *The Principles of Nuclear Magnetism*. Oxford University Press. Oxford, 1961.

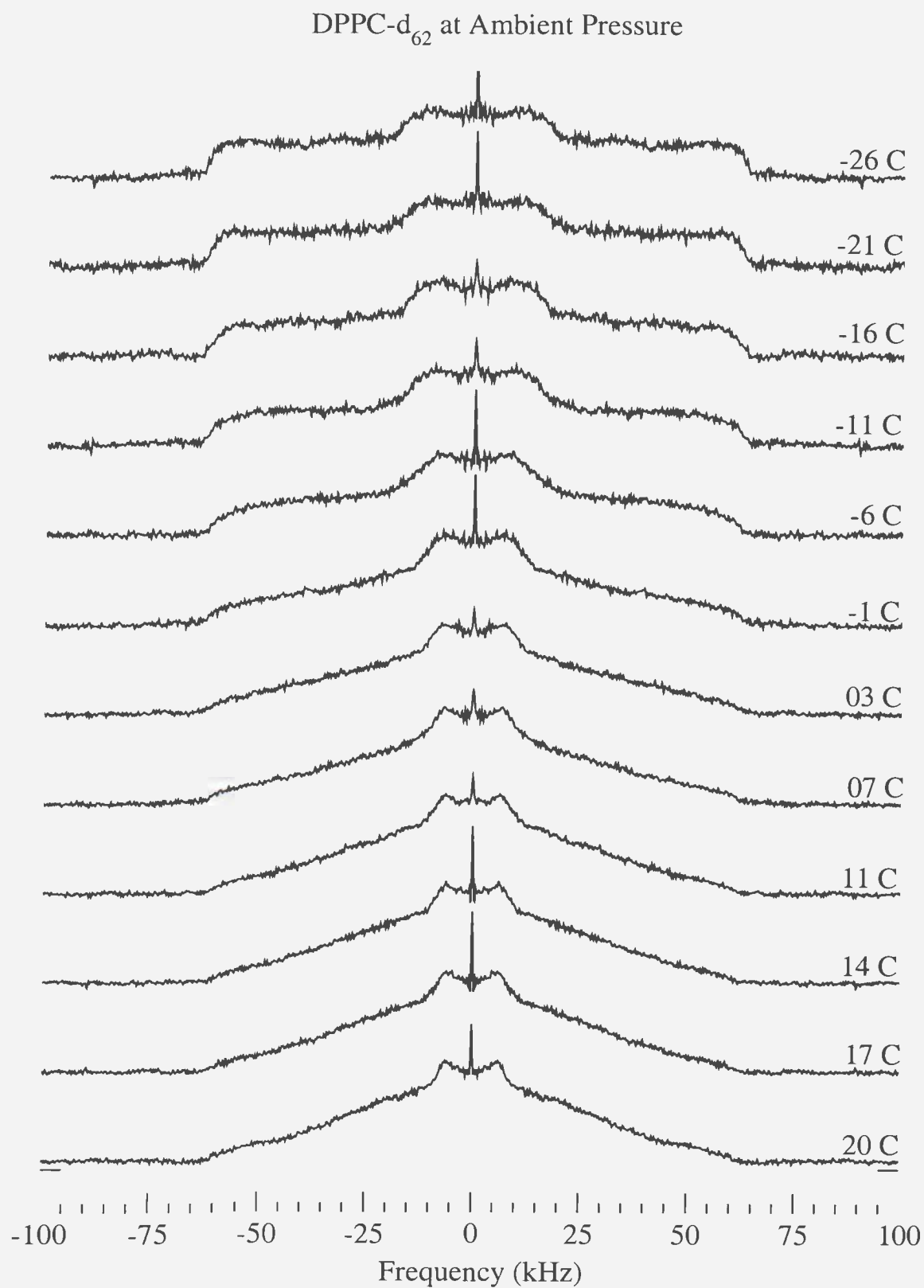
- [80] M. R. Morrow. Transverse nuclear spin relaxation in phosphatidylcholine bilayers containing gramicidin. *Biochimica et Biophysica Acta.*, 1023:197–205, 1990.
- [81] B.B. Bonev. *PhD Thesis*. Memorial University of Newfoundland, St. Johns, 1996.
- [82] M. R. Morrow, S. Taneva, G. Simtos, L. A. Alwood, and K. M. W. Keough. *Biochemistry Journal*, 32:11338–11344, 1993.
- [83] R S. Prosser, J. H. Davis, F. W. Dahlquist, and M. A. Lindorfer. ^2H Nuclear Magnetic Resonance of the gramicidin a backbone in a phospholipid bilayer. *Biochemistry*. 30:4687–4696, 1991.

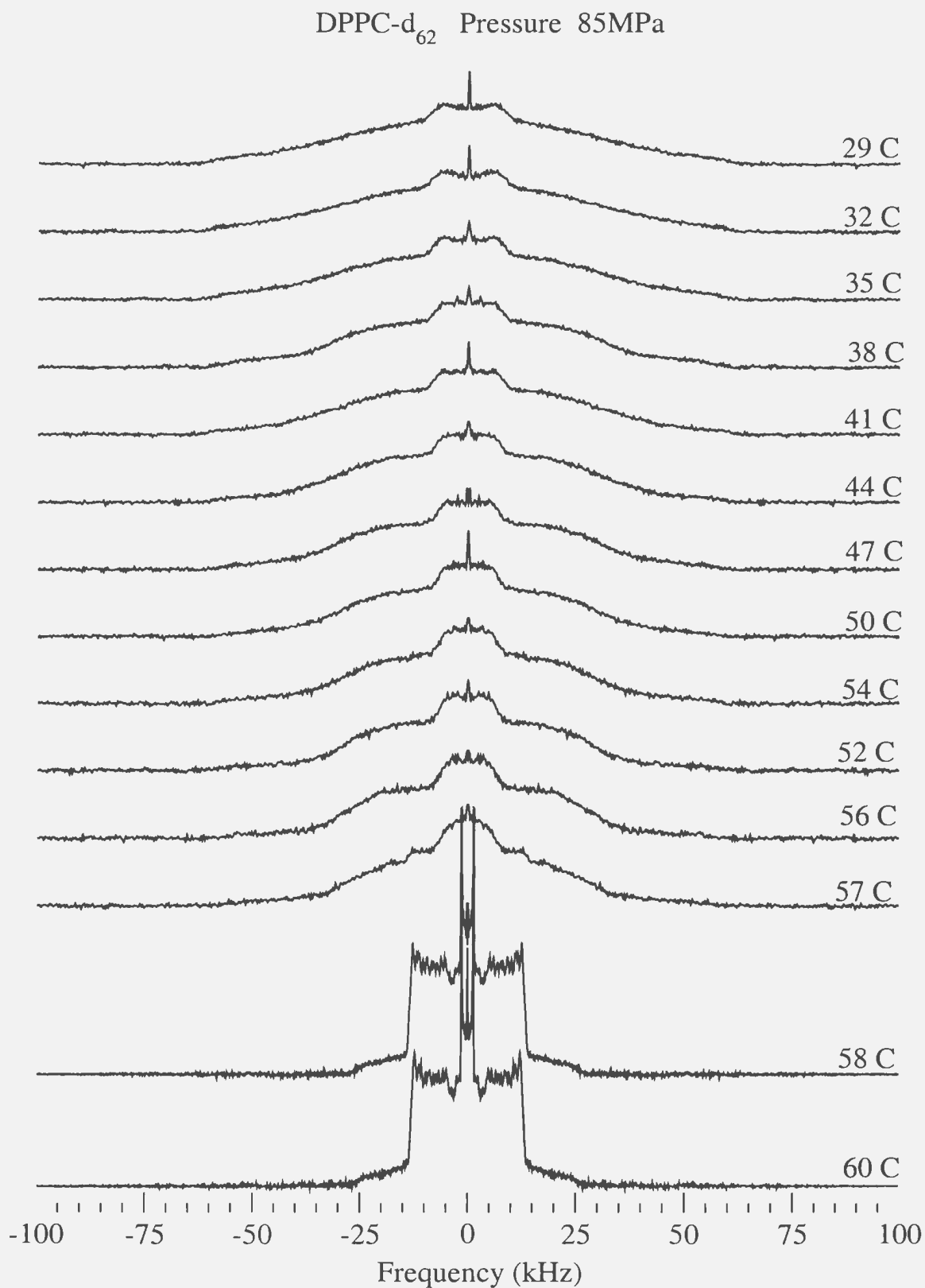
Appendix A

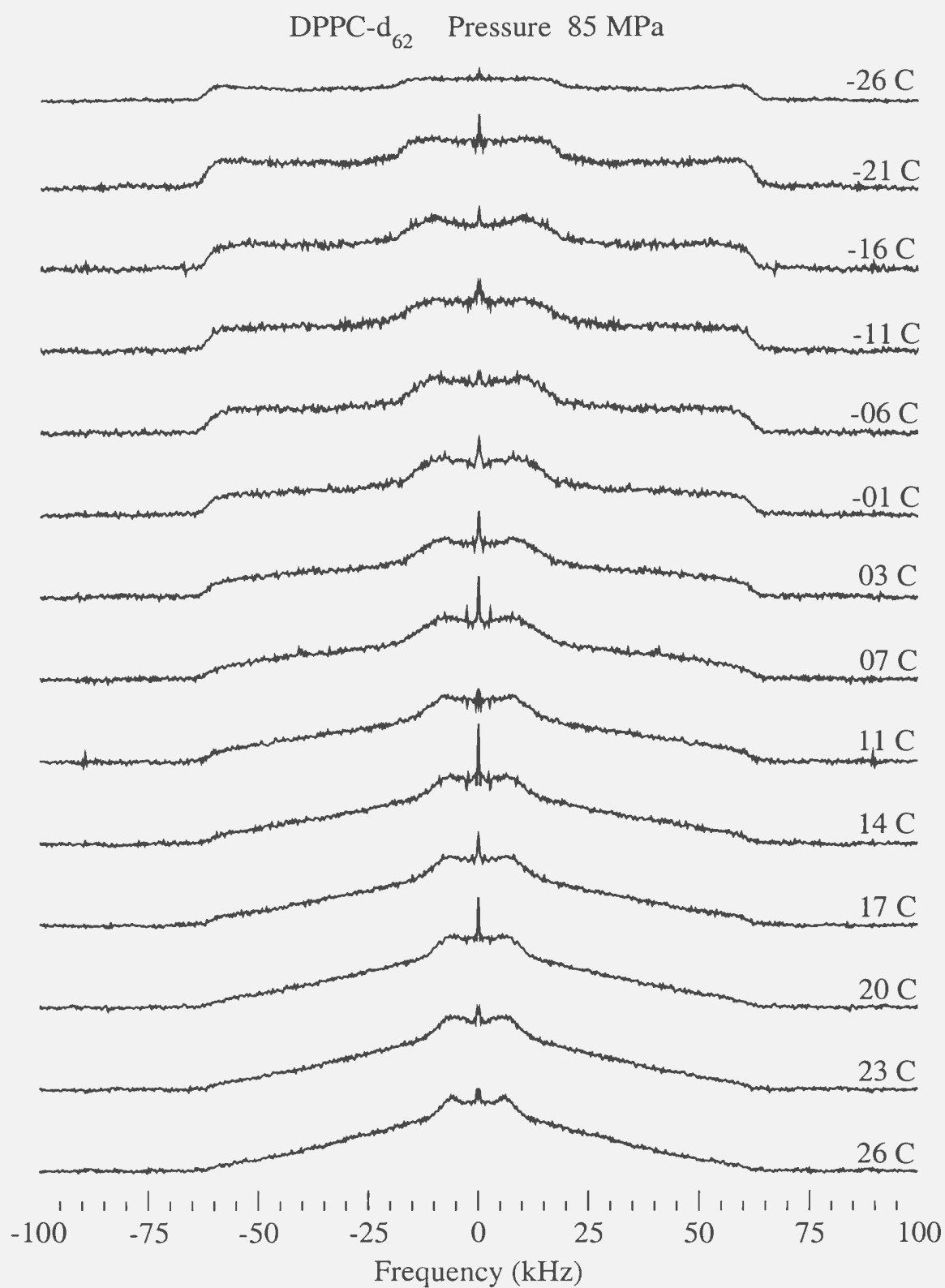
^2H NMR Spectra

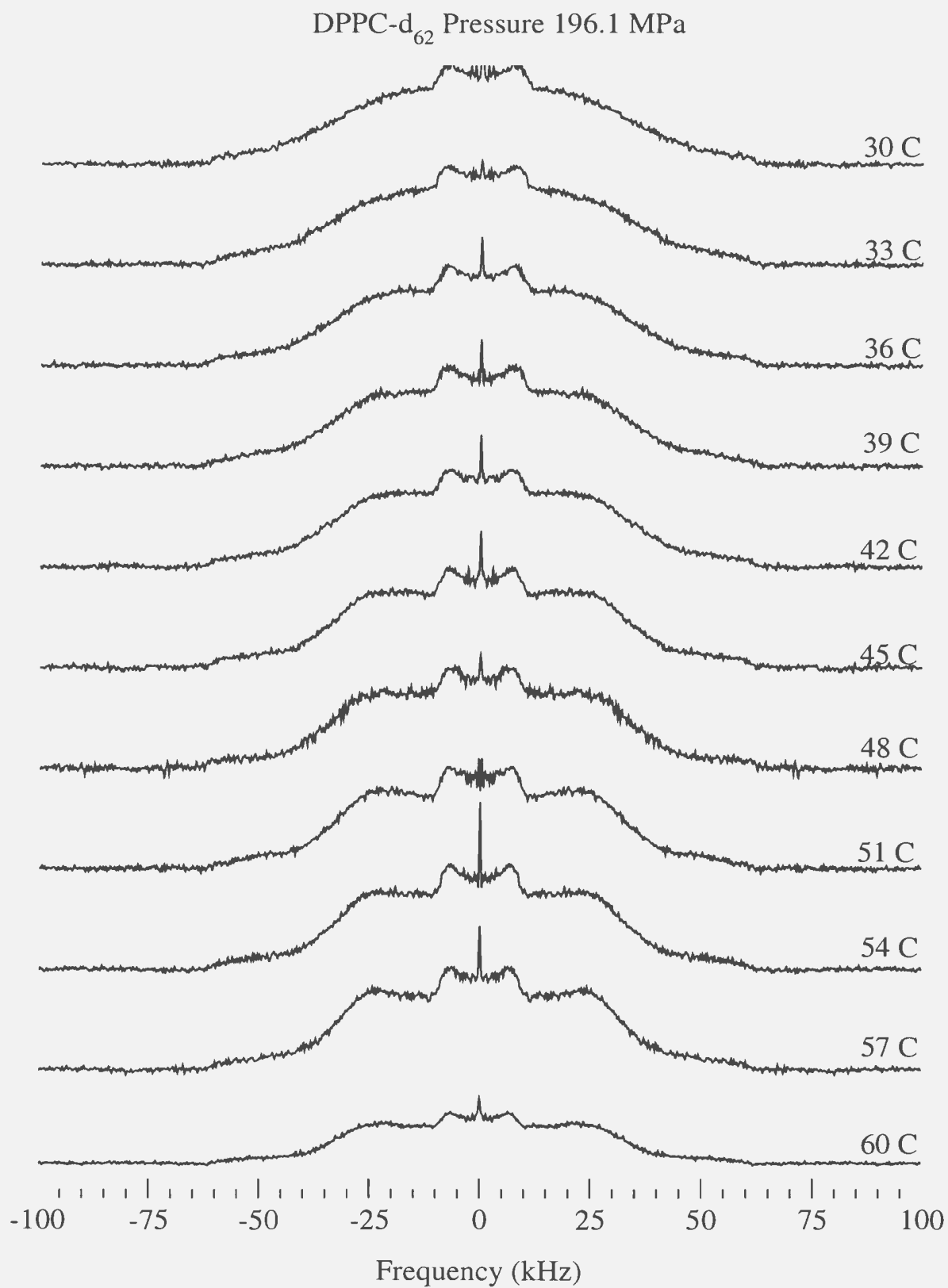
This appendix includes spectra of DPPC- d_{62} and DPPG- d_{62} at ambient pressure and pressure of 85 MPa and 196.1 MPa.

Figure A.1: ^2H NMR spectra for DPPC- d_{62} at ambient pressure, 50°C to 23°C.

Figure A.2: ^2H NMR spectra for DPPC- d_{62} at ambient pressure, 20°C to -26°C.

Figure A.3: ^2H NMR spectra for DPPC- d_{62} at pressure of 85 MPa, 60°C to 29°C.

Figure A.4: ^2H NMR spectra for DPPC- d_{62} at pressure 85 MPa, 26°C to -26°C.

Figure A.5: ^2H NMR spectra for DPPC- d_{62} at pressure 196.1 MPa, 60°C to 30°C.

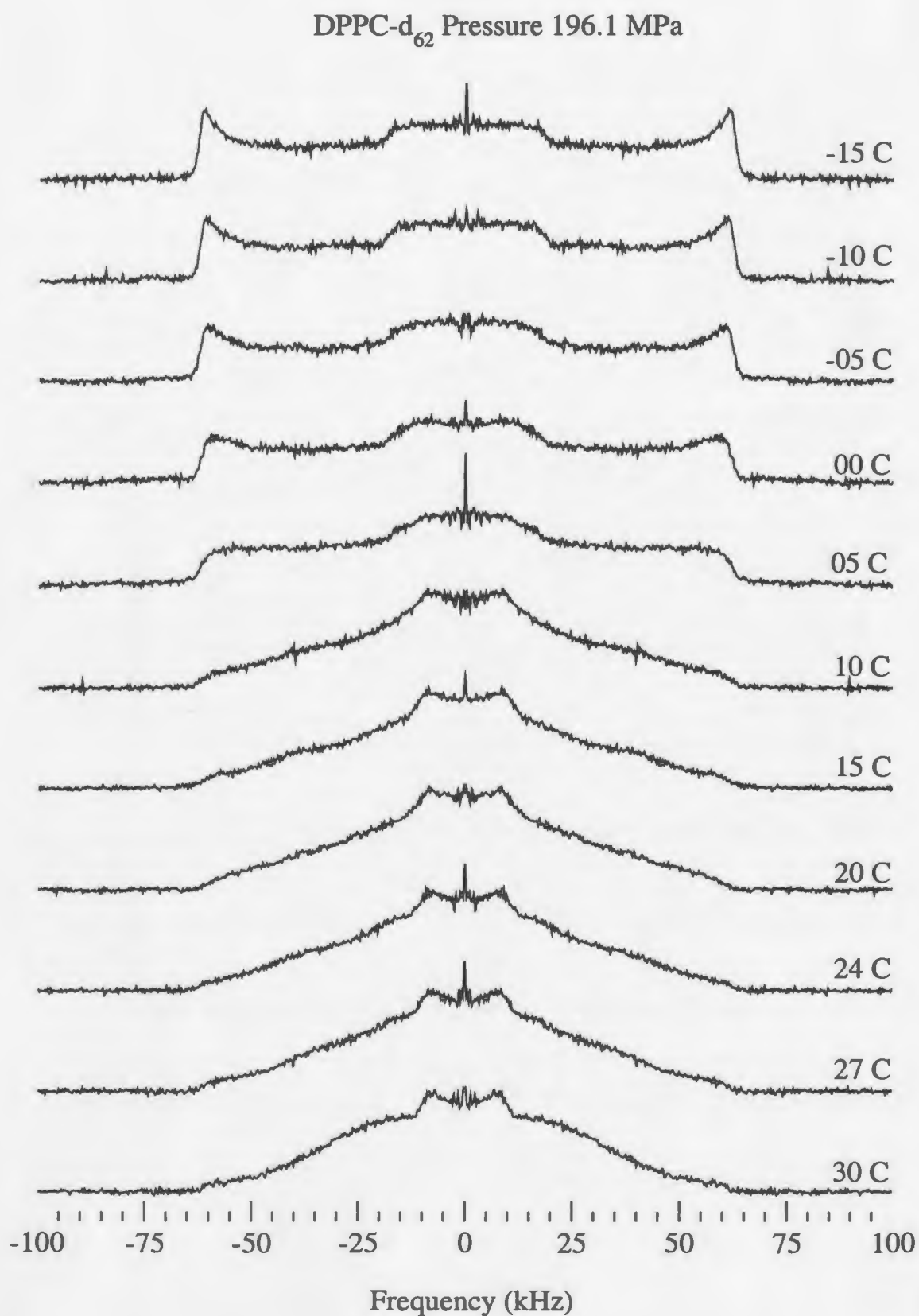
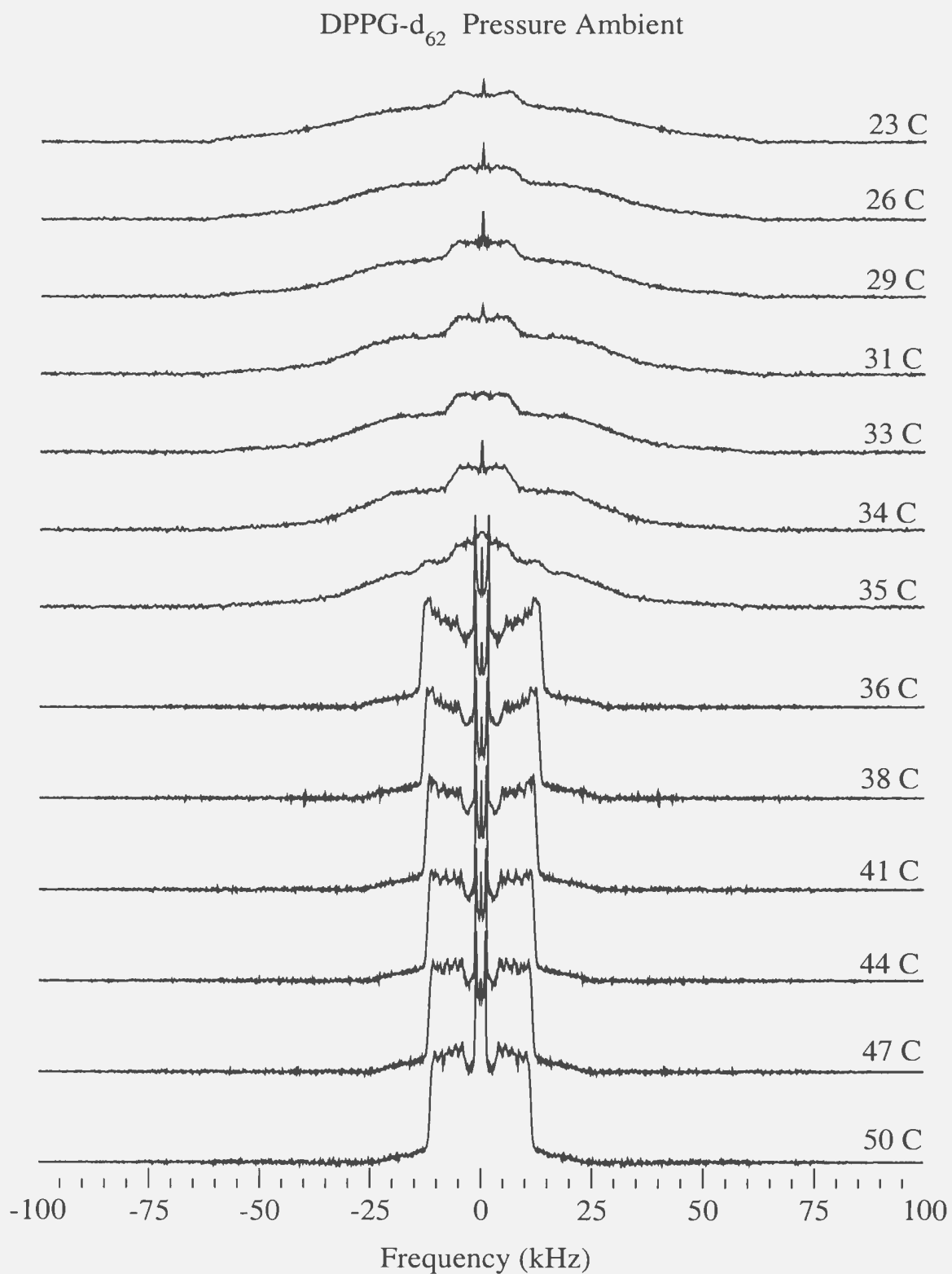
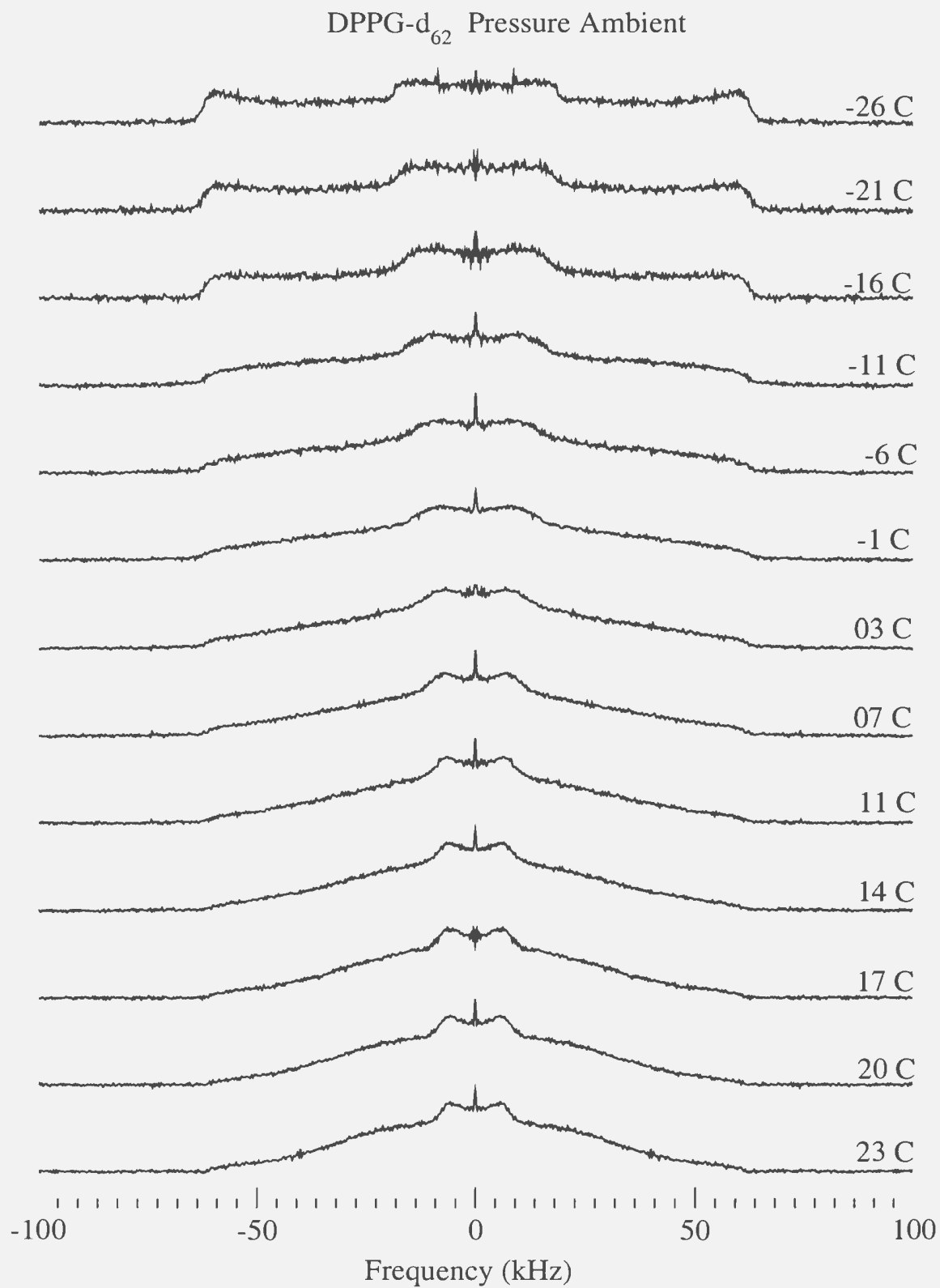
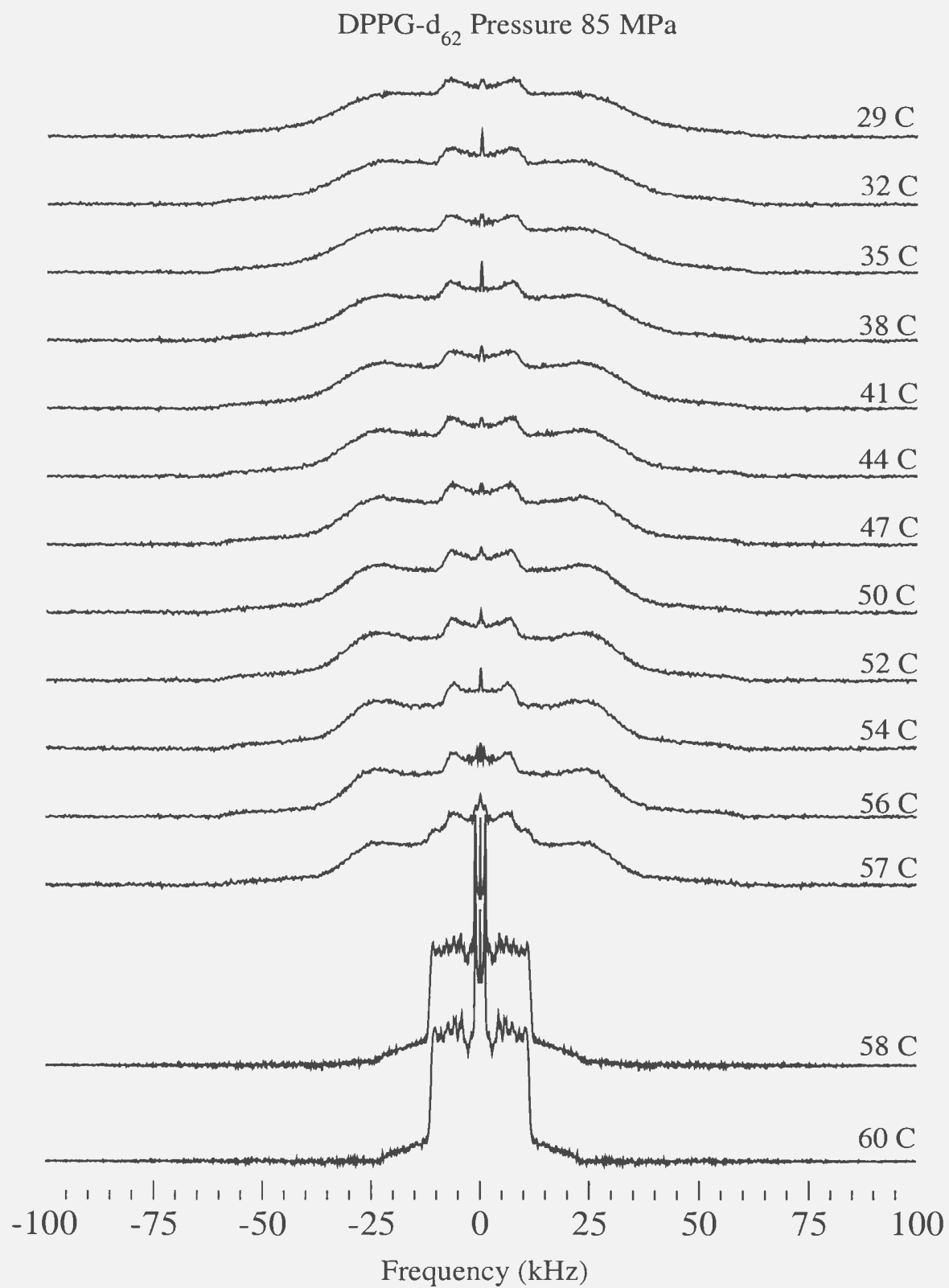
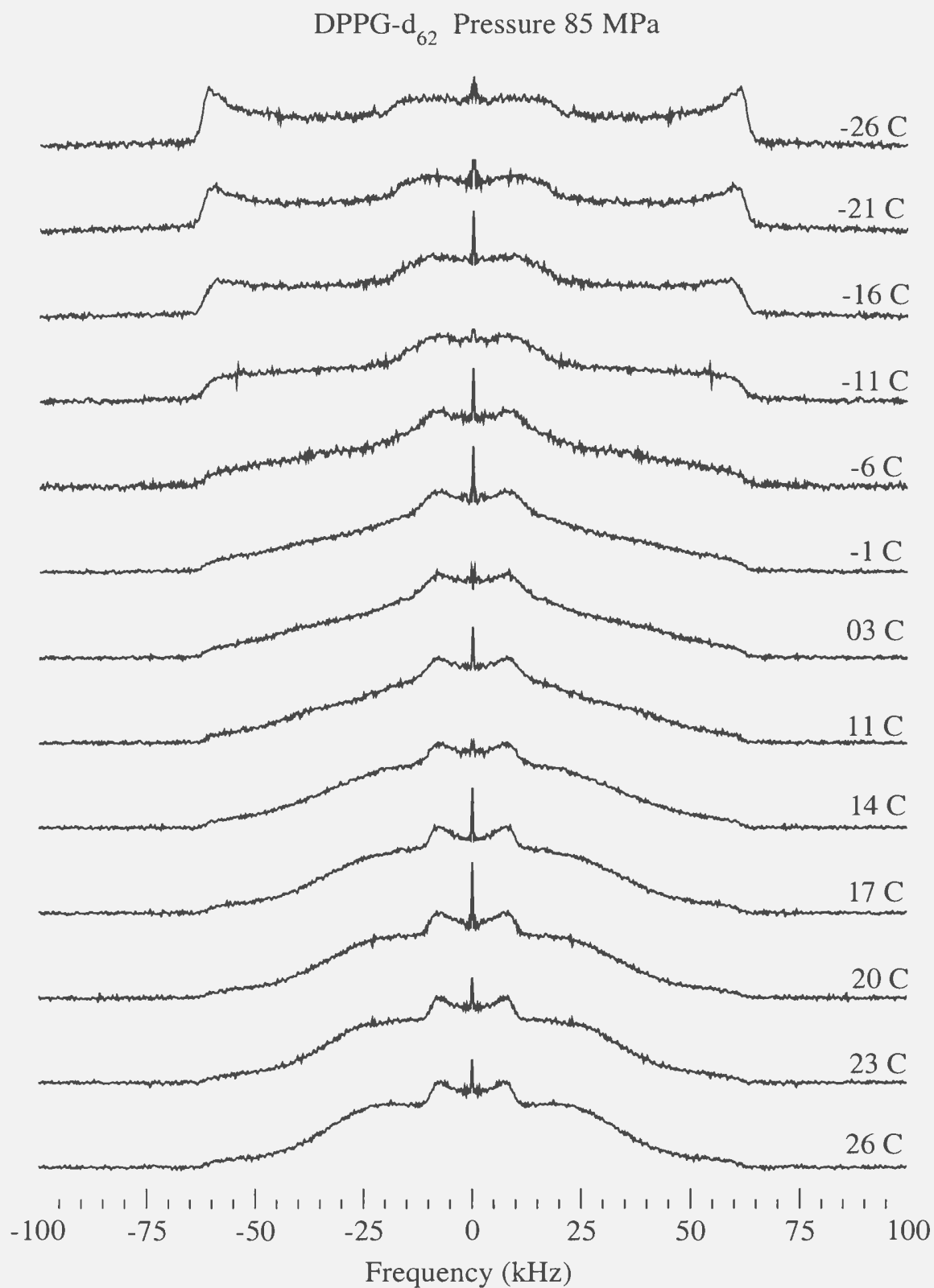


Figure A.6: ^2H NMR spectra for DPPC- d_{62} at pressure 196.1 MPa, 30°C to -15°C.

Figure A.7: ^2H NMR spectra for DPPG- d_{62} at ambient pressure, 50°C to 23°C.

Figure A.8: ^2H NMR spectra for DPPG- d_{62} at ambient pressure, 23°C to -26°C.

Figure A.9: ^2H NMR spectra for DPPG- d_{62} at pressure of 85 MPa, 60°C to 29°C.

Figure A.10: ^2H NMR spectra for DPPG- d_{62} at pressure 85 MPa, 26°C to -26°C.

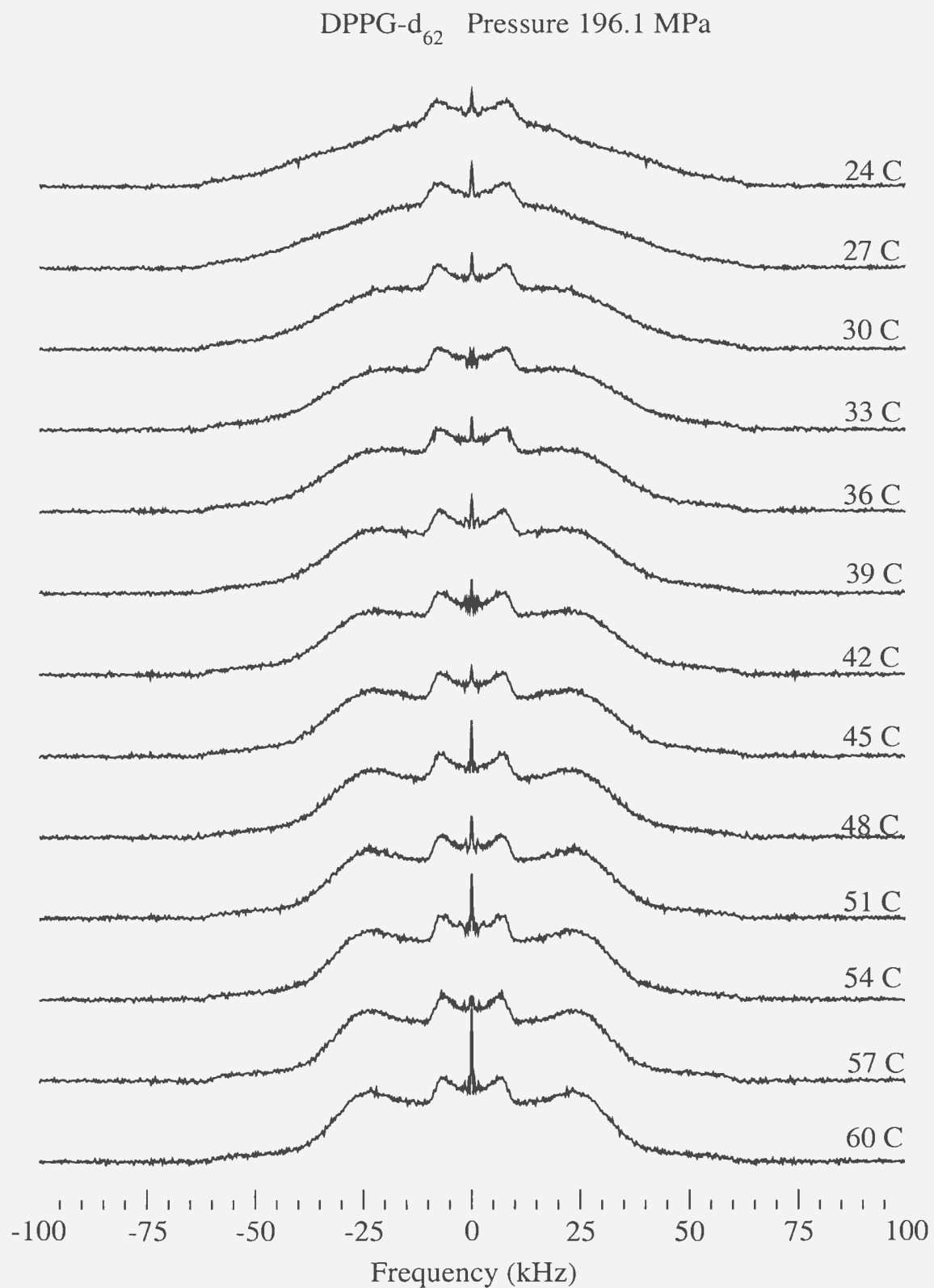


Figure A.11: ^2H NMR spectra for DPPG- d_{62} at pressure 196.1 MPa, 60°C to 24°C.

